Materials Science & Engineering R 145 (2021) 100621

Contents lists available at ScienceDirect

Materials Science & Engineering R

journal homepage: www.elsevier.com/locate/mser

Shaping and structuring 2D materials via kirigami and origami

Ziyang Zhang [a,1], Ziao Tian [a,1], Yongfeng Mei [b,*], Zengfeng Di [a,*]

[a] State Key Laboratory of Functional Materials for Informatics, Shanghai Institute of Microsystem and Information Technology, Chinese Academy of Sciences, Shanghai 200050, China

[b] Department of Materials Science, State Key Laboratory of ASIC and Systems, Fudan University, 220 Handan Road, Shanghai 200433, China

ARTICLE INFO

Keywords:
2D materials
Kirigami
Origami
3D structures

ABSTRACT

Two-dimensional (2D) materials such as graphene and molybdenum disulfide et al. offer significant new prospects for electronics, optics, and biosensing applications due to their unique physical and chemical properties. The controlled manipulation of such materials to create three-dimensional (3D) architectures is an intriguing approach to favorably tuning their properties and creating new types of 3D devices with small form factors. However, 2D materials exhibit extremely low bending stiffnesses compared with traditional functional materials, therefore, it is rather challenging to obtain stable 3D structures under van der Waals (vdW) interaction despite the easier out-of-plane manipulation. The centuries-old paper-shaping techniques named as 'kirigami' and 'origami' may provide a potential solution to this deadlock. The general idea is that through pre-patterning and mechanical deformations, 2D materials can be reshaped and transformed into 3D structures on demand, which extends the application of kirigami/origami from conventional functional films to atomically thin nanosheets. This kind of shaping and structuring strategy not only integrates 2D materials with 3D micro/nano-structures in a controllable manner, but also offers a new paradigm for tailoring the properties of 2D materials, thus enabling more functions beyond the capability of planar geometry. Such 3D micro/nano-architectures containing engineered 2D materials can provide a platform to explore the frontier physics and produce micro/nano-devices with improved performance or unprecedented functionalities. Hence, it is necessary to review the recent progress in this emerging field, which combines the exemplary kirigami/origami strategy with promising 2D materials to increasingly inspire the multidisciplinary applications. This review focuses on 2D materials kirigami/origami, including intrinsic and engineered properties, mechanisms, methods and applications. The research challenges and opportunities are also discussed to promote future theoretical and technological studies in this blooming interdisciplinary field.

1. Introduction

Two-dimensional (2D) materials that are only single or few atoms thick often exhibit extraordinary properties, e.g. very large specific surface areas, quantum-confined intrinsic electronic properties, and excellent stimuli-responsiveness [1–4].

One feature that especially benefits from the small atomic thicknesses of these 2D materials is their pronounced band tunability, which gives rise to the possibility of tuning their electronic and photonic performance effectively by mechanical deformations [5–7]. Indeed, the reported strain-induced tunability has attracted great interest and opened up a diverse range of next-generation devices (field-effect transistors, optoelectronic devices, and devices for storing energy, to name but a few). To achieve tunable properties, much effort has been made to ensure that the inherently planar geometries of 2D materials are assembled macroscopically on a three-dimensional (3D) scale.

However, the atomically-thin nature of 2D materials turns out to be both a blessing and a curse. On one hand, the bending stiffnesses of 2D materials tend to be extremely low, which means they are more easily bent or folded to form 3D structures compared to thicker or bulk materials. In other words, shaping and structuring 2D materials requires only a small amount of energy, which is important from a practical standpoint when facilitating low-power, highly-sensitive devices. On the other hand, their ultrathin nature means that 2D materials are too soft to support their own weight, which makes them highly susceptible to destruction and renders them unlikely candidates for directly creating

* Corresponding authors.
E-mail addresses: yfm@fudan.edu.cn (Y. Mei), zfdi@mail.sim.ac.cn (Z. Di).
[1] These authors contributed equally to this work.

https://doi.org/10.1016/j.mser.2021.100621
Received 3 December 2020; Received in revised form 9 April 2021; Accepted 20 April 2021

stable 3D structures. For example, hollow 3D graphene structures with ultrathin walls readily collapse into multifolded structures. In addition, strong van der Waals forces between nanosheets of 2D materials are difficult to control in general and often result in aggregation and restacking. Consequently, manipulating 2D materials to create 3D architectures with controllable geometries is currently very challenging.

Origami, the art of paper shaping, is one possible strategy that could be considered to achieve the creation of nano-, micro-, and macro-sized 3D objects via the folding of the initially-planar sheets. By simply imposing pre-designed patterns of creases, complex 3D architectures should be possible by the continuous and direct 2D-to-3D transformation of the sheets via folding, bending and twisting. This kind of shape-changing strategy has been demonstrated for various materials, e.g. metallic conductors, semiconductors, dielectrics, oxide insulators, hydrogels, piezoelectric ceramics, etc. [8]. In recent years, the origami concept has been extended to the realm of graphene and other 2D materials which are actually ideal origami materials due to their excellent mechanical strength, intrinsic flexibility, and strain-engineered behavior. As a result, many genuinely 3D structures (tubes, wrinkles, cages, etc.) have been fabricated from 2D materials by exploiting the origami approach. Furthermore, another strategy called 'kirigami' that similarly originates from the papercraft technique can introduce the cut patterns into the assembly and enrich the architectures of shaped and structured 2D materials.

Fig. 1 summarizes the main 2D materials (graphene, hexagonal boron nitride (h-BN) and transition metal dichalcogenides (TMDs)) that have been shown to be capable of being assembled into various out-of-plane structures via different methods, ranging from simple ones (folding [9], rolling [10], wrinkling [11] and buckling [12]) to more complex kirigami/origami-based schemes [13,14]. These predictable, controllable, and scalable approaches to generating 3D structures not only provide an innovative perspective to tailor the properties of the shaped and structured 2D materials but also inspire the creation of high-performance devices in a wide range of applications [15–26].

Over the past few years, several excellent reviews on origami and kirigami have been published [27–31], ranging from comprehensive ones to specific ones. However, as a frontier concept, 2D materials origami/kirigami is only mentioned and briefly discussed as a section in some reviews [28–30]. In fact, 2D materials integrated with origami/-kirigami have been investigated extensively recently, which unveils the potential of origami/kirigami assembly of 2D materials for novel applications in the multidisciplinary [19–26]. In particular, some major breakthroughs have been made in the related frontier area and demonstrated the promising prospect of 2D materials kirigami/origami, e.g. atomically precise graphene nano-origami [32] and high-order superlattices fabricated by rolling up van der Waals heterostructures [33]. In recognition of the unique advantages and potential of 2D materials integrated with origami/kirigami, it will be rather instructive to summarize the latest research progresses on 2D materials kirigami/origami and articulate their significance to interdisciplinary researchers. In this review, we focus on the kirigami and origami approaches to shaping and structuring 2D materials. In order to discuss the feasibility of 2D materials kirigami and origami, the relevant mechanical properties of 2D materials are firstly introduced. Then, some emphasis is placed on the driving forces for triggering the process of mechanical assembly. The following section describes the creation of diverse geometries from well-defined planar patterns via different shaping and structuring schemes of 2D materials, covering the basic elements of kirigami/origami assembly (folding, rolling, wrinkling, buckling) and more complex designs. Thereafter, we summarize the unique properties and promising applications of 2D-to-3D transformation in fields such as flexible electronics, energy harvesters, sensors, actuators, robotics, and

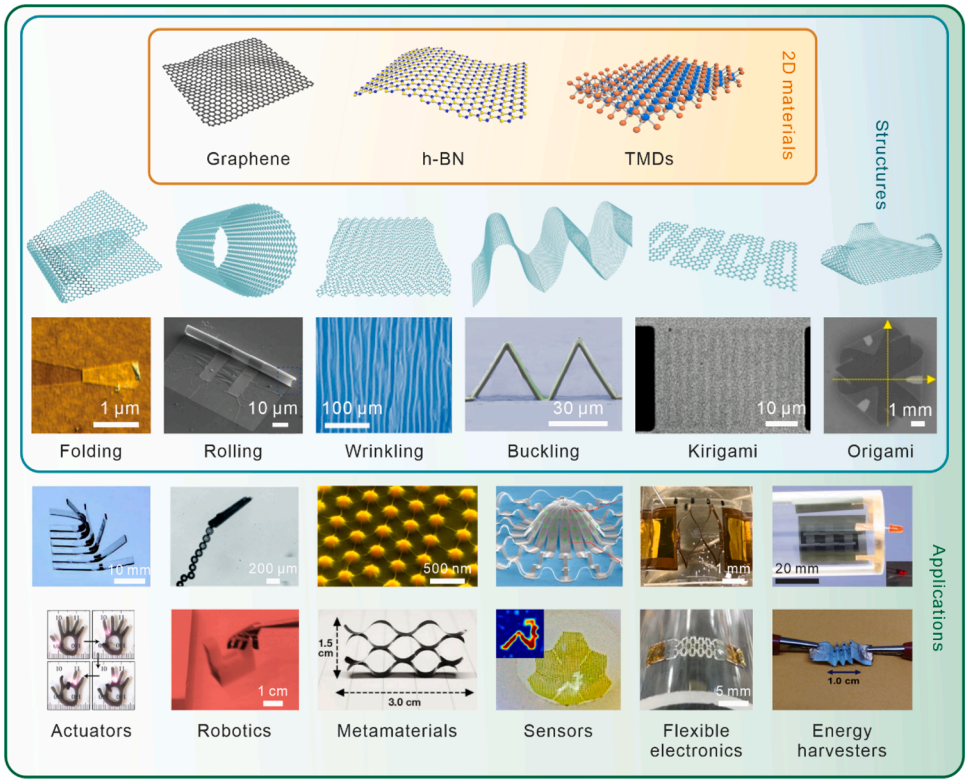

Fig. 1. An overview of six typical kirigami/origami-assembly structures based on three kinds of representative 2D materials and various applications. Schematic illustrations show representative 2D materials: graphene, hexagonal boron nitride (h-BN) and transition metal dichalcogenides (TMDs). Schematic illustrations and experimental examples of assembly structures via six kinds of shaping methods are exhibited as folding [9], rolling [10], wrinkling [11], buckling [12], kirigami [13], and origami [14]. Various applications inspired by 2D materials shaping and structuring are shown with representative examples: actuators, graphene-based polymer bilayers for light-driven hinge actuator (top) [15], light-controlled graphene-elastin composite hydrogel actuator (bottom) [16]; robotics, graphene oxide rolled-up micromotors (top) [17], origami-inspired light-triggered robotic hand (bottom) [18]; metamaterials, optoelectronic crystal of artificial atoms in strain-textured MoS_2 (top) [19], graphene oxide kirigami structure with ultra-positive Poisson's ratio (bottom) [20]; sensors, functional 3D architectures of 2D materials for photodetection and imaging (top) [21], human eye-inspired MoS_2-graphene curved image sensor arrays for implantable optoelectronic device (bottom) [22]; flexible electronics, 2D $PtSe_2$ layer kirigami conductors with outstanding stretchability (top) [23], highly stretchable nanoscale devices by MoS_2 kirigami (bottom) [24]; energy harvesters, rollable graphene hydroelectric generators (top) [25], flexible supercapacitors based on reduced graphene oxide (bottom) [26].

metamaterials. Finally, the challenges and future directions of this research area are outlined.

2. Mechanical properties of 2D materials

The mechanical properties of 2D materials used are one of the first elements when considering the suitability of the material for structural transformation as they play a fundamentally important role in determining the feasibility and stability of the kirigami/origami assembly. Atomically-thin 2D materials exhibit exceptional mechanical properties in comparison to their bulk counterparts. In particular, their mechanical properties make them ideal for fabricating nanoscale structures and tailoring their properties for various frontier applications.

However, the mechanical properties of 2D materials are affected by a wide variety of factors, which makes this research area rather complicated (from the atomic mechanisms underlying their transformations to their use in actual applications). In order to comprehensively investigate this key aspect of the research, a great deal of effort has been paid to the characterization of various significant mechanical properties, e.g. elasticity, fracture properties, and interfacial properties [34–36]. Many of the methods traditionally used to determine the mechanical characteristics of bulk materials cannot be adopted to characterize 2D materials. Therefore, new methods have had to be developed to realize even straightforward measurements in 2D materials, for example, in-situ microscopy techniques [35]. In this section, the mechanical properties of 2D materials are described in detail to demonstrate both the advantages and disadvantages for 2D materials kirigami/origami in terms of mechanics. We also highlight the opportunities and challenges of shaping and structuring 2D materials via mechanical deformation or manipulation.

2.1. Elasticity

The elasticity of 2D materials describes their most basic mechanical behavior when they experience elastic deformation (i.e. when the deformation is small enough that the material returns to its initial state upon removal of the applied stress). It is worth noting that some 3D morphologies created from 2D materials can be obtained via bottom-up elastic deformation, which ensures both the integrity and reconfigurability of the desired structures during the process of kirigami/origami assembly. It is the in-plane and out-of-plane moduli corresponding to stretching and bending in the elastic regime that are the critical parameters needed to interpret the in-plane stiffness and bending rigidity of such materials, respectively.

The elastic properties of monolayer graphene were first measured by Lee et al. based on a method of nanoindentation conducted by atomic force microscope (AFM) [37]. As shown schematically in Fig. 2a, the AFM tip can be used to apply load to a graphene monolayer suspended over a circular well and the load is usually applied at the center of the well to achieve nearly uniform stretching. The graphene monolayer clamped over the circular hole was in a tautly-stretched state and the tip load could be estimated at the center point [37]. The data from AFM-induced nanoindentation produced in the monolayer graphene flake over holes of different diameters (Fig. 2b) were recorded and used to generate force–displacement curves (Fig. 2c), thus revealing the elastic characteristics of graphene. A series of nanoindentation tests

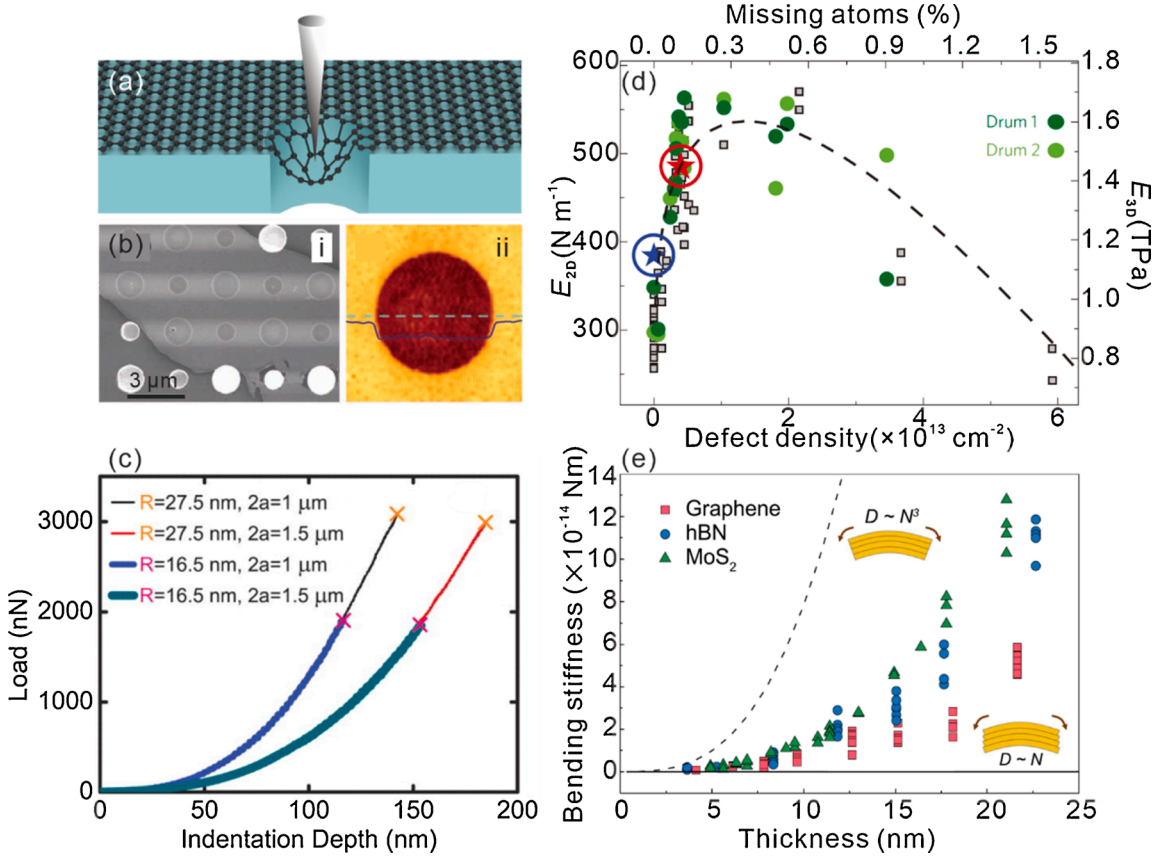

Fig. 2. The elasticity of 2D materials. (a) Schematic illustration of the measurement of elastic properties by AFM-based nanoindentation. (b) Images of suspended graphene for measuring elastic properties [37]: (i) scanning electron microscopy (SEM) image, (ii) AFM image. (c) Loading curves as the test results of monolayer graphene with different tip radii and film diameters [37]. (d) 2D elastic modulus of graphene modulated by defect concentration [45]. (e) Thickness-dependent bending stiffness of multilayer 2D materials directly measured by pressurized bubbles, between the values of theoretical prediction for perfectly glued (D ~ N^3) and ultra-lubricated (D ~ N) cases [61].

were analyzed to show that monolayer graphene had an outstanding elastic modulus corresponding to an average 2D Young's modulus of 342 ± 30 $N m^{-1}$.

Other experiments involving nanoindentation [38,39] and other techniques (e.g. pressurized blister tests [40]) also showed that the elastic modulus of pristine graphene was surprisingly high, a phenomenon that was ascribed to the effect of intrinsic ripples in some cases [39]. Similar experimental studies were extended to investigate the mechanical properties of other 2D materials and also observed high elastic moduli, e.g. 180 ± 60 $N m^{-1}$ for monolayers of molybdenum disulfide (MoS_2) [41] and 220–510 $N m^{-1}$ for the hexagonal boron nitride (h-BN) films [42]. The intrinsic superior stretchability of 2D materials ensures that they can sustain considerable tensile strain as load capacity is increased, which facilitates the in-plane manipulation of 2D materials for shaping and structuring.

It has been found that the existence of defects in 2D materials is usually unavoidable and has a remarkable effect on their elastic properties. According to some predictions, defects can generally cause the degradation of the elastic modulus [43,44]. It was surprising that a systematic investigation demonstrated that the elastic modulus of graphene could also be enhanced by controlling the introduction of defects [45]. The control on the defects density was realized by bombarding graphene samples (previously prepared for AFM mechanical testing) with known doses of Ar^+ ions. Fig. 2d shows the relationship subsequently obtained between the elastic moduli of the graphene samples and defect density. It was clear that the 2D elastic modulus of graphene firstly increased as defects were introduced until a maximum value (550 $N m^{-1}$) was reached at a defect density corresponding to 0.2 % of atoms missing. Further increase in the defect concentration led to a decrease in the 2D elastic modulus.

Structural defects in MoS_2 can also tune its mechanical properties, but the effects are more complex than those in graphene because of its binary elemental composition and three-atom layered structure [46,47]. For instance, grain boundaries in MoS_2 can behave as weak links that induce a remarkable weakening of the elastic modulus [48].

The engineered elastic properties of 2D materials by introducing defects has been investigated in-depth in other defect-dependent studies [49,50]. Such studies offer an opportunity for improving the ability of 2D materials to undergo elastic deformation in a controllable way. It is also shown that defects may occur during the fabrication or transfer process of 2D materials, thus causing unavoidable detrimental effects.

The traditional membrane models employed to interpret the above experimental results commonly neglect the effect of the material's bending moduli. Nevertheless, the influence of bending moduli is necessary to be included in a more rigorous analysis, which can obtain more precise results and elucidate the thickness-dependent elastic properties. The bending modulus also plays an important role in describing the flexibility of 2D materials with different thicknesses. However, it has always been challenging to directly measure the bending rigidity of 2D materials and the underlying mechanisms are full of controversy [51–53].

An estimate for the bending modulus of monolayer graphene was initially derived from the phonon spectrum of graphite, giving a value of ~1.2 eV [54]. The bending rigidity of convex, pre-buckled, graphene membranes was later determined from the critical electrostatic voltage that actuated the 'snap-through' phenomenon [55]. The bending rigidity of bilayer graphene was obtained by the above method as ~35.5 eV. Reassuringly, this value fell between two extreme theoretical values: 3 eV, for the case of two monolayers assumed to be independent [56]; 160 eV, for a coupled, plate-like, bilayer [52]. Meanwhile, the rough estimate for the bending rigidity of the graphene monolayer was still quite low (~7.1 eV), in spite of the high uncertainties.

As might be expected, the bending moduli of 2D materials become increasingly more significant in multilayer systems. In theory, the mechanical behavior of 2D materials will transform from membrane-like to plate-like as the thickness is augmented. This proposition has been verified by the mechanical investigation of pressurized graphene bubbles [57] and other 2D materials with thickness effects [58,59]. However, the out-of-plane elastic behavior of such materials remains somewhat puzzling as more complex factors like interlayer sliding need to be considered [60].

Recently, Wang et al. [61] directly measured the bending rigidity of multilayer van der Waals (vdW) materials based on pressurized bubbles. A layer-dependent function was introduced to explain the surprising result that the bending rigidities (D) of graphene, h-BN, and MoS_2 increased in the order: $D_{graphene} < D_{h\text{-}BN} < D_{MoS_2}$, which was in conflict with classical plate theory (Fig. 2e). The bending rigidity of 2D materials measured naturally increased as the thickness increased, and all of the values shown in Fig. 2e lay between two theoretical limits (i.e. the perfectly-glued and ultra-lubricated cases) due to the interlayer shear effect. Although the bending rigidity of multilayers could be stiffened by interlayer shear interactions, it was found that the above 2D materials were still flexible enough to be formed into various out-of-plane structures via buckling, wrinkling, scrolling, and folding.

In general, the unique elastic properties including high in-plane stiffness and low flexural rigidity are collective characteristics common to 2D materials and render these ultrathin nanomembranes shapeable. It is important to emphasize that the coexistence of in-plane stiffness and low flexural rigidity endows 2D materials with certain advantages that favor a diverse range of deformations and structural transformations, thus avoiding the disruption of the crystal lattice during the 3D assembly process. Nevertheless, their flexibility may also have a detrimental effect on the stability of the 3D structure after the assembly process, especially in cases involving liquid phases. For example, 3D hollow structures will be liable to collapse during the usual drying processes. In addition, the complicated effects of defects on elastic properties not only remind us that the quality of 2D materials used can determine the assembly result (to a large extent), but also open up the possibility of directing and controlling the defects to regulate the properties of 3D structure constructed.

2.2. Fracture properties

As shown schematically in Fig. 3a, when the load applied by the AFM tip gradually increases, the test material will begin to deform nonlinearly and fracture eventually occurs. Given the possible large deformation of shaped 2D materials, the fracture strength or toughness of 2D materials used need to be carefully considered to avoid the structure failure and guide the mechanics design.

For example, Fig. 3b shows morphologies of three different nanobubbles with different degree of deformations, which were formed by applying programmable AFM tip bias to graphene grown on a Ge (110) surface [62]. In this specific case, Ge–H bonds existing at the interface between the graphene and Ge (110) surface were broken by absorbing energy from the negative tip bias, thus generating hydrogen molecules to fill the graphene nanobubbles. Furthermore, the change of tip bias could vary the numbers of Ge–H bonds broken and the amount of hydrogen molecules, thus regulating the deformation of the graphene nanobubbles. The graphene nanobubbles produced therefore exhibited strain distributions and corresponding line profiles that evolved as the applied bias increased, as shown in the upper panel of Fig. 3c. It is evident that the deformation degree of shaped 2D materials can be tuned by the extent of the strain produced. Meanwhile, the fracture strength and toughness of 2D materials set limitations on the desired deformation, requiring an appropriate strain range to avoid the potential fracture like crack propagation (Fig. 3c, lower panel) [63].

Graphene and other 2D materials are highly susceptible to defects (e.g. vacancies, dislocations, and grain boundaries). These defects will also have a remarkable effect on the fracture behavior of 2D materials according to various mechanisms [64,65]. For example, Fig. 3d shows the schematic illustration of two typical grain boundaries that occur in graphene with different lattice orientations and tilted angles. Such

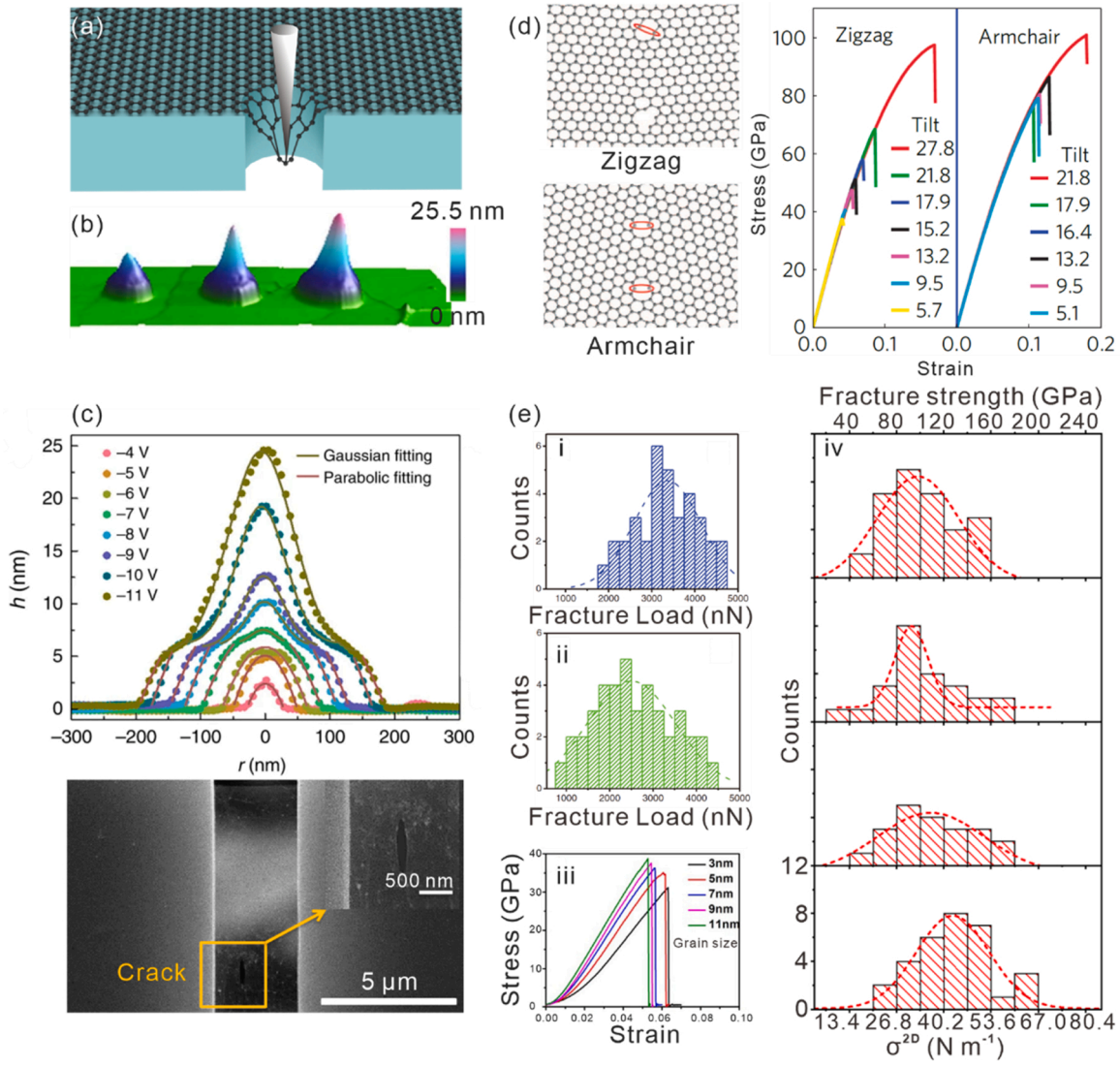

Fig. 3. Fracture properties of 2D materials. (a) Schematic illustration of largely deformed 2D materials when the load of AFM tip increases. (b) AFM images of programmable graphene nanobubbles with tunable deformations [62]. (c) Line profiles extracted from graphene nanobubbles with parabolic/Gaussian fitting showing two different deformation stages [62] and usual crack propagation in graphene [63]. (d) Two types of grain boundary in graphene [66] and stress-strain curve of graphene influenced by grain boundary [67]. (e) Tensile stress-strain curves and fracture strength for polycrystalline graphene modulated by grain size, shown as (i–iii) different grain sizes [38,70] and (iv) nanocrystalline [72].

typical defects composed of pentagon/heptagon rings can either enhance or weaken the strength of the graphene [66,67]. On the one hand, the strength of graphene can be enhanced by the increasing defect density of grain boundaries with large tilt angles [66]. On the other hand, both the tilt angle and specific arrangement of defects will influence the relationship between the strength and defects. Therefore, strength increases monotonically with tilt angle when 'armchair' defects are involved, but this is not the case with 'zigzag' ones [67].

As polycrystalline 2D materials with abundant grain boundaries are generally easier to produce (especially when large-scale manufacturing processes are involved), they have attracted enormous research interest [68]. For the example, the strength of polycrystalline graphene is not only affected by the grain boundaries but also by the grain size. Fig. 3e shows a comparison of the results of fracture tests performed on polycrystalline graphene samples grown by chemical vapor deposition (CVD). The results obtained from a sample consisting of large or small grains are shown in Fig. 3e (i) and Fig. 3e (ii), respectively [38]. Nanoindentation on samples with well-stitched, large-grain, grain boundaries therefore produced a slightly higher fracture load (3370 ± 340 nN) compared to those with small-grain grain boundaries (2590 ± 380 nN). Both of these values were comparable with pristine graphene. The grain-size dependency of the fracture load of polycrystalline graphene was further explored using molecular dynamics simulations, leading to the establishment of the pseudo-Hall-Petch [69] and inverse pseudo-Hall-Petch relationships [70], according to different models.

Fig. 3e(iii) shows stress–strain curves for polycrystalline graphene samples with different grain sizes. It is observed that the fracture strength in this case increases as the grain size increases, thereby following the inverse pseudo-Hall-Petch relationship [70]. This behavior is also consistent with the results of previous experimental measurements [71]. Recently, the effect of grain size on the strength of nanocrystalline graphene samples was explored using an ultrafast quenching technique [72]. Fig. 3e(iv) shows that the fracture strength of nanocrystalline graphene films can be regulated by the grain size and also follows an inverse pseudo-Hall-Petch relationship. This behavior is opposite to that found in nanocrystalline metals.

Enhanced in-plane stiffness and fracture strength with increased grain size (i.e. the inverse pseudo-Hall-Petch effect) has also been verified in polycrystalline MoS_2 [48]. The relatively complex and fickle circumstances imposed by defects will bring limitations and challenges

when choosing a 2D material for shaping and structuring in practical applications. Meanwhile, the grain boundary defects can enhance the potential of polycrystalline 2D materials, namely providing the opportunity for the materials to be toughened by engineering the defects in a controllable manner.

Besides conventional defects, micro/nanofabrication conducted in 2D materials enables the cut patterns, which can be viewed as another kind of special 'defects' with larger sizes. These microscale defects can play a creative role in the shaping and structuring of 2D materials. Such an approach is generally referred to as kirigami. The first attempt to introduce kirigami into graphene was performed in 2015 [13]. As mentioned in that article, the ratio between the in-plane stiffness and bending rigidity of graphene suggests that graphene can be stiffened by ripples to such an extent that it resembles standard paper. As a result of fabricating cut patterns, the toughness and stretchability of graphene can be further enhanced, showing that graphene kirigami is able to be an inspiring approach to designing novel mechanical metamaterials.

2.3. Interfacial adhesion and friction

The large surface to volume ratios of 2D materials has also attracted enormous attention because surface forces play a significant role at the interface. Whether these forces act at the interfaces between the layered materials or between 2D materials and substrate, the effects of adhesion and friction are intimately connected with any out-of-plane manipulation attempted, and are especially important for the development of transfer techniques. Interestingly, features induced during the synthesis and transfer processing of 2D materials originally thought to be detrimental (e.g. self-tearing [9], self-folding [60], and wrinkles [73]) have been exploited to investigate the properties of the interfaces and mechanisms underlying the out-of-plane deformation of 2D materials. This information has helped build a more solid theoretical basis for strain engineering and 3D manipulation.

Because of the relatively weak interlayer interactions in 2D materials, the competition between adhesion energy and bending rigidity will induce a certain amount of local out-of-plane deformation, as shown schematically in Fig. 4a. Fig. 4b also shows some experimental deformations corresponding to: (i) buckle delaminations [74] and (ii) blisters [75]. These kinds of deformations provide valuable information about the interfacial interactions. For example, utilizing the height profiles of blisters naturally formed in 2D materials on different substrates or vdW heterostructures, work of adhesion values extracted from various systems are summarized in Fig. 4c, thus demonstrating the interfacial adhesion between 2D materials and substrates [75].

Interfacial properties play a dominant role in determining whether interlayer adhesion or separation occurs. Knowing the adhesion between suitably strained and structured layers can be used to achieve selective delamination and facilitate the initialization of out-of-plane deformation, thus guiding the assembly process. Moreover, weak adhesion will be easily overcome in general, allowing even a small disturbance to activate a considerable out-of-plane motion. For example, as shown in Fig. 4d, self-tearing and folding of graphene nanoribbons from graphene films on SiO_2 were thermally activated using a nanoimprint, which allowed the competition between adhesion energy and

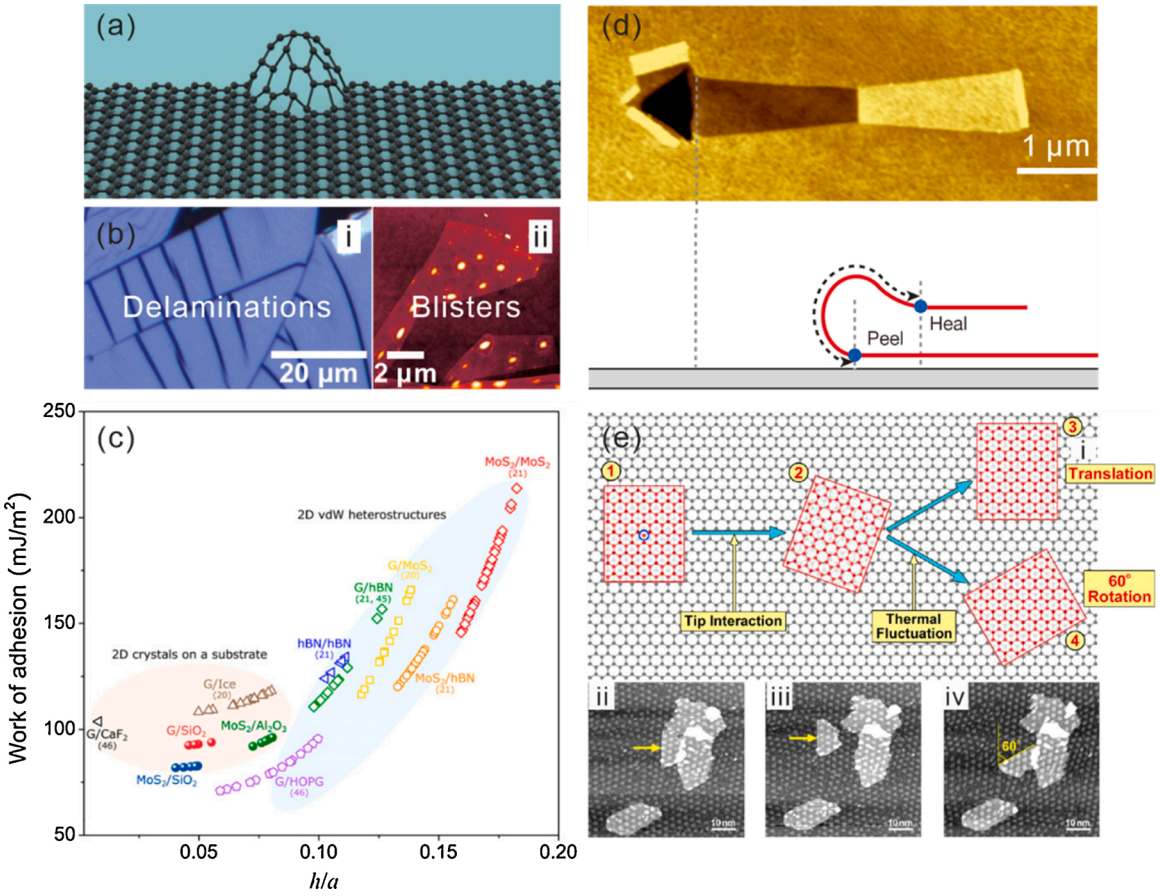

Fig. 4. Interfacial properties of 2D materials. (a) Schematic illustration of the bubble delaminated from the substrate commonly existing in 2D materials. (b) Two examples of out-of-plane patterns in 2D materials closely correlated to interfacial properties: (i) optical image of delaminations in an exfoliated MoS_2 flake [74] and (ii) AFM image of blisters formed in graphene [75]. (c) Work of adhesion values for various 2D material interfaces estimated according to blister profiles [75]. (d) AFM image of self-tearing and peeling of graphene induced by thermal activation and the corresponding schematic illustration [9]. (e) (i) Schematic illustration and (ii–iv) AFM images of translation and rotation behavior of graphene nanoflakes on larger graphene surface [80]. All scale bars are 10 nm.

exotic actuation to be leveraged [9].

In view of the fact that out-of-plane bending is required for layer separation, interlayer shear and sliding at the interface will also make important contributions to the synergistic effects. The quantitative measurements of the bending rigidities of multilayer vdW materials mentioned above indeed introduced the effect of interlayer shear in order to interpret the finer features of the coupled bending/stretching mechanism involved [61].

The layered structures and relatively low levels of interlayer friction in 2D materials lead to them being widely used in tribological applications [76,77]. They are also of interest when interpreting atomic friction mechanisms. The frictional properties of exfoliated 2D materials weakly adhered to a substrate have been explored using friction force microscopy [78]. The general trend is that thinner nanosheets are subject to greater interlayer friction because they have enhanced sensitivity to bending motion. Nanomechanical experiments involving more regulated variables can provide a deeper insight into the underlying slippage mechanisms. For example, the results of deflection tests on multilayer graphene depended on stacking orientation and showed that the finite shear strength between layers could account for the thickness-dependency of the strength of the material [79].

Another important facet of 2D materials is that they can be manipulated in directions parallel to the underlying surface when the adhesion forces are sufficiently weak, as illustrated in Fig. 4e. The figure shows AFM images of graphene nanoflakes on graphene after being manipulated using a frictional force microscope at low temperatures (e.g. 5 K) [80]. The schematic illustration and corresponding AFM images clearly shows the translation and rotation of an individual nanoflake which was initiated by the movement of frictional force microscope tip and was subsequently pushed forward by thermal fluctuations. Furthermore, the nanoflakes were found to exhibit superlubric behavior even at 5 K as long as they were in commensurate positions. These kinds of experiments may inspire more shaping and structuring schemes to be developed (perhaps initiated by microscope manipulation or other external stimulus) which is beneficial to the nanoscale assembly/self-assembly of 2D materials in particular.

3. Fabrication techniques

Considering the mesoscale involved, the shaping and structuring processes cannot be achieved 'by hand' due to the limited space. Instead, the transformations need to be triggered by some indirect driving force. Here, we summarize several driving forces that can be used to stimulate the shaping and structuring of 2D materials, including residual stresses, responsive stresses, capillary forces, van der Waals forces, external mechanical stresses, and other driving forces.

3.1. Residual stresses and responsive stresses

In multilayer systems, a strain mismatch between the different

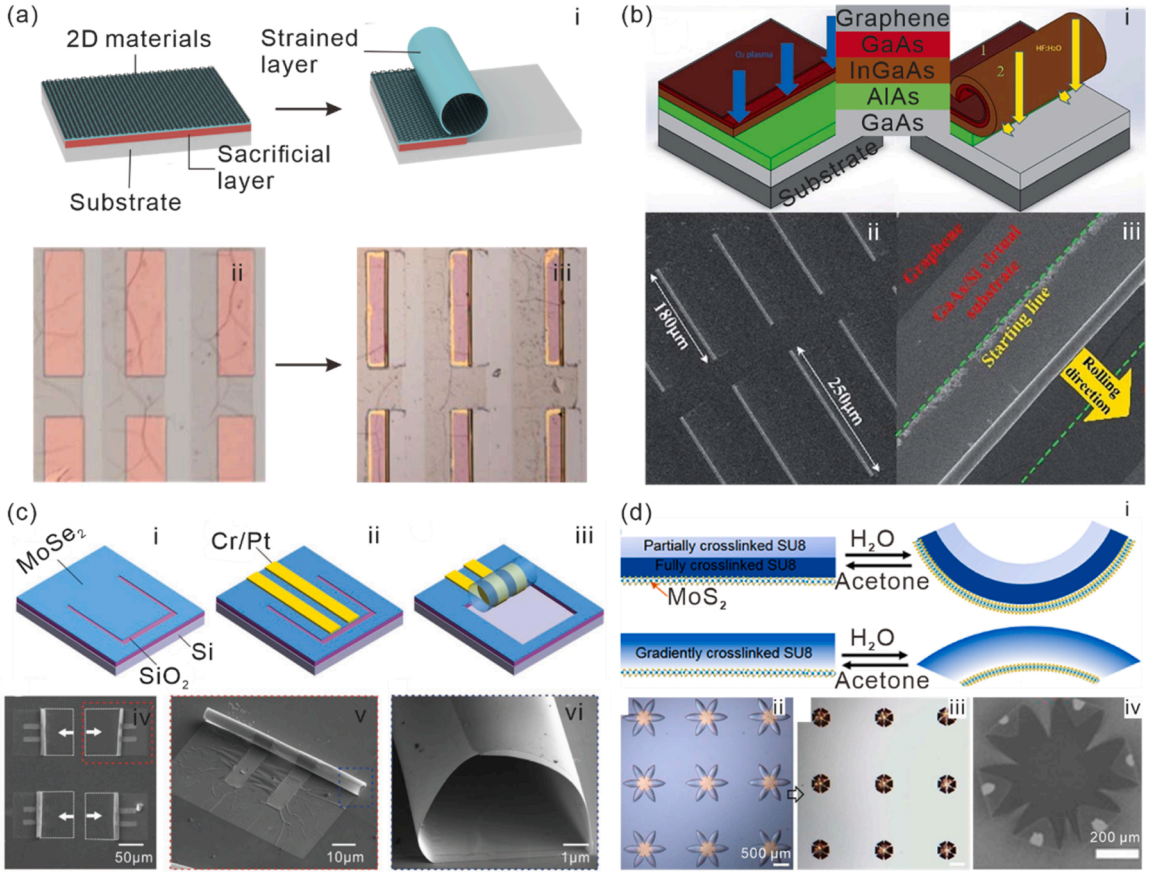

Fig. 5. Residual stress and responsive stress. (a) (i) Schematic illustration of the fabrication process of rolled-up 2D materials by strain gradient. Optical microscopy images of rolled-up tubes (ii) before and (iii) after releasing from the substrate [83]. (b) (i) Rolling process and mechanism of graphene driven by strain gradient in heteroepitaxial InGaAs/GaAs bilayers [83]. (ii) SEM image of the rolled-up InGaAs/GaAs/graphene microtubes array. (iii) SEM image of a InGaAs/GaAs/graphene microtube with the exposed starting mesas guiding the rolling direction. (c) Rolled-up $MoSe_2$ triggered by prestrained Cr/Pt layer [10]. (i–iii) Schematic illustration of the rolling process of $MoSe_2$. (iv–vi) SEM images of $MoSe_2$ tubes array, a single tube and the side view of the opening tube. (d) The reversible MoS_2 origami leveraging different swell properties of the responsive polymer layer (SU8) [14]. (i) Two approaches to form the SU8 strained layers for the reversible MoS_2 origami in the different solvent. Optical microscopy images of flower-shaped 2D patterns on the MoS_2/SU8 bilayer (ii) before and (iii) after folding, (iv) corresponding SEM image of flower-shaped 3D sturctures formed by folding.

materials can lead to the generation of stress [81,82]. However, the thin nature and weak vdW interactions between layers in 2D materials make it very difficult to directly generate enough strain gradient for providing driving force. As a result, a strained layer is needed to be combined with the targeted 2D material to introduce pre-defined strain. The pre-defined strain can then be released to guide the transformation of 2D materials from planar shape to 3D structure. The specific driving force can be the residual stress existing in the strained layer or the responsive stress generated by the response of active materials to the external stimuli.

As shown schematically in Fig. 5a(i), a strained layer is employed to provide driving force to roll up a 2D material into the tube after the sacrificial layer is released, which is also shown in optical microscopy images (before release, Fig. 5a(ii); after rolling, Fig. 5a(iii)). In such experiments, 2D materials is usually transferred onto a strained heteroepitaxial bilayer (e.g. InGaAs/GaAs). The heteroepitaxial crystalline bilayer experiences an internal strain gradient as it tries to accommodate the lattice mismatch between the two layers. Transferring a 2D material onto the strained bilayer thus creates a pre-strained multilayer system with considerable mechanical strength. As shown in Fig. 5b, a CVD monolayer of graphene was successfully rolled up along with the heteroepitaxial InGaAs/GaAs bilayer to form a iii–v semiconductor/graphene microtube after the sacrificial layer (AlAs) was etched [83].

A multistep photolithography scheme should be used in actual fabrication processes to assist in the production of the required arrays and expose the mesas which provides the critical etching front for rolling up the 2D material when the strain is relaxed. For example, when a GaAs layer was epitaxially grown on an $In_{0.2}Ga_{0.8}As$ layer, the upper layer (GaAs) with smaller lattice constant became stretched to accommodate the lattice mismatch [83]. On the other hand, the lower layer (InGaAs) became compressively strained. The selective etching of the sacrificial layer in such a heteroepitaxial crystalline bilayer system could be used to trigger the strain relaxation, which caused the top layer (GaAs) to shrink and the bottom layer (InGaAs) to expand. The consequent opposite movement induced a bending moment which drove the rolling up of the InGaAs/GaAs bilayers, along with the graphene layer on the upper surface. The rolled-up process introduced the uniaxial tensile stress in the rolled monolayer graphene. Therefore, this approach can be used to regulate the strain in the rolled-up graphene by varying the diameter of the microtube formed. In an earlier experiment, a strain-free rolled-up CVD graphene monolayer was produced on an InGaAs/Cr bilayer with a homogeneous radius of curvature [84]. In this case, the in-plane lattice parameter of polycrystalline Cr was almost equal to that of the GaAs. Therefore, the strain gradient generated at the InGaAs/Cr interface was similar to that in an InGaAs/GaAs bilayer and produced corresponding driving force.

Pre-strained layers deposited nonepitaxially on target nanomembranes can also actuate the assembly process. As shown in Fig. 5c, arrays of rolled-up $MoSe_2$ microtubes were successfully fabricated through the self-rolling of a strained layer of Cr/Pt deposited by e-beam evaporation [10]. $MoSe_2$ nanomembranes were firstly deposited on the SiO_2/Si substrate by high-vacuum co-evaporation. Then, the 'windows' were patterned onto the $MoSe_2$ nanomembranes for the rolling process via photolithography and reactive ion etching. The next step was to define the deposition area of the Cr/Pt strained layer, which also served as electrodes. Upon the selective etching of the sacrificial layer (SiO_2), the strain gradient in the strained layer was sufficient to drive the rolling of the $MoSe_2$ nanomembranes and formed microtubes, as observed by scanning electron microscope (SEM) in Fig. 5c(iv–vi). The core competitiveness in this example is the ability to control the key parameters involved in the deposition of the strained layer so that the strain gradient can be modified to control the geometry of the 3D product. The strain gradient in the strained layers can be controlled by varying the growth rate, thus producing different levels of driving force. The thickness of the strained layer is another key factor. For instance, there is a critical thickness that determines whether the strain gradient is sufficient to activate the assembly process. It also controls the winding numbers and diameters of the tubes produced. It should be noted that although it is convenient to be able to control driving force via the growth rate used to deposit the strained layer, the actual growth rate employed should be chosen cautiously to ensure that no damage is caused to 2D materials.

Physical or chemical reactions in suitably active materials may produce the internal stress responsive to a stimulus, which allows smart or reversible origami-like assembly processes to shape 2D materials [29]. In other words, an external stimulus (e.g. temperature change, application of light, contact with certain liquids, etc.) is able to change the responsive stress between the interlayers of a multilayer structure, thus behaving as a driving force for responsive deformation. As a result, the formation of the predetermined 3D architecture can be triggered by changing the environmental conditions. For example, it was shown that swelling stress could be induced between bilayers of graphene and graphene oxide (GO) with different swelling properties [18]. Upon light illumination or heating, the active layer that swelled due to the adsorption of water would shrink as it lost water. This generated a strain gradient relative to the other layer which resulted in self-folding.

Note that light/heat-induced humidity responses, like the one mentioned above, tend to be very sensitive and rapid, which means that the corresponding device will have a high sensitivity and response speed. It has been shown that the integration of graphene with shape-morphing active materials like stimulus-responsive polymers can realize the reversible transformation between the original 2D configuration and the desired 3D structure in response to a solvent [85] or temperature [86].

Fig. 5d shows mesostructures fabricated from a differentially photo-crosslinked photoresponsive polymer material (SU8) and MoS_2 [14]. The reconfigurable mesostructures were fabricated through the reversible swelling and shrinking of the SU8 in response to the solvent. The schematic illustration in Fig. 5d(i) presents two different layer configurations for realizing self-folding. The first one has a bilayer configuration consisting of two crosslinked SU8 layers, one is partially crosslinked and the other is fully crosslinked. The second configuration has a single layer of crosslinked SU8 wherein the extent of the crosslinking follows a gradient (fabricated via exposure to a low dose of UV so that the UV intensity decays exponentially as it penetrates the SU8). The integration of active materials is becoming a more favorable approach to shaping and structuring 2D materials because of its intelligent nature, controllability, and reversibility. In particular, it is an inspirational approach to 4D printing and creating smart devices.

3.2. Capillary forces

Capillary forces arise due to surface tension which originates from the tendency of a liquid to shrink for the minimized surface energy. These forces can be used to shape thin materials with small dimensions and this approach is becoming a major driving force in the field.

When a liquid droplet makes contact with the surface of a thin film, the capillary force acting at the interface is prone to induce the wrapping of the thin film around the droplet. Another form is the metal 'hinges' that can be melted to produce a liquid 'solder' whose surface tension causes the folding of two adjacent panels. Capillary origami was realized as early as 2007 [87]. In that work, the authors used droplets of water to cause the self-wrapping of polydimethylsiloxane (PDMS) sheets, tuning the initial sheet pattern to generate various encapsulated designs. It was later predicted theoretically (in 2009) that graphene nanostructures could also be activated and guided to fold up using nanodroplets [88]. In this case, molecular dynamics simulations were used to demonstrate that the nanodroplets could help the planar graphene sheets to overcome deformation barriers, resulting in conformal folding according to the sites where the nanodroplets were deposited.

Due to the relatively considerable size of capillary forces on the micro/nanoscales, capillary origami can be adopted as a universal approach to shaping and structuring 2D materials. It can therefore play a

very important role in self-assembly over a wide range of sizes/applications. Fig. 6a shows schematically how the self-folding of 2D materials can be triggered by capillary forces in the liquid phase and used to construct 3D structures by appropriately designing hinges and rigid panels. The pioneering application of capillary-force manipulation to graphene resulted in the formation of high-quality carbon nanoscrolls [89]. In this experiment, nanoscrolls were fabricated with assistance of a solution of isopropyl alcohol. Fig. 6b shows the results of self-scrolling of transition metal dichalcogenides (TMDs), where (i) shows the TMDs before droplet intercalation, and (ii) shows the scrolls produced after self-scrolling [90]. It was apparent that the applied liquid droplets permeated into interface from the edge of 2D materials thus creating a 'no-adhesion' area, where the delamination process was initiated and the capillary force facilitated the ensuing rolling-up process. Due to the capillary forces from the droplets, the spontaneously-delaminated 2D material experienced bending moments and started to undergo self-scrolling. However, it needs to be emphasized that although this kind of scrolling is a simple approach to producing high-quality nanoscrolls with high yields, it is not controllable (in terms of rolling direction and geometries) unless the liquid flow is well guided.

Self-wrapping behavior can, nevertheless, inspire the shaping of 2D materials around the liquid phase in a more controllable way. For example, driven by the capillary force, graphene could be induced to wrap itself around water to form multiwall nanoscrolls with the water encapsulated within the nanochannel [91]. Moreover, as shown in Fig. 6c, atomically thin MoS_2 sheets could be folded into 3D shapes using a micropipette with a droplet of liquid (driven by the competition between surface energy and bending energy) [92]. The bending stiffness of the MoS_2 sheets was found to be such small that the capillary force from the droplet was sufficient to make folds on a length scale of about 10–100 nm. Depending on the design of the 2D pattern, more complex 3D architectures could be fabricated using a combination of rigid metal panels and flexible MoS_2 hinges. Meanwhile, parallel folding of MoS_2 sheets was realized by adding chloroform emulsions to deionized water containing the patterned MoS_2 sheets instead of using a micropipette. The self-wrapping approach makes a further step in the development of capillary origami. Therefore, shaping and structuring 2D materials by droplets is convenient in spite of its relatively weak controllability. It is also a very promising technique when applied to massive self-assembly. However, these kinds of wet assembly processes are limited as their application is confined to the liquid environment and the advanced drying techniques (e.g. critical point drying) will be required for the subsequent structural stabilization.

When the meltable solder used to create 'hinges' experiences a phase transformation, the surface tension produced can induce the self-folding to complete the formation of an entire closed structure. As illustrated in Fig. 6d, the self-assembly of a 3D graphene structure was realized by applying hinges to certain parts of the 2D graphene net according to a pre-designed pattern. Then, the self-assembly could be triggered when the hinges became molten [93]. The hinges were poly(methyl methacrylate) (PMMA) and the panels were Al_2O_3, respectively. The net of monolayer graphene was used to guide the folding of the panels into the final polyhedron arrangement according to the surface tension generated by the molten PMMA. Fig. 6d(i) shows a schematic illustration of the components before self-assembly and corresponding SEM image. Fig. 6d(ii) shows the 3D configuration after self-assembly. These kinds of hollow and closed polyhedrons integrated with graphene can be easily designed by customizing the 2D pattern. Meanwhile, these polyhedrons can be further utilized for potential optical applications.

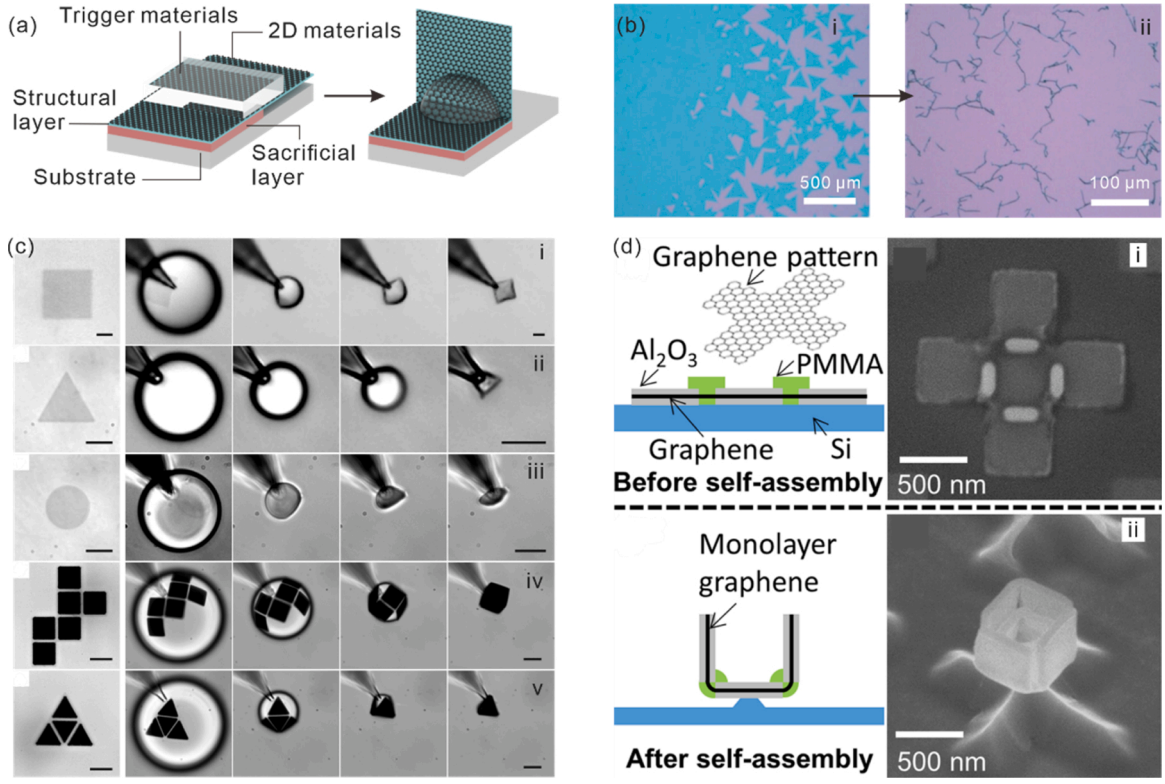

Fig. 6. Capillary forces. (a) Schematic illustration of the fabrication process of 2D materials folding by capillary force. (b) Optical image of (i) monolayer MoS_2 flakes and (ii) MoS_2 nanoscrolls rolled by capillary force from the drop of ethanol on SiO_2/Si substrate [90]. (c) The sequential images of the capillary origami of monolayer MoS_2 by the droplet with different patterns of (i–iii) individual shapes and (iv–v) shape nets. The leftmost figure in each row shows the initial 2D precursors and the following figures are shown in time series, all scale bars are 20 μm [92]. (d) Schematic illustrations and their corresponding SEM images of 3D graphene-based polyhedrons fabricated via capillary force from the molten polymer hinges (i) before and (ii) after self-assembly [93].

3.3. Van der Waals forces

Although van der Waals (vdW) interactions are relatively weak compared with ionic or covalent bonds, they constitute a kind of fundamental force that dominates many properties of nanomaterials. As they play a significant role in the exfoliation and transformation of 2D materials, vdW forces can be used as an effective tool to assist the shaping and structuring of 2D materials in a natural way.

It was shown in some early theoretical studies involving molecular dynamics simulations that vdW forces could be strong enough to form carbon nanoscrolls by scrolling planar graphene sheets around a core template structure such as a carbon nanotube, silicon nanowire, or platinum nanocluster [94–96]. The vdW force between the core and the nanoribbon could induce the nearby area to undergo self-wrapping and the hybrid system gradually developed into rolling to create the nanoscroll shell. In both cases, as vdW forces were strongly distance-dependent, the diameter of the central part had to exceed a certain critical value. Otherwise, the corresponding vdW force would be insufficient to activate the self-scrolling and form a stable core/shell structure.

It has also been found that the enhanced aggregation between decorated particles is another way in which vdW forces can contribute to the fabrication of nanoscrolls. For example, it was shown that graphene oxide (GO) sheets with nanoparticles such as Ag and Fe_3O_4 attached could be rolled up into nanoscrolls in a controllable way [97]. In this case, it was energetically favorable for the adjacent nanoparticles to approach to each other due to the vdW forces. In addition, nanosheets rolled up on a tubular substrate via a layer-by-layer assembly method was demonstrated [98]. In this method, free-standing nanofilms (e.g. graphene) on the surface of water were brought into contact with a tubular substrate. The rotation of the substrate could enhance the vdW force at the substrate–nanofilm interface, thus driving the rolling-up process as the nanofilm moved away from the water.

A micromanipulator or microscope tip can also utilize the vdW forces to guide the deformation of 2D materials (folding or unfolding, etc.) in a more precise manner, as shown schematically in Fig. 7a. A real example of the nano-origami of graphene is presented in Fig. 7b [32]. In this method, graphene nanoislands (GNIs) were controllably and reversibly folded and unfolded on a highly-ordered pyrolytic graphite (HOPG) substrate using the tip of a scanning tunneling microscope (STM). The manipulation process involved the following steps: (1) working at low temperature (4.2 K), the tunneling resistance in the STM junction was firstly reduced to make the STM tip approach the GNI, (2) the edge of the GNI was then lifted and moved along a predesigned direction, and (3) the lifted part was finally lowered to construct a folded nanoisland (i.e. with 2D stacked bilayer and 1D tubular edge). The non-destructive nature of the manipulation process was demonstrated by recording STM images before and after repeated folding and unfolding along different directions (Fig. 7c). It was clear from the high-resolution images recorded that the atomic structure presented in the initial state was preserved in the final state. Unlike previous efforts to fold graphene using the microscope tip [99–103], this method can choose an atomically-precise folding direction and be operated in a non-destructive way. Furthermore, this STM origami applied on a

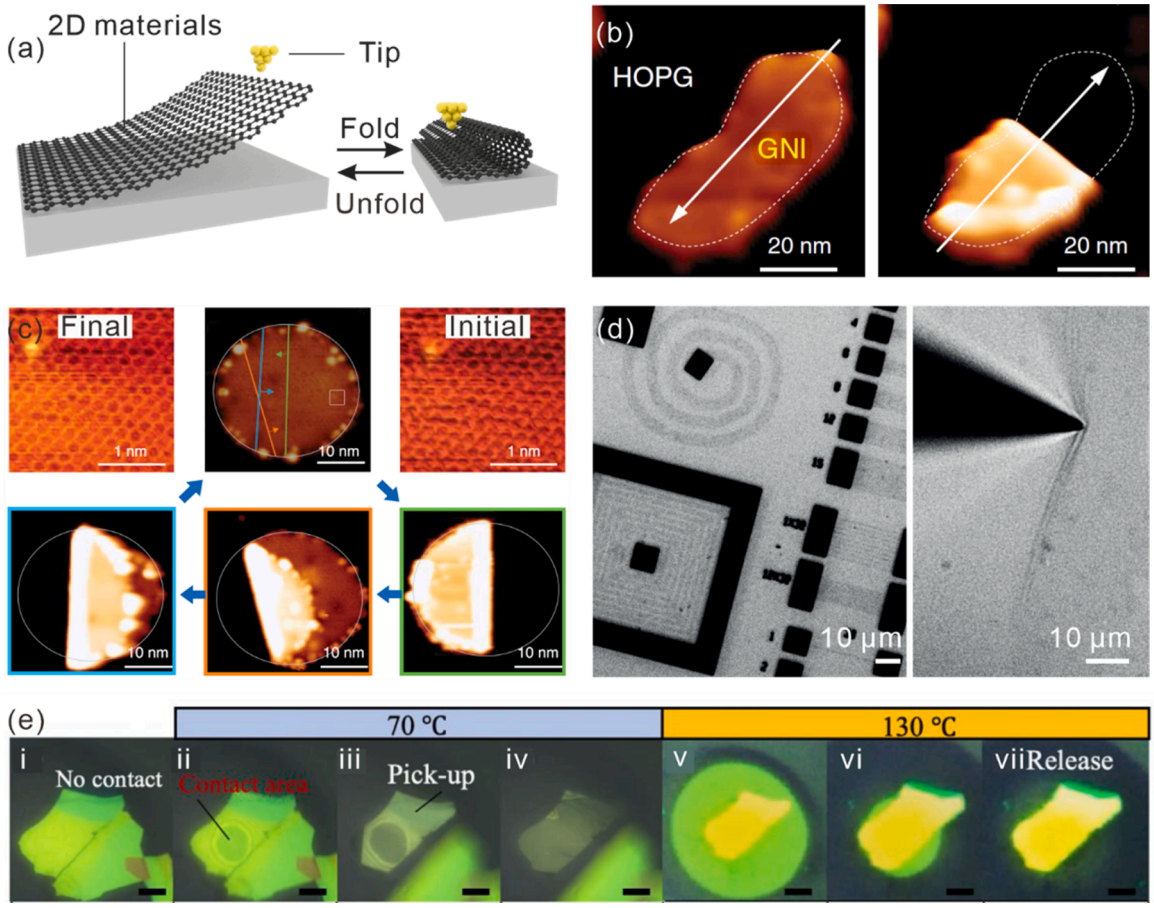

Fig. 7. Van der Waals forces. (a) Schematic illustration of the fabrication process of 2D materials folding and unfolding by tips utilizing vdW force. (b) STM images of the folding and unfolding of a graphene nanoisland by tips moving along the direction indicated by the white arrows [32]. (c) STM images showing repeatable folding and unfolding of a graphene nanoisland along different controlled directions by STM origami [32]. (d) Transmission white-light images of patterned graphene and crumpling a large sheet of graphene through a micromanipulator [13]. (e) Optical micrographs of the pick-up and subsequent release process of 2D materials using PVC-microdome polymer (MDP), all scale bars are 10 μm [104].

nanoscale can realize the in-situ characterization of the nanostructures for quantum investigation purposes, thus exhibiting an unprecedented potential to produce desired nanostructures with novel properties stemming from 2D materials.

On the microscale, vdW forces between the micromanipulator and 2D materials can work as an effective driving force as well. For example, Fig. 7d shows that a polycrystalline monolayer of graphene could be folded and crumpled by a probe tip like ultrathin paper [13]. Recently, a series of 3D manipulations of 2D materials (folding, sliding, rotating, etc.) was performed using a microdome polymer (MDP) as the point-contact manipulator (a technique that is similar to the dry transfer technique commonly used for the fabrication of vdW heterostructures) [104]. Firstly, a layer of poly(vinyl chloride) (PVC) was coated onto the polydimethylsiloxane (PDMS)-MDP to create a strong force of adhesion between the MDP and 2D materials. The strong adhesion enabled 2D materials to be manipulated in spite of the limited contact area between them and the microdome. Furthermore, the adhesive force was temperature-dependent, and the corresponding contact location and area could be controlled, so the lateral and more complex manipulations became feasible to realize different purposes. In detail, the PVC-coated MDP could contact a flake of 2D material and picked it up at 70 °C as the adhesive force was strong at this temperature. Then, the flake was placed on a heated substrate at 130 °C to accomplish the release process of the flake as the adhesive force was weak at the elevated temperature (Fig. 7e). The lifting and releasing of the edges of flakes could be accomplished following the above process, thus allowing folded structures to be obtained. The partial contact in the above case could also reduce the pick-up area to facilitate tearing. The MDP-based method is quite useful for the construction of vdW heterostructures, and it may aid in the application of vdW forces in term of building 3D microstructures from 2D materials.

3.4. External mechanical stresses

In this context, 'external mechanical stress' refers to a stress caused by the release of a pre-stretched elastomeric substrate with bonding constraints. Rogers and his coworkers have utilized such external mechanical stress to achieve 3D shaping of 2D micro/nanostructures, proposing the well-known mechanically-guided assembly method called 'compressive buckling' [105–108].

As shown schematically in Fig. 8a, the 2D precursor is firstly patterned onto a sacrificial layer which is then transferred to a pre-stretched elastomeric substrate and selectively bonded. When this strain is released, compressive stresses are induced at the bonding sites and cause the non-bonded regions of the 2D layer to 'pop-up'. The resulting out-of-plane deformation thus forms the desired 3D structure. Mechanical buckling can be used to drive the 3D assembly of various advanced materials across a broad range of length scales, facilitating the fabrication of sophisticated 3D mesostructures inspired by kirigami/origami [106,107]. The pattern and thickness of the 2D precursor used are both tunable and can be precisely defined using modern planar technologies. Thus, different schemes can be designed to generate specific features, e.g. filaments, origami-based patterns with creases, and kirigami-based patterns with cuts [108]. Through the rational design of appropriate 2D precursors and selective bonding sites, a wide range of desired 3D structures can be constructed with specific configurations and strain distributions, consistent with those structures predicted using finite element analysis (FEA).

To date, the use of compressive buckling to shape and structure 2D materials remains challenging because pristine 2D materials hardly ever form stable free-standing structures. Consequently, the integration of the fundamental elements consisting of 2D materials (the use of an elastomeric substrate as an assembly platform and integrating 2D

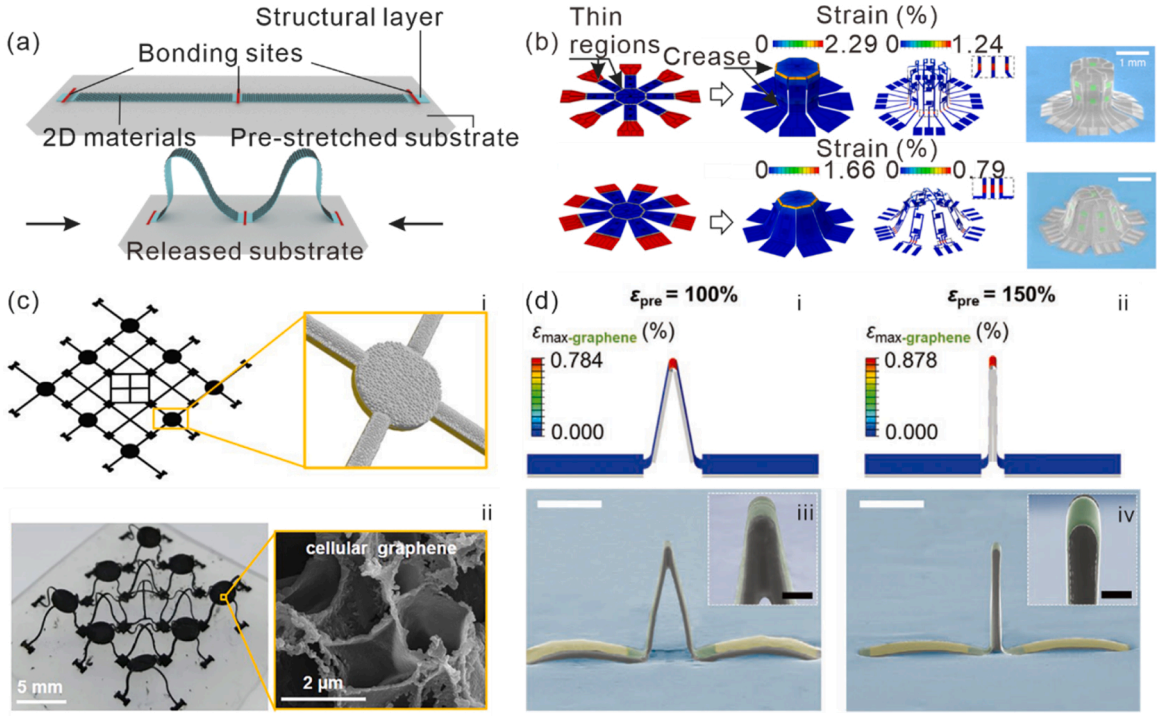

Fig. 8. External mechanical compressive stress. (a) Schematic illustration of fabrication process of 3D mesostructure by mechanical buckling of 2D materials. (b) Finite element analysis (FEA) results and colorized SEM images of the photodetector arrays based on graphene and MoS_2 in the 3D functional structures with shape of octagonal prism (upper) and octagonal prismoid (lower). The magnitude of the maximum principal strain is shown in the colorized configuration and materials are indicated as MoS_2 (green), graphene (light gray), and SU-8 (gray) [21]. Scale bars are 1 mm. (c) (i) Schematic illustration of the 2D precursor with the 'mixed table and tent' pattern in cellular graphene/PI bilayer. (ii) Optical image of 3D 'mixed tables and tents' consisted of cellular graphene after mechanical buckling, SEM image of laser-induced cellular graphene [109]. (d) (i, ii) FEA results evaluating the maximum principal strain distributions and (iii, iv) corresponding SEM images of foldable 3D microstructures using graphene hinges [12]. Scale bar, 20 μm in white color, and 3 μm in black color. (For interpretation of the references to colour in this figure legend, the reader is referred to the web version of this article).

materials with another thin-film material to act as a bottom structural layer for support, or by adopting a 2D material-based composite material) has become the most feasible approach. As observed in Fig. 8b, the 3D shapes of an octagonal prism (upper) and an octagonal prismoid (lower) were fabricated by compressive buckling [21]. The assembly process started with the sequential patterning of a negative photoresist (e.g. SU8), graphene, and MoS_2 on the SiO_2 sacrificial layer. Thin regions were defined in the SU8 layer to act as 'creases' for the subsequent assembly process. After the etching of the sacrificial layer and the subsequent transfer printing, the polymer with graphene and MoS_2 were transferred onto the pre-stretched elastomer. To accomplish selective bonding, the photoresist was selectively exposed to UV-induced ozone, which resulted in the exposed SU8 regions being strongly bonded to the elastomeric substrate. As the pre-strain in the elastomer was released, buckled 3D structures were formed from the 2D pattern designed. The fabricated 3D structures in the colorized SEM images are in good agreement with the FEA results while it is clear that the induced creases follow the thin regions predefined in the 2D patterns.

As shown in Fig. 8c, patterns fabricated on 2D polyimide (PI) via laser treatment were reported to be transformed to complicated 3D cellular graphene structures driven by external mechanical compressive stress [109]. In this case, a so-called 'mixed table and tent' pattern in the bilayer of cellular graphene and PI was prepared using the CO_2 laser illumination of the pre-patterned PI layer. Following the usual process of compressive buckling after strain release, the compressive stresses exerted at the covalent siloxane bonding sites triggered the formation of the final 3D hierarchical structure.

The above examples are based on 2D materials with a continuous supporting layer. In the following case, however, the structural layer can be thinned so that 2D materials work as the hinges (in the thin regions) while the more rigid parts of the layer (in the thick regions) provide the support. Recently, CVD-grown graphene was employed as hinges to complete the reversible assembly and recovery of foldable 3D microstructures based on a deterministic buckling process [12]. The traditional compressive buckling strategy was followed but the supporting (SU8) layer was thinned at the designated hinge segments to reduce the bending rigidity. At these locations, graphene experienced bending to form the pop-up structure. Fig. 8d presents SEM images of the buckling geometries produced by different pre-strain levels. It is shown that the corresponding strain distributions in the graphene can be maintained within an appropriate range. Thanks to the control over the thickness of the hinge area and pre-strain level, programmed 3D microstructures can be constructed from a diverse range of 2D precursors using this method. It would be very valuable if the technique can be expanded to make high-strength hinges in other 2D materials.

3.5. Other driving forces

There are many other kinds of driving forces that can be used to shape and structure 2D materials. This means that the manipulation methods available are likely to be enriched constantly as specific applications are developed. Some typical examples are outlined below. The supplementary methods introduced are intended to reveal the feasibility of an extensive range of possible strategies and indicate some potential directions for further development.

Surface adsorption is a very important feature of 2D materials as it allows the properties of the material to be modified via physical interaction or chemical bonding. 'Decorating' the surface by the adsorption of nanoparticles may bring the functionalization of exotic properties and actuate the reshaping of 2D materials through the mutual interactions that occur between the nanoparticles. In addition to vdW-driven aggregation, reshaping processes can be triggered by other properties of the adsorbed nanoparticles, e.g. magnetic properties. Sharifi et al. demonstrated that nanoscrolls could be fabricated from sheets of nitrogen-doped reduced graphene oxide (N-rGO) via the adsorption of magnetic γ-Fe_2O_3 nanoparticles at the nitrogen defects [110]. Furthermore, the synthesis was highly efficient and could be reversed by removing the magnetic nanoparticles. The rolling up of the homogenous N-rGO nanoscrolls (Fig. 9a(i)) was initiated by the magnetic interaction between the γ-Fe_2O_3 nanoparticles strongly adsorbed at the nitrogen defects, as shown in Fig. 9a(ii). Density functional theory was used to elucidate the most energetically favorable configuration for the iron oxide clusters adsorbed by the N-rGO sheets (Fig. 9a(iii)), and it was proven that the nitrogen defects were crucial to stabilize the adsorption process. Fig. 9a(iv) depicts in a step-by-step manner how the rolling process occurred based on an analysis of the rolling energy at each step (bottom to top). Rolling was initiated by the attraction between the adsorbed γ-Fe_2O_3 nanoparticles which lowered the energy barrier for preventing scroll formation. As two adjacent nanoparticles were approaching, there was a further decrease in the rolling energy due to the enhanced spin–spin interaction between them. Finally, the rolled N-rGO sheet could form new bonds with the nanoparticles as the physical contact was formed at the flat end, which further decreased the rolling energy.

As 2D materials are highly flexible, out-of-plane deformation can be induced by the surface stress created by the adsorption of gas molecules. Naturally, the magnitude of this stress increases with the degree of adsorbate coverage. For example, it has been found that the selective atomic adsorption of hydrogen and fluorine can cause graphene nanoribbons to bend and be converted into carbon nanotubes simply by controlling the adsorbate coverage [111]. Taking hydrogen adsorption as an example, it is apparent that the adsorption of a hydrogen (H) atom at a particular carbon (C) atom in graphene will generate an sp^3 hybridized C—H bond at that site. Accordingly, the corresponding three neighboring C atoms with their initially planar sp^2 C—C bonds will be repelled, leading to an out-of-plane tension and hence bending moment.

Zhu and Li simulated the folding of graphene induced by single-sided hydrogenation along certain lines of the graphene structure [112]. They also demonstrated that the folding angle could be well-regulated by the extent of the hydrogenation and the number of lines used, as shown in Fig. 9b(i). This so-called 'hydrogenation-assisted graphene origami' has become well known because it opens up the possibility of programmable graphene nanocage assembly for molecular mass uptake, storage, and delivery, as shown in Fig. 9b(ii). Based on a similar theoretical mechanism, experiments involving the electrostatic deposition of graphene in a selective gaseous environment further verified the possibility of rolling up graphene through hydrogen and nitrogen adsorption [113].

A shear force is always a powerful tool for accomplishing the exfoliation and scrolling of layered materials. For example, graphene nanoscrolls have been fabricated through friction and wear via the sliding of diamond-like carbon (DLC) balls [114]. Fig. 9c shows another example wherein graphite and h-BN flakes were successfully exfoliated and rolled into nanoscrolls using a shear force [115]. In this case, a rapidly rotating spinning disc was used to apply a shear force which firstly exfoliated multilayers and then further scrolled the flakes. There was a competition between the surface energy and bending energy and the increment of scroll yield could be obtained when a higher spinning rate was utilized over an extended period of time.

Ultrasonication is often a necessary step in the fabrication of nanoscrolls by the chemical process, as the ultrasonic energy applied to 2D materials can initiate the scrolling [116–118]. For example, as depicted in Fig. 9d, high energy ultrasonication could rapidly work to exfoliate graphite via alkali intercalation, thus forming carbon nanoscrolls [116]. It was found that a very good conversion rate (over 80 %) could be obtained by optimizing the sonication time.

Many different driving forces including internal stresses or external forces have been extensively utilized for shaping and structuring various 2D materials. However, most studies are only conducted in laboratories to circumvent the problems associated with controllability, scalability, and efficiency. Meanwhile, the versatile driving forces that are anticipated to guide the massive and facile fabrication of shaped and structured 2D materials are still in their primary stages of exploration. This

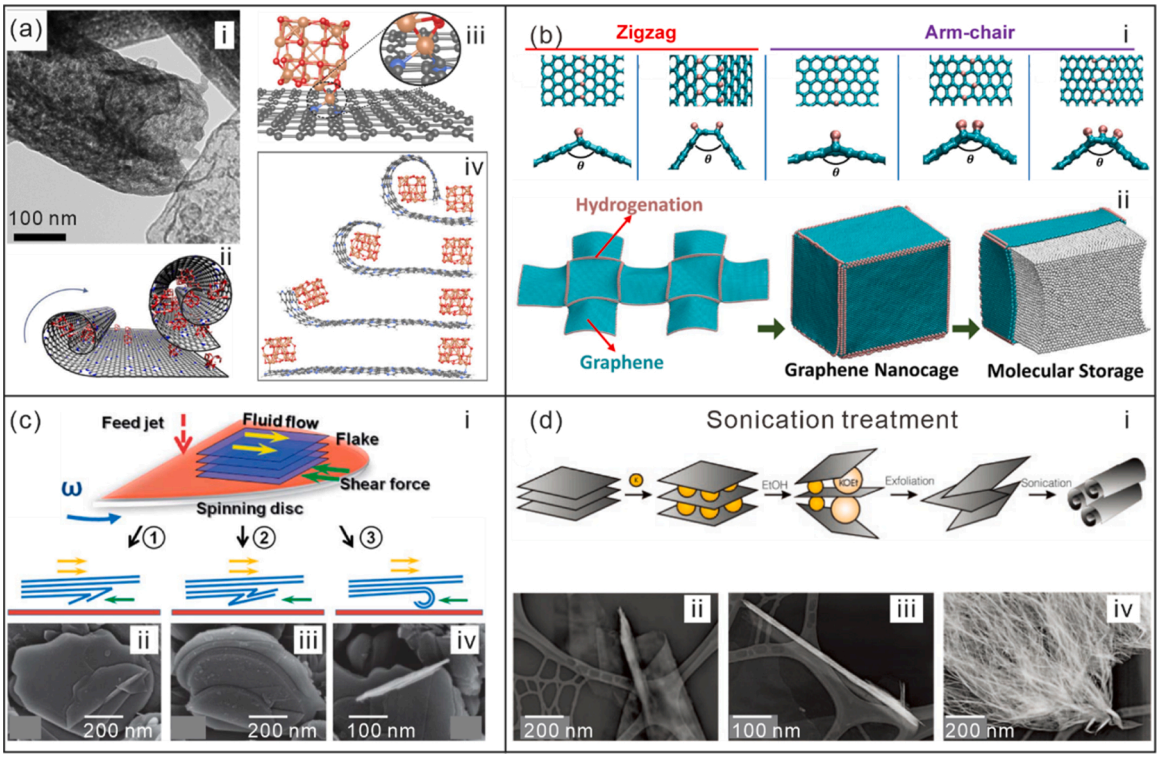

Fig. 9. Other driving forces. (a) Nitrogen-doped graphene nanoscrolls by adsorption of magnetic γ-Fe_2O_3 nanoparticles [110]. (i) Transmission electron microscopy (TEM) image of nitrogen-doped graphene nanoscrolls. (ii) Schematic illustration of the rolled-up process. (iii) Simulated stable configuration of an iron oxide cluster at the nitrogen defects. (iv) Simulated geometrical structure of nitrogen-doped graphene nanoscrolls at each rolling step. (b) (i) Self-folding of hydrogenated graphene by molecular dynamics simulations. (ii) Graphene nanocage with controllable opening and closing enabled by hydrogenation-assisted graphene origami. Reprinted from [112]. (c) (i) Schematic illustrations and (ii–iv) SEM images of boron nitride nanoscrolls formed by shear force [115]. (d) (i) Schematic illustration and (ii–iv) SEM images of carbon nanoscrolls formed with the assistance of sonication treatment [116].

can be continuously updated by exploiting other promising sources of driving forces, e.g. electrostatic forces [119] and applied magnetic fields [120].

4. Shaping and structuring schemes

In the previous section, driving forces that guide the shaping and structuring of 2D materials have been reviewed in some detail. Using the procedures outlined, a diverse range of geometries and 3D functional structures encompassing 2D materials can be realized via various shape transformations. According to the individual deformation characteristics, the basic elements of 2D materials kirigami and origami can be organized as folding, rolling, wrinkling and buckling. These shaping strategies can transform 2D materials into the simple 3D structures and facilitate more sophisticated kirigami and origami schemes using patterned 2D materials.

Each individual shaping strategy involves a particular principle, which dictates the corresponding strategic design of the 2D precursors and resultant reconfiguration schemes. The specific geometric parameters and structural properties of the reshaped 2D materials (which play a critical role in determining the suitability of the final device for further application) can be well-controlled by delicately regulating the implementation process of these shaping strategies. In this section, we introduce the recent advances made in the shaping and structuring schemes of 2D materials. We discuss the controllability of the various strategies and assess the extent to which they are developed. In recognition of the state-of-the-art nature of these shaping and structuring schemes, both research opportunities and challenges can be identified in them. As these are circumvented and exploited, innovative advances are expected to achieve in the future.

4.1. Basic out-of-plane strategies

Folding is the most basic operation in shaping 3D structures. Similarly, localized bending mechanisms can be adopted that flip paper-like nanomembranes over to form folds at especially-creased regions. Moreover, folding can fabricate the complicated origami-like mesostructures based on an elaborate arrangement of creases, or a combination of bendable hinges and rigid panels. Here, folding itself, which seems to be the simplest shaping manipulation possible with 2D materials, is focused upon to highlight the actual structural complexity and tunability of folding 2D materials.

As shown schematically in Fig. 10a(i), the folded structure of a 2D material is composed of the stacked planar layers and a folded edge. The stacking orientation of the planar layers varies with the folding angle. The atomic structure in the localized bending region is unexpectedly complex, especially in multilayer materials. Rooney et al. have recently investigated the atomic bending mechanism by characterizing the twin boundaries in the localized bending region of multilayer 2D materials [121]. Fig. 10a(ii) shows two different bending modes found: discrete twin boundaries (in orange) and nanotube-like curvature (in green). It is found that these modes are often mixed together.

Many novel physical phenomena may exist in folded 2D materials due to the folded configuration and strain engineered. For example, a zero Landau level [122], gauge fields [123], and a strong magnet ophotoelectric effect [124] have all been observed in folded graphene. It is even more fascinating that the presence of a twist angle between stacked layers of 2D materials provides an additional degree of freedom, which has opened up a vast area of researches named as ‘twistronics’ [125–128]. As the twist angle changes, the electrical properties of the folded 2D materials change accordingly. This has caused new research booms and has resulted in the groundbreaking finding of correlated

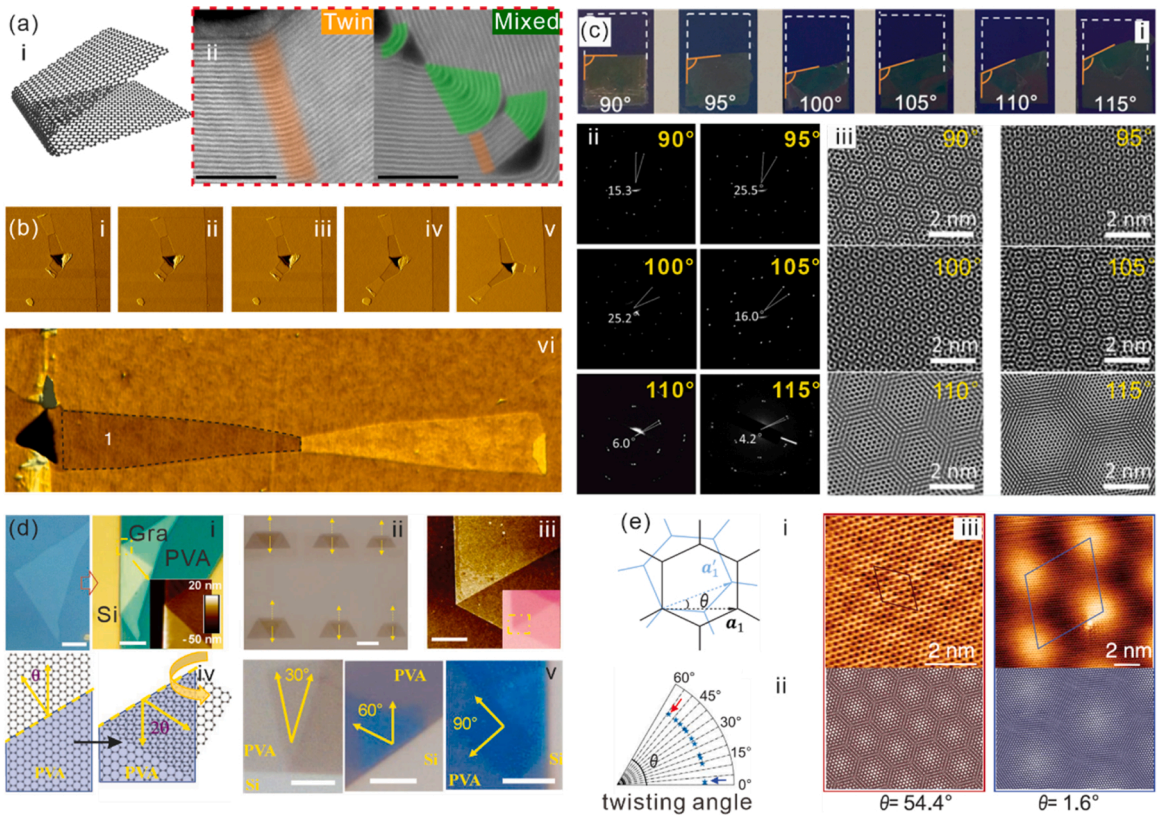

Fig. 10. Folding shaping strategy. (a) (i) Schematic illustration and (ii) High-angle annular dark field-scanning transmission electron microscopy (HAADF-STEM) images of different bending modes in the fold of multilayer graphene [121]. All scale bars are 5 nm. (b) (i–v) Sequential AFM images of the room temperature growth process of three ribbons nucleated from single fretted nanoindentation contact, and (vi) simultaneous growth of a ribbon in bilayer graphene with a certain starting width [9]. (c) Controlled folding of single crystal monolayer graphene with an established correlation between controlled folding direction and stacking orientation. (i) Optical images show a series of folded graphene with indicated folding angles. (ii) The selected area electron diffraction (SAED) patterns and (iii) Moiré patterns of these folded graphene samples show the stacking orientation corresponding to the different folding angles [145]. (d) Fluidic flow assisted deterministic folding of vdW materials [146]. (i) A graphene flake before and after folding, (ii) folded arrays with consistent directions, and (iii) a sharp folded interface. (iv) Schematic illustration of the correlation between folding and twist angles. (v) Optical microscopy images of graphene flakes with different folding angles and indicated twist angles. All scale bars are 5 μm. (e) Atomically precise control of graphene nano-origami twisting angle by STM tip [32]. (i, ii) Schematic illustrations show the relationship between the folding direction and twisting angle, as well as the precise control of twisting angles with tunable range. (iii) STM images and corresponding models show moiré patterns of two exemplary folded graphene with 54.4° and 1.6°, indicated as the red and blue arrow in (ii).(For interpretation of the references to colour in this figure legend, the reader is referred to the web version of this article).

insulator behavior [129] and unconventional superconductivity [130] in magic-angle twisted bilayer graphene.

In particular, 'twisted graphene bilayers' has become one of the hottest research topics, inspiring significant progress in frontier physics involving electron-correlation behavior and quantum physics [131–138]. Furthermore, twistronics investigations have been extended to other 2D materials including topological excitons in twisted TMD heterostructures [139–142], interlayer magnetism [143], and photonic magic-angles in twisted α-MoO_3 bilayers [144]. These significant achievements are stimulating the exploration of controllable approaches for constructing twisted superlattices of 2D materials. Meanwhile, as the precision of the folding process can be controlled and improved continually compared to other approaches, folded 2D materials may provide an ideal platform for twistronics research.

As the most classical 2D materials and 'superstar' in twistronics, graphene has been the widely studied 2D material in the context of controlled folding. Initially, the folding of graphene is something routinely observed in studies involving AFM characterization. Graphene often spontaneously undergoes self-folding but the folding geometry in the absence of human intervention is unintentional and lacks controllability. Fig. 10b shows an example of the self-peeling and folding of graphene ribbons caused by thermal activation. It was observed that the peeled layers could gradually grow outwards from the nucleation location (images i–v), which corresponded to a nanoindentation or nanocrater [9]. The ultimate geometry of the growing ribbon was closely related to the starting width but the relevant observation was not sufficient to provide quantitative control in principle. In addition, the self-folding of graphene can also be induced by the multiple scans of the surface with an AFM tip [101], whereby graphene nanoribbons can be formed by applying suitable normal loads. It was found that the folding direction could be determined by setting the scan line. Self-folding was also found to occur along either 'zigzag' or 'armchair' directions in the vicinity of a nearby crack.

In order to achieve controlled folding and precise stacking, it is essential to define the folding direction and the stacking orientation in an appropriate way. Fig. 10c shows an example where single crystal monolayer graphene films were controllably folded along defined directions by the chemical modification of the underlying substrate [145]. The SiO_2/Si substrate was pretreated using photolithography and surface modification to create a surface consisting of both hydrophobic and hydrophilic areas separated by a well-defined boundary. When graphene was transferred to the modified substrate and immersed in water, the part of the graphene in contact with the hydrophilic area detached from the surface and folded over onto the other part (still attached to the substrate) when the sample was slowly withdrawn from the water. By making a comparison of: (i) optical images of graphene folded along

different predefined lines, (ii) selected area electron diffraction (SAED) patterns, and (iii) moiré patterns, a relationship was successfully established between the folding and twisting angles. That is, every 10° change in twisting angle requires a 5° change in folding angle. In general, this technique is quite versatile to be utilized for controlling the folding of other 2D materials. However, resolution limitations and possibility of contamination occurring during the photolithography and modification processes remain problematic.

Recently, Zhao et al. proposed an innovative and universal deterministic folding strategy for 2D materials via microfluids [146], as shown in Fig. 10d. 2D materials was firstly transferred onto a SiO_2/Si substrate coated with a layer of polyvinyl alcohol (PVA). Then, electron beam lithography (EBL) was used to crosslink the PVA layer in exposed regions to make them insoluble in water. As EBL has a high resolution (< 100 nm), precisely defined edges could be created. The unexposed PVA regions were then dissolved in warm (50 °C) deionized water so that the parts of the upper 2D material became suspended in the fluid. The final step was to use the flow of deionized water to guide the detached 2D material towards the attached side. In other words, microfluidic forces were used to fold 2D materials along the predefined boundary. The images in Fig. 10d of: (i) a graphene flake before and after folding, (ii) folded arrays with consistent directions, and (iii) a sharp folded interface, all demonstrate the excellent controllability and scalability of this method. Fig. 10d(iv) further illustrates the correlation between folding and twist angles. Accordingly, the graphene sheet on the modified PVA layer can be folded along the pre-designed direction to form the desired twist angle, as shown in Fig. 10d(v). Despite its convenience and sub-micrometer spatial resolution, the fluidic-flow assisted strategy is still not capable of producing the atomically-precise results required for in-depth frontier research.

Recently, Chen et al. [32] reported the STM nano-origami technique, which represents a groundbreaking strategy for folding graphene. As shown in Fig. 10e(i) and (ii), the STM tip could be used to accurately define the folding direction on an atomic scale, thus producing a tunable range of twisting angle. Fig. 10e(iii) shows two examples of moiré superlattices (top) formed in the folded graphene nanoisland that are consistent with models (bottom). In spite of the unavoidable dilemma that STM-based strategies are hardly likely to be scalable, the intriguing concept of custom-designing nanostructures using 'nano-origami' will undoubtedly stimulate similar trials in other 2D materials.

In contrast to folding, rolling is dominated by global bending. This is generally induced by strain gradients or forces acting across the vertical direction. The rolling assembly strategy has benefitted a great deal from the developments made in rolling-up nanotechnology. Thus, a wide range of advanced nanomembrane materials have been fabricated with interesting geometries, e.g. micro/nanotubes, helices, and rings [147].

Carbon nanotubes (CNTs) are the best-known rolling form of 2D materials. They were first reported as novel allotropes of carbon in the early 1990s [148,149], which is anterior to the discovery of graphene. However, rolled-up 2D materials have been subject to rapid development in recent years.

By combining them with a pre-strained or stimulus-responsive layer,

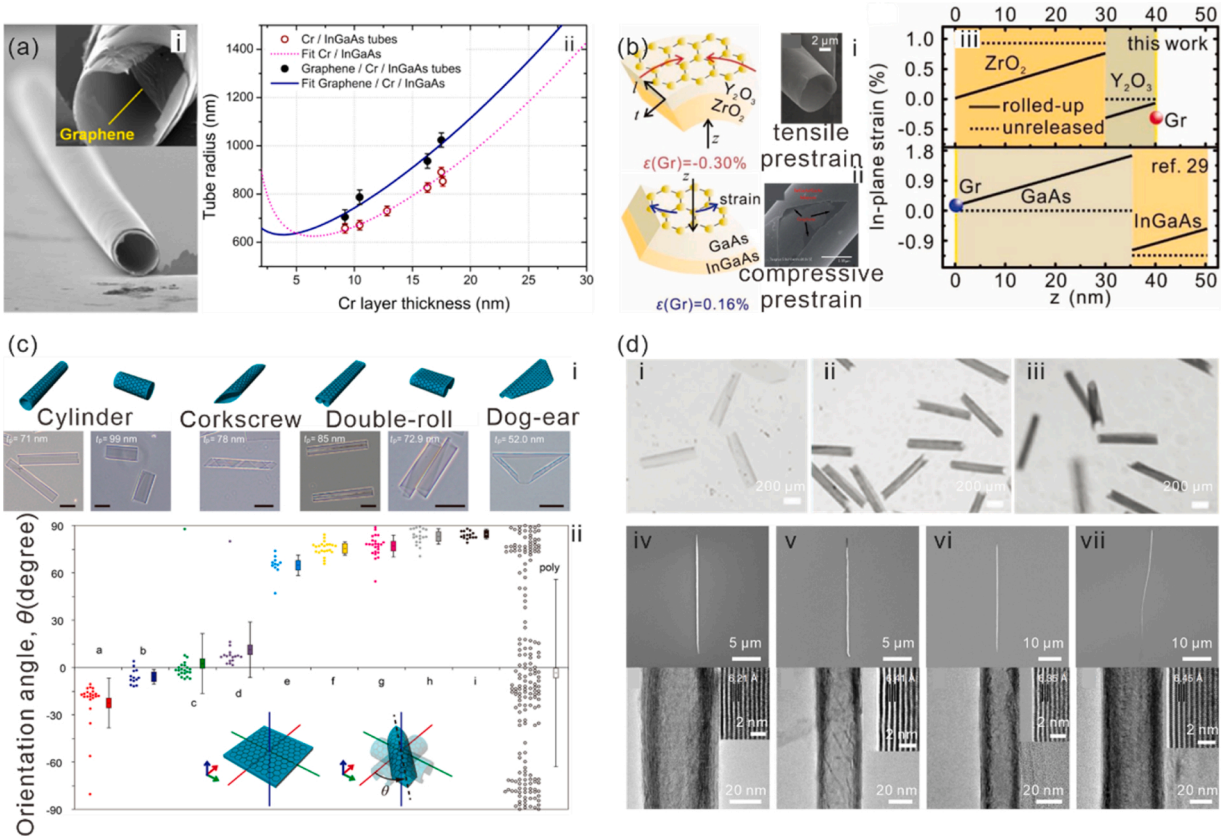

Fig. 11. Rolling shaping strategy. (a) The diameters of rolled-up graphene tubes controlled by strained layers thickness [84]. (i) SEM images of graphene/Cr/InGaAs tubes. The inset shows the magnified detail of the tube opening with the inside graphene layer. (ii) The tube radius of graphene/Cr/InGaAs tubes and Cr/InGaAs tubes as a function of the strained layer (Cr) thickness. (b) Tunable strain in rolled-up graphene based on the different strained layers [83,150]. Schematic illustrations and SEM images of rolled-up nanotubes under (i) tensile or (ii) compressive prestrain. (iii) Strain distribution before and after release in the above two cases. (c) (i) Various tubular graphene shapes fabricated through controlling of rolling direction, and (ii) the orientation angle distribution of folded single-crystalline/polycrystalline graphene [151]. All scale bars are 100 μm. (d) Nanoscrolls fabricated by different 2D materials [17,90]. (i) Graphene oxides nanscrolls. (ii, iii) reduced graphene oxides nanoscrolld with different C/O ratio. (iv–vii) SEM and corresponding TEM images of different TMDs nanoscrolls via drop of ethanol assistance: (iv) MoS_2 nanoscroll, (v) WS_2 nanoscroll, (vi) $MoSe_2$ nanoscroll and (vii) WSe_2 nanoscroll.

2D materials can be rolled up into cylindrical shapes as shown in Fig. 11. As mentioned in Subsection 3.1, the strain gradient and thickness of the thin film are two key factors that can be used to control the tube diameter. On the one hand, a larger strain gradient will lead to a more compact structure, as shown in Fig. 11a(i) [84]. On the other hand, the diameter of the tube increases as the thickness of the rolling layer increases. For example, the relationship between tube radius and thickness of the Cr layer is shown in Fig. 11a(ii) which well illustrates the above points. Here, a series of experimental tube radii are plotted as a function of the layer thickness, giving results in good agreement with the continuous elasticity multilayer model. This demonstrates that the tube radius increases with the Cr layer thickness as the result of enhanced bending rigidity. In addition, the radii of graphene/Cr/InGaAs tubes are larger than those of Cr/InGaAs tubes (with the same Cr layer thickness) due to their augmented total thickness.

The strain distribution in the rolling tube can be tuned by varying the pre-strain in the strained layer, thus allowing the properties of the rolled-up 2D material to be modulated. Raman spectroscopy can be used to investigate the strain states in graphene tubular structures created using layers strained to different degrees [83,150]. The images in Fig. 11b show a comparison of the strain distributions in: (i) a tensile pre-strained graphene/Y_2O_3/ZrO_2 layer, and (ii) a compressive pre-strained graphene/GaAs/InGaAs layer, which indicates that the strain in the rolled-up graphene is opposite to that in the unreleased pre-strained layers. The ability to control the strain in the rolled graphene structure provides a feasible approach to strain engineering in 2D materials, even in the context of massive, on-chip, fabrication processes [150].

Apart from tubes, more interesting structures can be constructed from 2D materials by tuning the rolling direction and 2D pattern. Fig. 11c(i) shows a variety of rolling shapes fabricated from graphene/poly(chloro-*p*-xylylene) (parylene-C) bilayers by the relaxation of internal strain gradients (cylinders, corkscrews, double-roll configurations, and dog-ears) [151]. The geometries of these microstructures are closely related to the micropatterns created before conducting autonomous rolling, and the thickness of the bilayer. In addition, the final rolling structure produced highly depends on the preferable rolling direction, which is subjected to the principle to overcome the smaller energy barrier. In the above case, the graphene utilized is polycrystalline with an elastic energy that is anisotropic. Thus, the rolling direction will follow the most compliant direction, thereby forming a diverse range of geometries. A statistical analysis of the folding orientations in single-crystalline and polycrystalline graphene is shown in Fig. 11c(ii). It is observed that the isotropic behavior of single-crystalline graphene leads to a relatively concentrated distribution of folding orientations, while the anisotropic behavior of polycrystalline graphene yields a random distribution.

It is commonly found in these kinds of experiment that the exact nature of the rolled-up material depends on the structure and property of 2D materials used. Fig. 11d illustrates several scrolls made from different 2D materials. Although they are similar in the general form, their specific structural parameters are different depending on 2D materials used [17,90]. SEM image in Fig. 11d(i) shows scrolls made from graphene oxide (GO), while those in (ii) and (iii) are made from reduced graphene oxide (rGO) with different C/O ratios. The scrolls have different radii due to their different hydrophobicities and mechanical properties [17]. In particular, rGO sheets that are more hydrophobic and rigid than GO sheets roll up more tightly and thus forming scrolls with smaller radii. Another example is shown in Fig. 11d(iv–vii) which presents SEM and transmission electron microscopy (TEM) images of a series of nanoscrolls made from different TMDs. It is shown that they all have compact and multiwalled structures. However, their interlayer spacings are different and match well the interlayer spacings found in their bulk counterparts [90].

Wrinkling is another form of out-of-plane bending deformation. However, a wrinkled material is subject to a much smaller strain gradient than a rolled material [152,153]. As the development of 2D materials has progressed, it has been found that wrinkles are often unavoidably (unintentionally) formed during the synthesis or transfer process. Meanwhile, the controlled (intentional) wrinkling of 2D materials is often desirable and introduces new parameters that can be used to tune the properties of the product (e.g. wrinkling amplitude, 'wavelength', and orientation).

In the case of free-standing graphene, wrinkles have long been considered to be a critical structural factor, which contributes to its thermodynamic stability. Fig. 12a shows suspended samples of graphene that can be manipulated thermomechanically so as to control the degree of wrinkling introduced [154]. The wrinkling morphologies shown in Fig. 12a(i) correspond to suspended graphene annealed at different temperatures (left: before annealing, middle: after annealing to 425 K, right: after annealing to 475 K). There is a clear manifestation in the images of a tendency for both the amplitude and wavelength of the wrinkles to increase with annealing temperature, which can be illustrated more quantitatively in Fig. 12a(ii). It shows that the amplitude of the post-annealed wrinkles increases linearly as a mixed variable (inclusion of both wavelength of the post-annealed wrinkles and the maximum annealing temperature) increases. It is also worth noting that the shape of the opening holes over which the graphene is suspended influences the orientation of the wrinkles produced (because of the boundary conditions created), as shown in Fig. 12a(iii).

The orientation of the wrinkles is also remarkably affected by the strain distribution. Fig. 12b shows SEM images of graphene wrinkles produced under 1D and 2D strain, respectively [155]. The wrinkles are even quasi-ordered when fabricated by a local patterning method. The amplitude of the graphene wrinkles can be modulated by varying the magnitude of the strain. It is clear that the orientations of the wrinkles in the 2D strain state are disordered, whereas in the 1D case they are well aligned. It is further shown that a soft skin layer patterned onto the graphene before strain relaxation results in the selective release of the strain in the patterned region. As a result, quasi-ordered wrinkles can be formed with a certain order parameter.

As mentioned above, the control of strain mismatch is an important approach to obtaining the controlled wrinkling, which inspires many strain engineering studies. However, larger strain than those of wrinkling can induce the delamination, which is the obvious characteristic of buckling that differentiates it from wrinkling. Lou et al. reported the existence of buckling-induced wrinkles in the strained edges of Bi_2Se_3/Bi_2Te_3 heterojunctions whose morphology could be controlled by changing the conditions used [156]. Due to the lattice mismatch involved, the Bi_2Se_3 parts were stretched while the Bi_2Te_3 parts were compressed, which led to a buckling of the edge area in order to minimize the system energy. Fig. 13a shows that the relationship between the wrinkle amplitude and wavelength, together with the edge width and thickness. In general, both the amplitude and wavelength increased as the edge width increased in order to maintain the balance between the in-plane strain energy and bending energy.

Strain engineering has also been used to generate buckling in $ReSe_2$ nanosheets [157]. As shown in Fig. 13b, the morphology of the buckled-up wrinkles has an obvious dependence on the number of layers involved. Guided-buckling can be achieved using the strain-release scheme shown in Fig. 13b(i). The exfoliated $ReSe_2$ flakes can be buckled-up to form distinct structures whose cross-sections vary with the layer number, as shown in Fig. 13b(ii), including ripples with multilayers, triangles with only a few layers, and needle-like structures with monolayers. It appears that thinner flakes experience more extensive out-of-plane buckling due to their lower bending rigidity.

Compressive buckling (also referred to here as simply 'buckling') is the deformation that occurs in response to an external compressive stress, as already outlined in Subsection 3.4. This buckling shaping strategy is a universal strategy that enables complex out-of-plane structures and covers a wide range of scale lengths. The general aim is to induce buckling in regions between the pre-selected bonding sites in

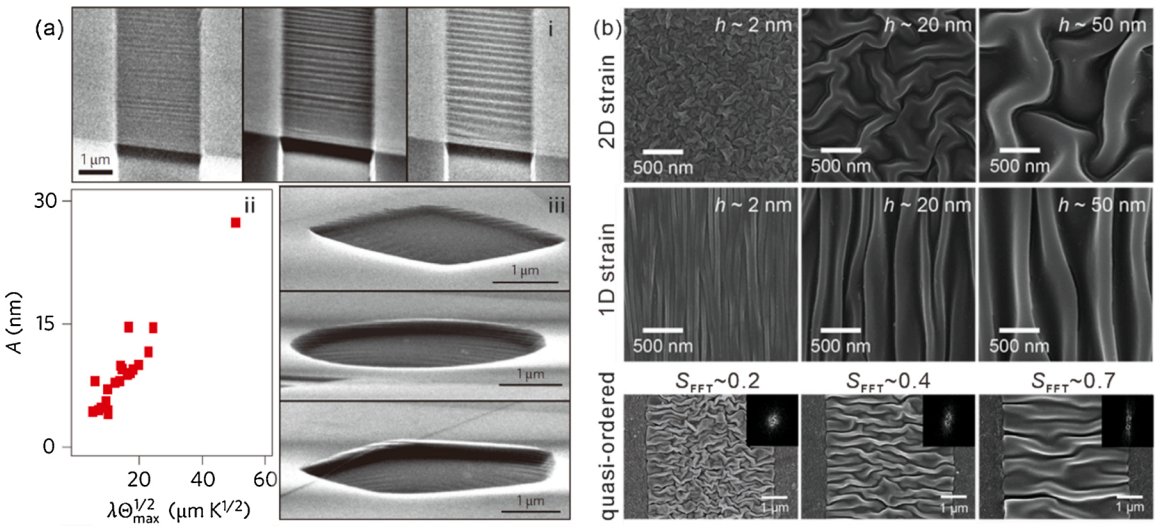

Fig. 12. Wrinkling shaping strategy. (a) Wrinkles of suspended graphene over opening holes of various shapes controlled by thermomechanical manipulation [154]. (i) SEM images of a suspended graphene membrane before annealing (left), after annealing to 425 K (middle) and to 475 K (right). (ii) Nearly linear relationship between the amplitude and $\lambda\Theta_{max}^{1/2}$ (λ, wavelength; Θ_{max}, the maximum annealing temperature rise above ambient) of the post-annealed wrinkles in the suspended graphene membrane. (iii) Various wrinkles formed in graphene membranes suspended over opening holes of different shapes. (b) SEM images of orientational and quasi-ordered wrinkles under various strains [155]. The insets in the third line are used to calculate fast Fourier transform order parameter (S_{FFT}) for quantifying the orientation of wrinkle.

order to generate desired structures.

However, relatively few examples are based on 2D materials as 3D shapes of suspended 2D materials tend to be fragile, readily succumbing to external compressive forces (above a certain critical value). The research on the fabrication of mesostructures by buckling 2D materials therefore still focuses on diversifying the geometries attainable, the customization and stabilization of the configurations produced, and controlling the strain distributions and mechanical deformations induced.

2D materials of interest are always transferred onto structural layers such as polymers in order to execute the compressive buckling routine required. The buckling technology used in the assembly of conventional nanomembrane materials is considered to be relatively mature [30]. In the previous studies, 2D materials essentially served as a functional component in the integrated 3D structure, adhering to the structural layer instead of supporting the mechanical deformation process [21]. However, as mentioned in Subsection 3.4, 2D material derivatives, or the hybrid systems composed of 2D materials and structural layers can be utilized, which integrates the superior mechanical properties of 2D materials with strain-stable performances of the exotic materials.

As illustrated in Fig. 13c, compressive buckling of cellular graphene/PI bilayers can produce a variety of 3D hierarchical structures inspired by kirigami/origami [109]. Finite element analysis (FEA) can be used to help rationally design the 2D precursor structures which is able to generate the desired 3D structures and predict the mechanical properties of the mesostructures formed. In this way, the assembly process can be mechanically-guided ensuring that the maximum principle strain distribution in the resultant 3D structure does not exceed certain critical values (fracture limits). The mesostructures experimentally fabricated via buckling are in good agreement with the FEA predictions.

A diverse range of 2D precursors with elaborate design patterns and selective bonding schemes have been devised to generate different kinds of hierarchical buckling structures. Some examples are exhibited in Fig. 13c. The structure shown in (i) is based on a filamentary design, wherein a network of buckling ribbons leads to the formation of a double-floored helical array. As shown in (ii), a kirigami-inspired design is used to create a jellyfish-like shape, and a windmill-like shape is depicted in (iii). These structures can be designed using a variety of different types of cut, e.g. circumferential cuts, radial cuts, and serpentine cuts. In addition to the tuning of the final 3D geometries, these cuts are beneficial to the structural stability of the designs by the significant reduction of the stress concentration. Origami-inspired folded structures can also be produced like the five-pointed-star shape shown in (iv) and 'alternating mountain' shape shown in (v). These can be realized through the addition of strategically placed creases (formed, in this case, by using laser irradiation to thin the layer by an appropriate amount). Multilayer layouts can also be employed to create even more complex structures such as networks fabricated with overlapping or entangled parts. Examples can be more complex including the double-layered helical coil shown in (vi), triple-layered cage shown in (vii), and quadruple-layered tree shown in (viii).

As mentioned above, by utilizing the graphene as hinges and rigid panels as beams, further foldable microstructures were developed, as shown in Fig. 13d [12]. Here, multiple folds were made employing biaxial compressive buckling, as shown schematically in Fig. 13d(i) wherein two different folding modes were achieved (outward at one hinge and inward at the other). By varying the pre-strain used, the buckling geometries shown in (ii–iv) could be prepared. The height of the table shape reached a maximum when the pre-strain is 50 %. A larger pre-strain caused the 'legs' of the table to be bent under the table so that the height of the table decreased. However, even though the strain in the table shape became concentrated at certain specific locations, the strain remained below the fracture limit and so failure was securely avoided.

Buckling is a versatile and widely compatible strategy for assembling 3D structures. As such, it has been proven to be fairly facile when applied to assemble sophisticated 3D architectures from 2D materials. However, there is an urgent demand for the technique to be expanded to 2D materials other than graphene in order to extend its usefulness. Meanwhile, there are plenty of creative 3D buckling geometries that can be assembled to enlarge the range of structures available and bestow novel functionality. The use of kirigami- and origami-based techniques is an important part of this process, as we will describe in the following two subsections.

4.2. *Kirigami-inspired strategy*

Kirigami is an ancient assembly strategy that involves cutting paper using scissors. In the current context, kirigami relates to making a

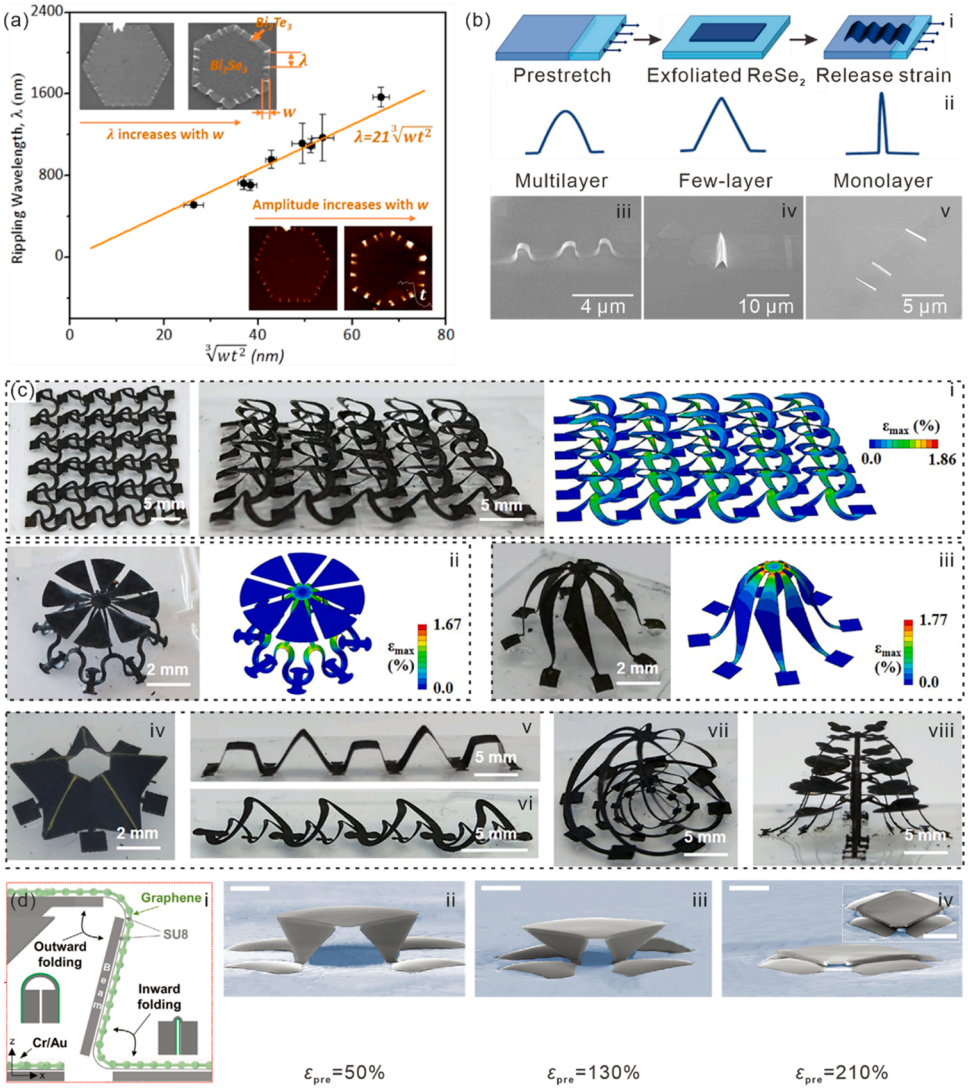

Fig. 13. Buckling shaping strategy. (a) Tunable amplitude and wavelength of buckling-induced wrinkles in strained Bi_2Se_3/Bi_2Te_3 heterojunction [156]. The amplitude and wavelength (λ) both increase with the indicated edge width (w). (b) Various shapes of wrinkles fabricated by buckling of $ReSe_2$ nanosheets with varied thicknesses [157]. (i) Schematic illustration of the fabrication process using prestrained elastomeric substrates. (ii–v) Schematic diagram and corresponding SEM images of buckling-induced wrinkle geometries for multilayer, few-layer and monolayer $ReSe_2$ nanosheets. (c) Various 3D mesostructures fabricated by mechanical buckling of cellular graphene [109]. Filamentary design: (i) double-floor helices array. Kirigami-inspired structures: (ii) jellyfish shape, (iii) windmill shape. Origami-inspired structures: (iv) five-pointed-star shape, (v) alternative mountain shape. Mutilayer network: (vi) double-layer helical coils, (vii) trilayer cages, (viii) four-layer trees. (d) Table-shaped foldable 3D microstructure by graphene hinges [12]. (i) Schematic illustration of two different folding modes in above structure: outward and inward folding respectively happens at the different locations of hinges. (ii–iv) SEM images show the tendency that the height of table shape reaches the maximum when prestrain is 50 % and further decreases as the prestrain increases. All scale bars are 40 μm.

pattern of 'cuts' in planar 2D precursors through photolithography or ion-beam irradiation. The size and layout of these patterned cuts can regulate the geometries and mechanical properties of the assembled 2D material, as mentioned in Subsection 2.2. They are mainly regular patterns with some kind of symmetry or periodicity and are often created using computer-aided design (CAD) techniques. This means that the design of the patterned cuts is very flexible and many unprecedented 3D structures can be constructed via stretching, curving, or compressive buckling, as discussed above. More importantly, kirigami patterns can be devised that improve the ductility and toughness of the structures by suppressing the concentration of stress at 'kink' positions.

Graphene kirigami was first proposed in 2015 by Blees et al. [13] who envisaged a broad application of the technique for preparing mechanical metamaterials. As mentioned in Subsection 2.2, the mechanical characteristics of polycrystalline monolayer graphene are analogous to paper, making it easy to apply the principles of kirigami to graphene. Kirigami patterns can be created using photolithography which allowed the formation of various interesting kirigami structures, e.g. in-plane kirigami springs, out-of-plane pyramidal springs, and a diverse range of cantilevers. The complex 3D structures created can also be remotely actuated by optical fields and controlled by magnetic fields after attaching iron 'pads'.

The kirigami assembly strategy has also been applied to other 2D materials, thus enabling the formation of a rich collection of 3D micro/nanostructures based on 2D materials. An example is shown in Fig. 14a wherein monolayers of CVD-grown MoS_2 were patterned into different kinds of kirigami structures after the layer transfer and etching. The images show two linear kirigami springs, kirigami pyramids, and out-of-plane kirigami springs with alternating C-shapes [24]. To create these structures, large-area MoS_2 films were firstly transferred onto kirigami-patterned polydimethylsiloxane (PDMS). Then, the MoS_2 films were processed by etching the exposed regions using plasma and the same kirigami structures present in the underlying PDMS were formed.

A novel kirigami strategy for utilizing chemically derived deposition and etching WSe_2 was also reported [158]. Fig. 14b schematically illustrates some of different kirigami configurations produced by multilayered WSe_2. SEM images show the kirigami structures of multilayers arising from the competition between deposition and etching during the CVD growth process. The etching process was governed by the stacking of the bottom layer and the growth temperature, which ultimately led to the evolution of the final geometrical result.

A direct-write patterning method can be applied to create graphene kirigami ('pulsed laser-assisted helium ion nanomachining') in an attempt to improve the processing precision [159]. A systematic investigation was conducted using the adopted laser in order to obtain the optimal operating conditions of the laser (laser power, pulse width, and laser frequency). A comparison of the resulting lines cut is given in Fig. 14c(i). As the laser power increased, carbon deposition decreased

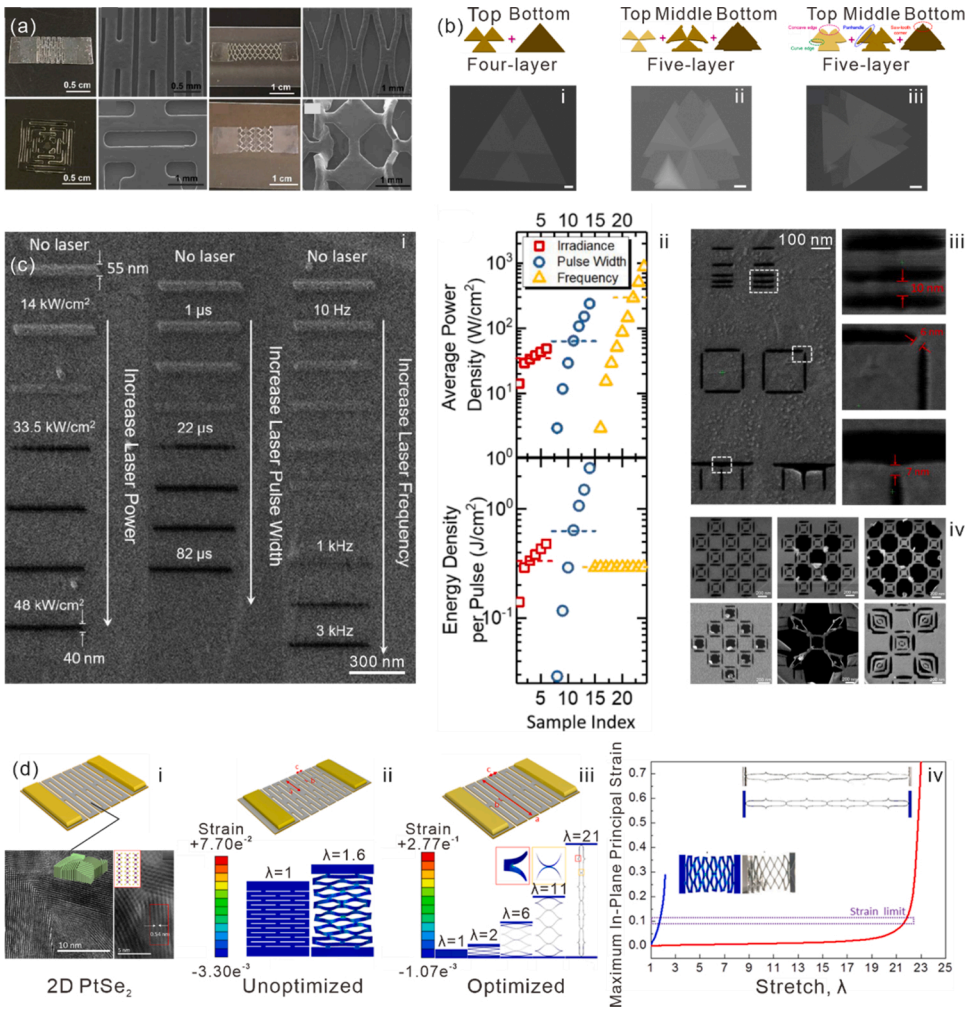

Fig. 14. Kirigami-inspired schemes. (a) Optical images and corresponding SEM images of diverse MoS_2 kirigami structures [24]. (b) Schematic illustrations and corresponding SEM images of hierarchical structures based on the chemically derived kirigami of WSe_2 [158]: (i) four-layer, (ii, iii) five-layer. All scale bars are 2 μm. (c) Direct-write kirigami patterns of monolayer graphene by pulsed laser-assisted helium ion milling [159]. (i) Patterns controlled by laser parameters. (ii) Average laser power density and energy density per pulse affected by laser parameters. (iii) Milling resolution in typical kirigami patterns. (iv) Various complex kirigami patterns fabricated by ion milling. (d) Optimized kirigami structures of $PtSe_2$ layer conductors with remarkable stretchability [23]. (i) Schematic illustration of 2D $PtSe_2$/PI kirigami patterns and vertically aligned 2D $PtSe_2$ layers shown in high-resolution transmission electron microscopy (HRTEM) and STEM image. Schematic illustrations define geometrical parameters and FEA simulations show the corresponding strain distribution of (ii) unoptimized and (iii) optimized kirigami pattern. (iv) Comparison of maximum in-plane principal strain versus stretch between the unoptimized (blue line) and optimized (red line) kirigami patterns. (For interpretation of the references to colour in this figure legend, the reader is referred to the web version of this article).

and ion milling increased. The milling process dominated when the laser power reached 33.5 kW/cm^2. Similar transitions from carbon deposition to ion milling were also found when tuning the pulse width and laser frequency (the critical values of these parameters for forming clear cut lines were found to be 10 μs and 100 Hz, respectively). The average laser densities corresponding to different values of the above factors are summarized in Fig. 14c(ii), and the dashed lines denote the threshold between deposition and milling behavior. Fig. 14c(iii) shows some kirigami patterns with high resolution can be even attained using an ion milling strategy (generally <10 nm at different critical positions). Fig. 14c(iv) shows that the ion milling technique is capable to produce a variety of complex geometrical kirigami patterns.

Optimized kirigami structures made from $PtSe_2$ have been found to have remarkable stretchability (Fig. 14d) [23]. Furthermore, the kirigami-based $PtSe_2$/PI bilayers exhibit enhanced stretchability without compromising its intrinsic electrical conductance. According to a comparison of unoptimized and optimized kirigami patterns, the maximum stress in the optimized structure can be reduced dramatically compared to the unoptimized structure under the same stretch strain. The extremely large stretchability of ~2,000 % can even be realized.

4.3. Origami-inspired strategy

Origami is the ancient art of paper folding. When applied to 2D materials, it has also evolved into an influential assembly strategy that enables the creation of intricate 3D micro/nanostructures through the use of creases or hinges. The geometry of the 3D mesostructure produced is, therefore, clearly governed by the pattern of folds created in the 2D precursors.

The required creases or hinges can be created in the constituent 2D membranes by strategically reducing the thickness of those regions to enhance their flexibility. 2D materials can also be selectively bonded to fix certain parts of the material and thus guiding the folding process. It is worth noting that the design process must consider the standard mechanical principles as the creased/hinged regions will be subject to an increase in stress concentration. Thus, they should be viewed as potential fracture sites.

As already mentioned, the origami assembly technique can also be extended to the construction of reconfigurable structures in an autonomous and even reversible manner (through the use of active or stimulus-responsive materials). This is likely to be a major stimulus promoting applications related to 4D printing and intelligent assembly.

The conception of ‘graphite origami’ was first proposed by Ebbesen and Hiura as early as 1995 [160]. They envisaged that creating 3D forms of graphene should be possible based on the results of AFM experiments characterizing multi-folded graphite layers on the surface of highly-ordered pyrolytic graphite (HOPG). Origami assembly of 2D materials has recently experienced a rapid period of development, resulting in the realization of complex 3D architectures.

Fig. 15a shows a graphene-based cube fabricated by the capillary forces induced by the melting of polymer hinges [93]. As the graphene was transferred onto an underlying support layer and etched to remove the portions outside the frame prior to assembly, the surfaces could be readily modified by, for example, the addition of metal patterns. Other

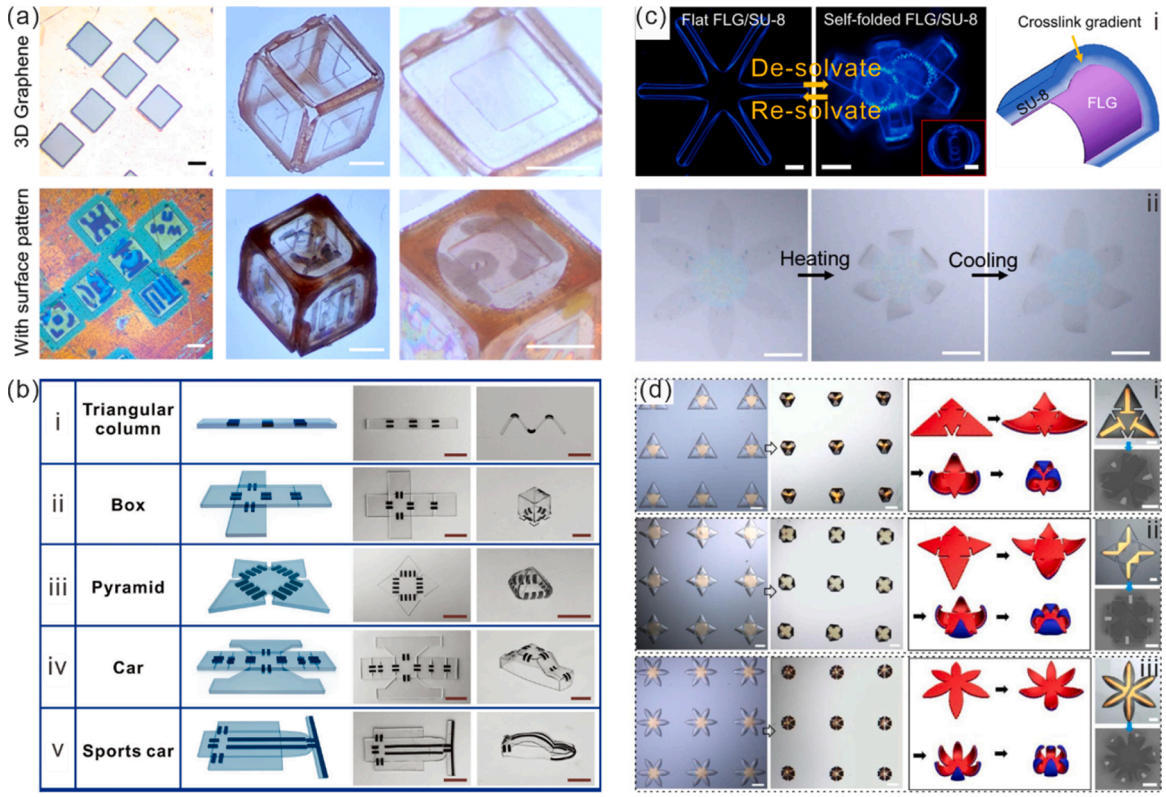

Fig. 15. Origami-inspired schemes. (a) Self-assembly of 3D graphene polyhedrons from predesigned 2D patterns [93]. All scale bars are 100 μm. (b) A series of 2D precursors and 3D structures enabled by light-driven origami assembly of graphene-based polymer bilayers [15]. All scale bars are 10 mm. (c) Reversible origami via the integration of graphene with polymer layer (SU8) responsive to stimuli like (i) solvate (scale bar, 200 μm) or (ii) heating (scale bar, 100 μm) [85,86]. (d) Reversible MoS_2 origami based on the differentially-crosslinked polymer and selective fixing: with shapes of (i) pyramid, (ii) square pyramid and (iii) flower [14].

2D sheets, e.g. GO, can also be folded in the same manner to form polyhedrons [161].

The excellent photothermal effects of rGO sheets make them work as useful constituents in light-driven functional structures. For example, an active layer incorporating rGO, thermally expanding microspheres, and PDMS can be used to achieve autonomic origami assembly based on the deflection of the active layer induced by light [15]. In this case, the active layer was combined with a passive layer of PDMS to form a bilayer. There is a mismatch in the Young's modulus and coefficient of thermal expansion within the bilayer that gives rise to a bending deformation when irradiated with infrared (IR) radiation. Furthermore, the folding angle was found to be controllable by tuning the active hinge length. Hence, a series of complex 3D structures could be assembled by connecting the different parts of the 2D design using appropriate hinges, as shown in Fig. 15b.

Apart from using light to stimulate assembly, other experimental stimuli have been investigated to achieve an assembly response and these continue to attract an increasing amount of attention. Fig. 15c(i) shows an example in which a crosslinking gradient inside a layer of SU8 was exploited to achieve the reversible folding of a graphene/SU8 bilayer via a process of de-solvation and re-solvation [85]. Moreover, the curvature of the folding effect was controlled by the swelling gradient. As a result, the 3D origami structure like flower shape was formed in combination with 2D patterning. Fig. 15c(ii) shows the reversible folding and unfolding of graphene in response to heating and cooling [86]. In this case, a layer of thermoresponsive polymer with a strain gradient sensitive to temperature was employed. Thus, the reconfigurable 3D graphene-based structure was formed and further stabilized by the attachment of rigid panels.

Another example of a reversible system is shown in Fig. 15d (based on MoS_2 and a differentially-crosslinked polymer, as discussed earlier). It is observed that the hybrid system can be used to assemble various 3D structures, e.g. pyramids, square pyramids, and flower shapes [14]. The selective fixing of the pattern center is another key procedure to ensure the targeted assembly of such origami designs.

In the field of smart devices, 2D materials are being combined with conventional shape changing materials (hydrogels, liquid crystals, shape memory elastomers, etc.) to assemble reconfigurable origami structures with additional advantages, e.g. significantly smaller form factors, low-power consumption, and fast response times, thanks to the ultrathin nature of 2D materials used. These advances pave the way for some promising applications of origami-assembled 2D materials in, for example, the adaptive and programmable design of smart devices [162].

5. Tailored properties and design strategies

Using the diverse range of assembly schemes discussed above, we can give 2D materials new vitality by transforming them into 3D structures and tailoring their properties for application in next-generation micro/nanodevices. In addition to the 3D configuration adopted, strain engineering can also be used to prominently regulate the properties of the reshaped 2D materials, thus endowing them with a new creative capability for a broad range of applications in mechanics, optics, electronics, and nanoscience.

In general, there are two primary considerations when shaping and structuring 2D materials: (i) preserving the unique inherent merits of the 2D material in the 3D structure created; and (ii) furnishing the new materials with novel functionalities that cannot be attained with the planar 2D materials alone. Consequently, an inverse approach to the design of both the geometry and mechanical characteristics of the structures is required in order to optimize them for future application. As the understanding of the atomic-scale mechanisms develops, more precise designs are expected to realized. This process can be further accelerated by adopting advanced methods of computer-aided design

(CAD).

5.1. Unique physical properties

Depending on the coupling between the materials' mechanical and other properties, 2D materials can be engineered via origami/kirigami to form a geometrical form with a favorable morphology and advantageous strain distribution. The key challenge is how to maintain the merits of 2D materials while exploiting the superiority of the targeted 3D structure.

It is interesting to see that 2D materials isolated from the bulk material can meet the growing demand for the novel functionalities in the form of an appropriate 3D structure. Meanwhile, compact 3D structures like rolled-up tubes can promote miniaturization, reducing the volume and footprint of material required. It is very important for the development of the microelectronics industry. It is noteworthy that various 3D geometries also provide a flexible platform for strain engineering in 2D materials. In particular, the desired strain distribution can be well-designed in the practical schemes of shaped and structured 2D materials and yield the exceptional physical properties required for specific applications.

As we are working on the nanoscale, custom-design nanostructures can be made that enable novel physical phenomena to be manifested for frontier physical investigation. Starting with graphene, out-of-plane deformation and strain engineering have become effective tools for tuning the material's transport properties, even in the quantum regime [163].

As the fundamental theory has developed and the computational methods are improved, numerous theoretical investigations on the engineered properties of deformable 2D materials have been conducted, spanning from frontier physics research to device conception. For example, as already mentioned, it was predicted that zero-energy edge states could be perfectly transmitted onto the opposite layer of a folded metallic graphene nanoribbon to generate a zero Landau level due to symmetry considerations [122]. This work unveiled the quantum Hall transport property in folded graphene nanoribbons with a vivid description of the Klein paradox. Another example concerns the instability of black phosphorus. In this case, the formation of nanoscrolls may be a possible strategy to encapsulating the reactive surface of black phosphorus for real applications. This is because, in addition to promoting stability, the calculated band structure of black phosphorus nanoscrolls suggests that the carrier mobility will be increased [164].

It has also been suggested that periodically-corrugated graphene can be applied to the study of origami-based spintronics [165]. In that work, spin-dependent conductance of graphene sheets with different corrugation parameters were calculated. It was found that the spin-orbit

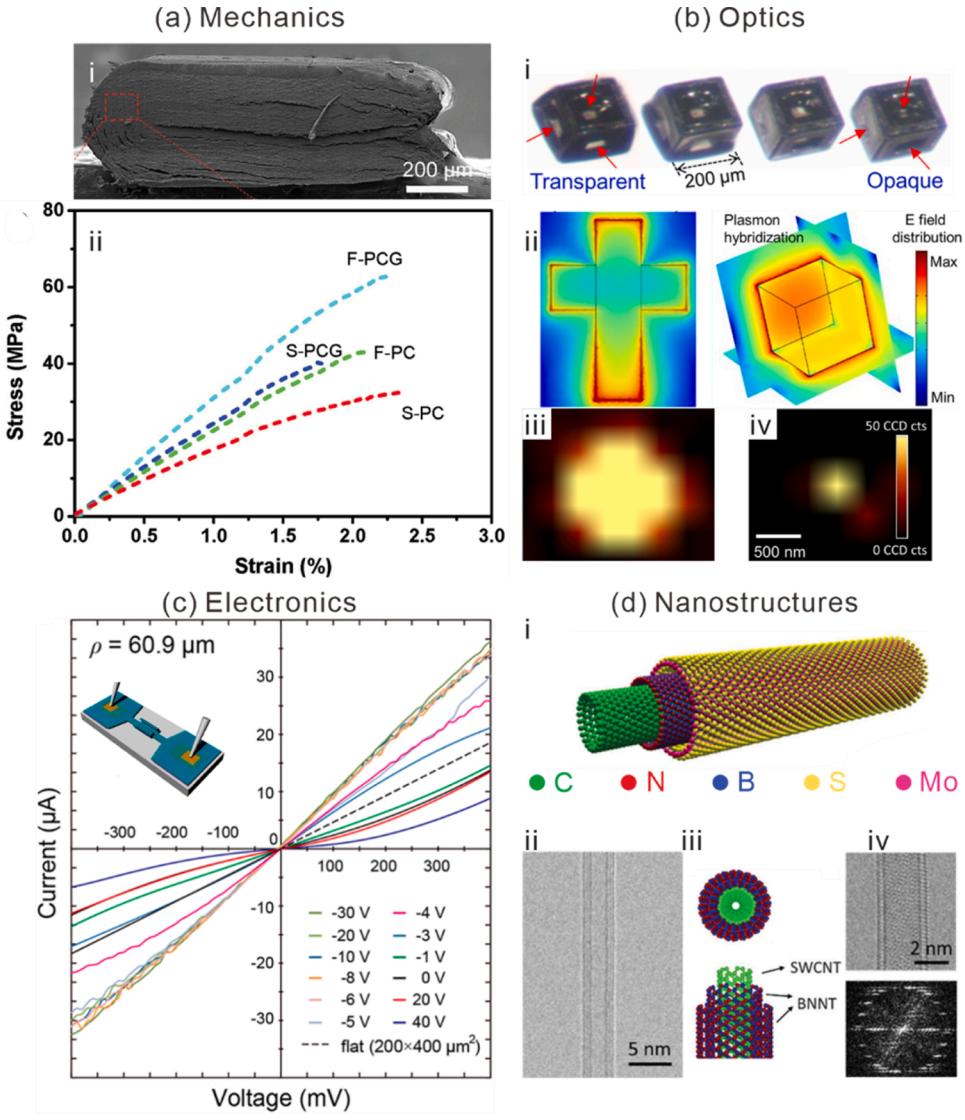

Fig. 16. Unique physical properties of origami/kirigami-engineered 2D materials. (a) Mechanics: remarkably enhanced mechanical performance of graphene-based composites through multi-folding [167]. (b) Optics: (i) tunable optical transparency of the graphene oxide polyhedron [161], (ii–iv) volumetric light confinement in self-assembled 3D graphene-based polyhedrons [93]. (c) Electronics: nonlinear electronical properties of self-folded graphene film with a curvature radius of 60.9 μm [151]. (d) Nanostructures: one-dimensional heterostructures via the assembly of different nanotubes [169]. (i) Schematic illustration of one-dimesional vdW heterostructure with the coaxial tubular structure. (ii) TEM image of one-dimesional vdW heterostructure formed by the inside single-wall carbon nanotube and outside bilayer boron nitride nanotube, (iii) the corresponding structural model and (iv) aberration-corrected TEM image.

coupling was improved due to the enhanced effect of the curvature. The improved spin-orbit coupling opens up the bandgap and induces a spin-polarized current that can be used in spintronic applications.

Inspired by such theoretical advances, scientists have attempted to realize these properties of origami/kirigami-engineered 2D materials in practice. Fig. 16 summarizes some representative examples of unique physical properties split into four broad categories: mechanics, optics, electronics, and nanostructures.

As mentioned above, graphene can be toughened and elongated beyond its previous limits through the use of kirigami [13]. In addition, composite films consisting of 2D materials can be readily reinforced through shaping and structuring. For instance, by using photolithography to create kirigami patterns in nanocomposites of GO–polyvinyl alcohol (PVA), the material's elastic properties can be engineered, thus promoting its ultimate strength [166].

It has also been found that a kind of macroscale laminated composite material formed from a multi-folded polycarbonate (PC)/graphene (G) film (PCG) possesses reinforced mechanical properties, thus yielding another strategy to further improve the mechanical stability and durability of such materials [167]. Fig. 16a(i) shows that a PCG composite film has been repeatedly folded in half to form a multilayered structure similar to that of a stacked multilayer (in the case shown, the composite was folded 10 times producing 1024 layers with an overall thickness of ~0.4 mm). The structures were further analyzed theoretically and the synergistic effect occurring between the folding and reinforcement process was quantified using finite element analysis (FEA) simulations. Bending tests were then performed on a series of samples including folded ones (F-PCG, F-PC) and stacking ones (S-PCG, S-PC). The highest strength was achieved using F-PCG, as shown by the stress–strain curves in Fig. 16a(ii). Such folded 2D material-based mechanical metamaterials or composite materials can be expanded on a large scale and may have potential applications in stretchable electronics.

The optical properties of 3D structures are also often very different from those of the 2D components. Fig. 16b shows examples in which tunable transparency [161] and volumetric light confinement [93] can be realized using graphene-based polyhedra produced via similar origami schemes. In the former case, the water-permeability of the 3D hollow GO structure was exploited to switch the transport path of the light. Thus, the transparency of the structure changed depending on whether the environment was dry or wet. In the latter case, 3D plasmon hybridization occurred on the graphene surfaces on the polyhedra, producing a highly confined electrical field inside the 3D structure.

The electrical properties of 2D materials can be effectively engineered in the 3D structure. For example, both the graphene tubes and edge-closed graphene ribbons were synthesized using palladium (Pd) nanowires as templates [168]. It was rather surprising that the edge-closed graphene ribbons exhibited a higher conductivity than the edge-open graphene ribbons, which was attributed to parasitic defects. Fig. 16c shows plots of the nonlinear electrical properties of self-folded graphene films with a certain curvature radius. In this case, graphene films with various curvature radii generated the varied strain, thus modulating their electronic structures and producing the tunable resistances accordingly [151].

Finally, Fig. 16d shows a recently reported method for assembling nanostructures in the form of 1D vdW heterostructures [169]. Layers of h-BN and MoS_2 were grown on single-walled carbon nanotubes by vapor deposition technique. It was shown that TEM images and electron diffraction results verified that the structure of the 1D vdW heterostructures involved nested nanotubes that were highly crystalline. Furthermore, the electrical properties of the 1D vdW heterostructures were found to be dependent on the close coupling between the nanotubes, modulated by their structural parameters, e.g. the diameters of the tubes.

5.2. Novel inverse designs

Both facile and accurate designs are essential for the pursuit of structures with desirable properties and thus building a solid basis for further applications. It is quite challenging to develop an inverse design approach when shaping and structuring 2D materials (especially in the context of nanostructures). Therefore, the understanding of the theoretical mechanisms utilizing computer-aided design (CAD) is becoming more necessary. By attaining an in-depth understanding of the design principles involved, it should be possible to accomplish suitable designs very rapidly.

The geometrical design of kirigami/origami patterns has made much progress via the use of mathematical methodologies, e.g. Miura-ori folds [170]. However, the design of patterns for shaping and structuring 2D materials is mainly limited by the material. This issue may be resolved by learning from the design experience gained from the prediction process of new materials. Prior to an experimental attempt to form a predicted novel or functionalized material, the 3D structure made from 2D materials can be simulated using theoretical methods, which allows the formation process to be explored and, perhaps, a more favorable structure to be proposed.

As an example, the possibility of forming subnanometer TMD origami structures was systematically investigated using density functional theory, including the critical role of the line defects in the origami assembly process [171]. The stability of the MoS_2 nanoribbons, with and without line defects, was firstly calculated. The results indicated that the line defects only caused a small energy penalty and were suitable for the construction of origami nanostructures. As shown in Fig. 17a, the evolution from MoS_2 nanotube to nanowire was simulated in S-rich (orange dots) and Mo-rich (blue dots) environments. Compared to optimal structures, the inset experimental observations demonstrated that vacancies were inclined to crease in TMD nanostructures, which suggested that line defects could effectively induce assembly of the origami structure.

In addition to traditional optimization algorithms that are based on finite element analysis (FEA), machine learning methods have emerged and gradually become an alternative and highly efficient approach for the design of materials or kirigami patterns. In general, the optimization of a series of cut layouts to obtain the desired mechanical properties would no doubt be a complicated and exhausting process. However, by machine learning, the optimized design of graphene kirigami (using 1000 training candidates) could be rapidly derived, thus yielding a design with outstanding elastic stretchability [172]. Fig. 17b shows the relationships obtained between stress and strain in three different representative kirigami patterns (left panel) which can be used to extract other important mechanical parameters. The elastic properties of the origami designs are correlated with both the cut density and arrangement (right panel). By the adequate sample training and the experimental results to optimize the cut pattern in the kirigami structure using a neural network search algorithm, the inverse design of a highly stretchable graphene kirigami structure was realized. The work also enriches our knowledge of the relationship between the kirigami cuts in a material and its elastic properties.

For the targeted design of shaped and structured 2D materials (especially at nanoscale) more effort needs to be devoted to understanding the atomic mechanisms involved. Recently, Han et al. studied the atomic-scale bending mechanism in few-layer graphene and found there was a decrease in bending stiffness resulting from interlayer effects [173]. Fig. 17c shows the potential bending mode identified in few-layer graphene. It was observed that interlayer slipping in the graphene softened the bending stiffness when the bending angle was large (bright-field STEM image) while bending was accommodated by the tensile and compressive strain (inserted schematic illustration).

As mentioned above, atomically-precise nano-origami performed using an STM tip is a promising approach to custom-designing graphene nanostructures. This is typified by the tubular carbon structures shown

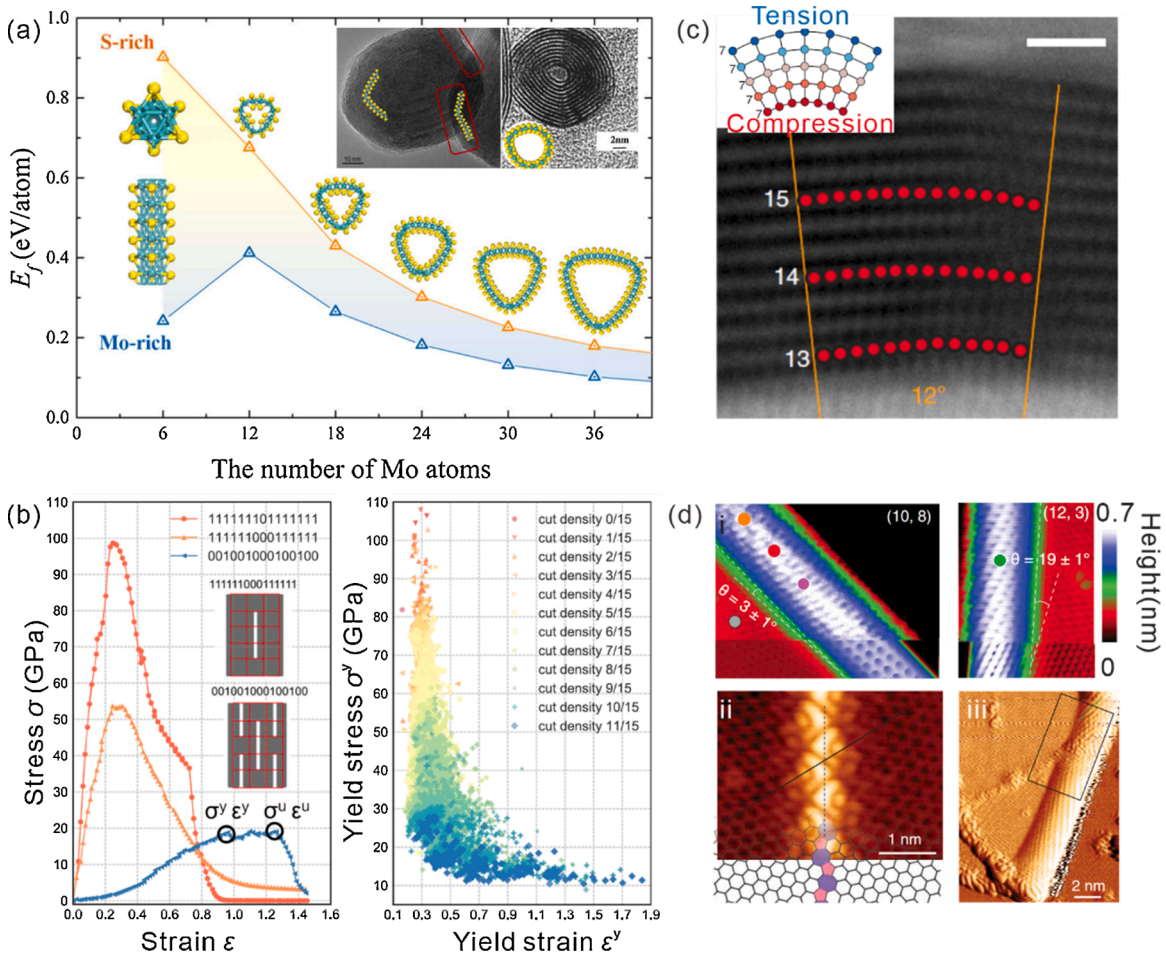

Fig. 17. Novel inverse designs. (a) The simulation of the evolution of MoS_2 nanotube in S-rich (orange dots) and Mo-rich (blue dots) environments [171]. (b) Accelerated search and design of stretchable graphene kirigami using machine learning according to the diverse kirigami patterns with different cut density, and the corresponding stress-strain curves [172]. (c) Atomically bending mechanism in few-layer graphene shown in bright-field STEM image and inserted schematic illustration [173]. Scale bar, 1 nm. (d) Atomically precise nano-origami toward the custom-design of graphene nanostructures, like (i) tubular carbon structures with tunable chirality, and (iii) intramolecular junctions formed by (ii) bicrystal graphene nanoisland [32]. (For interpretation of the references to colour in this figure legend, the reader is referred to the web version of this article).

in Fig. 17d(i) [32]. In this case, the graphene nanoisland (GNI) was folded using the STM tip to produce tubular part like the nanotube with tunable chirality. Fig. 17d(ii) shows the distinct grain boundary of a bicrystal GNI, which can be folded to create a fascinating intramolecular junction (Fig. 17d(iii)) via STM origami. These kinds of folded graphene nano-origami structures may also provide ideal design platforms to investigate the coupling effect that exists between their flat twisted and curved folded parts. Moreover, this design approach allows to investigate the important frontier physical concepts such as superconductivity in magic twist angle graphene, which can be studied in combination with the properties of attached nanotubes or intramolecular junctions.

6. Applications

The unprecedented ability to design and engineer the properties of 3D-assembled 2D materials opens up enormous opportunities for intriguing applications in various fields like flexible electronics, energy harvesters, sensors, actuators, robotics, and metamaterials. The unique geometries and enhanced performance of the 3D structures available via strain engineering will enable novel devices to be created that are unavailable with conventional planar 2D materials. In this section, we introduce some of the applications and devices that benefit from the use of the superior construction techniques inspired by kirigami/origami.

6.1. Flexible electronics

In recent years, flexible electronics have attracted an increasing amount of attention in the area of advanced electronics, especially in the context of implantable and wearable devices [174]. Naturally, devices intended for use in flexible electronics have totally different requirements imposed on them compared to those used in conventional, rigid applications. That is, they often need to be bendable, stretchable, twistable, and/or foldable [175].

The recent advances in the shaping and structuring of 2D materials to provide routes to assembled 3D functional structures opens up the possibility that 2D materials with favorable intrinsic electrical properties can be transformed to 3D structures with similar or even enhanced electrical properties. As inorganic and organic electronic materials have been successfully employed in flexible electronics in the past, it can be anticipated that the sophisticated design methods available for 2D materials will inspire a multitude of novel micro/nanodevices or even integrated systems. Various attractive characteristics such as durability and high performance in strained states should therefore be deliverable [176].

Fig. 18a shows stretchable micro-supercapacitors fabricated by creating suspended wavy graphene microribbons that are capable of maintaining outstanding electrical performance even when highly stretched [177]. The left panel presents optical and cross-sectional

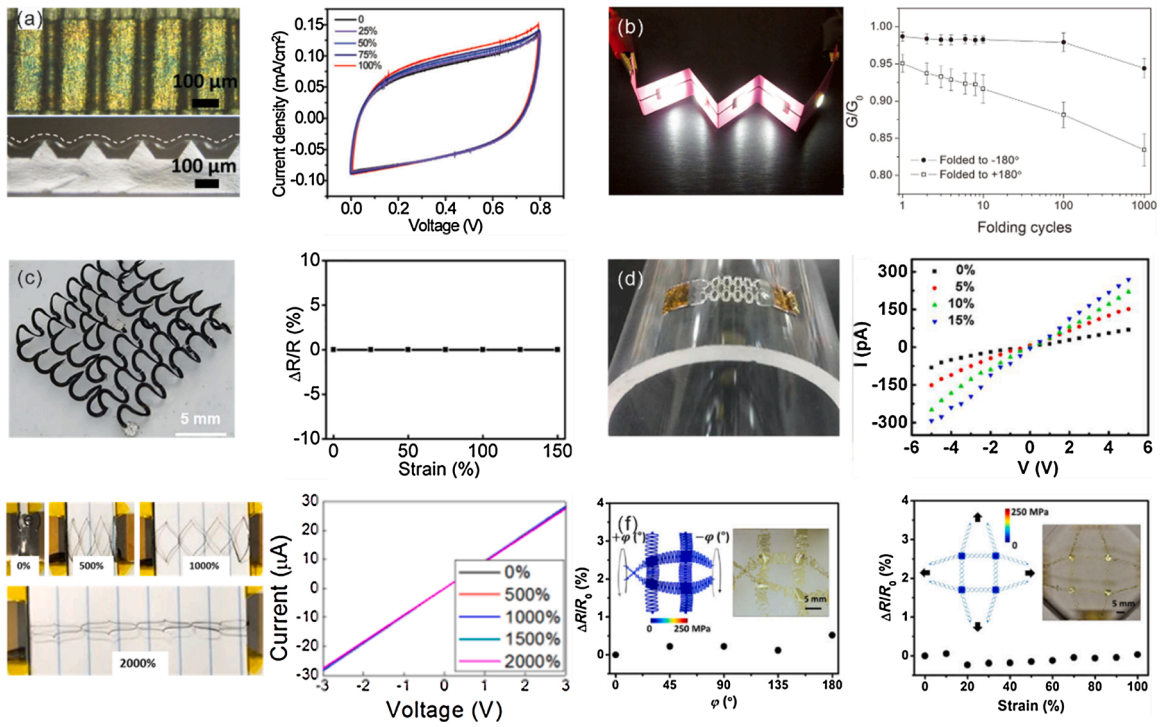

Fig. 18. Flexible electronics. (a) Stretchable micro-supercapacitors based on suspended wavy graphene microribbons with released status and its cross-sectional image (left panel). The current–voltage curves of the micro-supercapacitors in different strains (right panel) [177]. (b) Optical image of a folded graphene-based electronic circuit with an array of LED chips working well under negative and positive angle folding (left panel). The stable relative resistance in folding cycles (right panel) [178]. (c) Optical image of 3D helical coils of cellular graphene with outstanding electromechanical properties (left panel). The nearly invariable resistance at different biaxial tensile strains (right panel) [109]. (d) Optical image of the highly stretchable device adopting MoS_2 kirigami structures on the curved surface (left panel). Enhanced electrical properties and strain-sensing behavior under deformation induced by kirigami structures (right panel) [24]. (e) Optical image of kirigami-inspired 2D $PtSe_2$ layer conductors with 2,000 % stretchability (left panel) and corresponding current–voltage curves under different strains (right panel) [23]. (f) Kirigami-patterned mesh design for strain-insensitive electrical resistance under different twisting angles (left panel) and biaxial strains (right panel) [179].

images that clearly show the wavy geometry of the suspended graphene microribbons in the released state. It is this geometry that allows the material to accommodate a very large tensile strain and thus avoiding the failure of the device in the stretched state. A series of electrical tests demonstrated that the electrical properties of the material were almost invariable under stretching. For instance, the current–voltage curves measured using micro-supercapacitors under different strains (right panel) are nearly identical, confirming that the highly stretchable wavy graphene micro-supercapacitors are ideally suited to application in flexible electronics.

Creating foldable electronic devices is another very important step in many applications. However, the problem of degradation induced by repeated folding is a very challenging aspect in such devices. If the device is to be foldable, then the substrate as well as the conductor must be foldable. For example, Hyun et al. used paper substrates to successfully fabricate foldable electronic circuits made from graphene [178]. Fig. 18b shows a folded graphene-based electronic circuit with an array of LED chips (left panel) which work very well regardless of the direction it is folded in (i.e. positive or negative folding angle). In addition, the relative conductance of the circuit was found to change very little after repeated positive–negative folding cycles (right panel).

Another example is to be found in the 3D helical coils of cellular graphene (Fig. 18c, left panel) that were mentioned earlier [109]. These were constructed using compressive buckling, and their structure made them retain the intrinsic high conductivity even when a large stretchable strain was applied (i.e. they have outstanding electromechanical properties). As shown by the minimal variation in the relative resistance with strain (right panel), the relative resistance is practically unchanged under increasing biaxial tensile strain. This kind of stretchable 3D conductive helical coil can serve as an excellent interconnect for situations where stretching is likely to occur, e.g. between devices located on a flexible curvilinear surface.

Ever since the concept of graphene kirigami was first proposed, the desirable properties (toughness and stretchability) of such kirigami structures have been expected to make them ideal for use in making ‘stretchable’ electrodes [13]. Fig. 18d (left panel) shows an example of a MoS_2 kirigami structure on a curved surface that is highly stretchable due to its kirigami design [24]. The electrical properties of the structure under deformation can be improved by its kirigami design. It was found that the structure’s current–voltage behavior was sensitive to the strain, which suggested a possible application as a strain sensor. Fig. 18d (left panel) shows that the conductivity increased slightly in the 0–5 % strain range but much more dramatically in the 5–15 % strain range. A maximum value of the conductivity was reached when the applied strain increased up to 15 %, after which conductivity decreased as the strain was increased further. The variation observed arised from the deformation behavior of the kirigami-regulated 2D material and also a possible piezoresistive effect.

There are other kirigami-structured 2D materials whose designs have been specifically optimized to make them insensitive to strain. Fig. 18e shows kirigami-inspired conductors made from 2D layers of $PtSe_2$ that have extremely high stretchability [23]. The current–voltage curves recorded under different strains are also shown (right panel). Remarkably, according to stretching tests (left panel), the kirigami-patterned $PtSe_2$ layers were able to maintain their conductivity even when stretched up to 2,000 %.

A device-scale kirigami-patterned mesh design has been recently proposed for graphene sensor devices that incorporates relatively more complex strain states, e.g. biaxial strains and twists [179]. The stable relative resistance measured in the twisted (left panel) and

biaxially-strained (right panel) states are shown in Fig. 18f. The insets show the deformed devices and well-matched strain distributions simulated using finite element analysis (FEA). It was found that the out-of-plane deformation of bridges in kirigami meshes accommodated stress concentrations very well and vastly improved the material's multiaxial stretchability. Kirigami designs are so inspiring that more applications will undoubtedly emerge in the near future that add to the progress made in flexible strain sensors [180] and flexible multifunctional devices [181].

6.2. Energy harvesters

Energy harvesting has long been a topic of interest because of concerns about the need to achieve sustainable development. The research conducted to date has inspired a diverse range of energy harvesting techniques involving various energy sources.

Due to their flexibility and ultrathin nature, deformable 2D materials have been widely used in energy-related applications, e.g. lightweight and adaptive power-supplies for wearable devices [182], origami lithium-ion batteries [183], and surface-textured solar cells [184]. The reshaping of 2D materials not only enlarges the range of the corresponding energy harvesters that can be accessed, but also inspires innovative 3D design schemes that can be used to resolve practical problems in applied devices.

It is clear that 2D materials are well-suited for harvesting energy because of their large specific areas. Meanwhile, reconfiguring 2D materials into 3D form can endow it with additional advantages and functionalities. A typical example is shown in Fig. 19a. In this example, photovoltaic (PV) cells were fabricated using a textured silicon surface and kirigami graphene as the effective transparent electrode [184]. The PV cells thus formed were found to have improved conductivity and power conversion efficiency. Graphene has long been considered as a promising substitute for replacing conventional transparent conductive films (e.g. indium tin oxide). The kirigami strategy is able to achieve conformal mapping of a planar sheet onto a textured 3D surface, thus generating a larger surface area for light harvesting. The upper figure schematically illustrates this central idea (in this hybrid PV cell, the kirigami graphene employed has a cross-pattern to enhance the effective contact between the transparent electrode and a surface that is textured in the form of inverted pyramids). The conformal overlaying of the kirigami graphene on the textured surface is validated by SEM and TEM images presented. The comparison shown in the bottom figure clearly demonstrates that the use of kirigami graphene successfully increases the power conversion efficiency by up to 9.8 %.

Fully utilizing the available sunshine plays a significant role in the harvesting of solar energy. Remarkably, kirigami can be used to help the

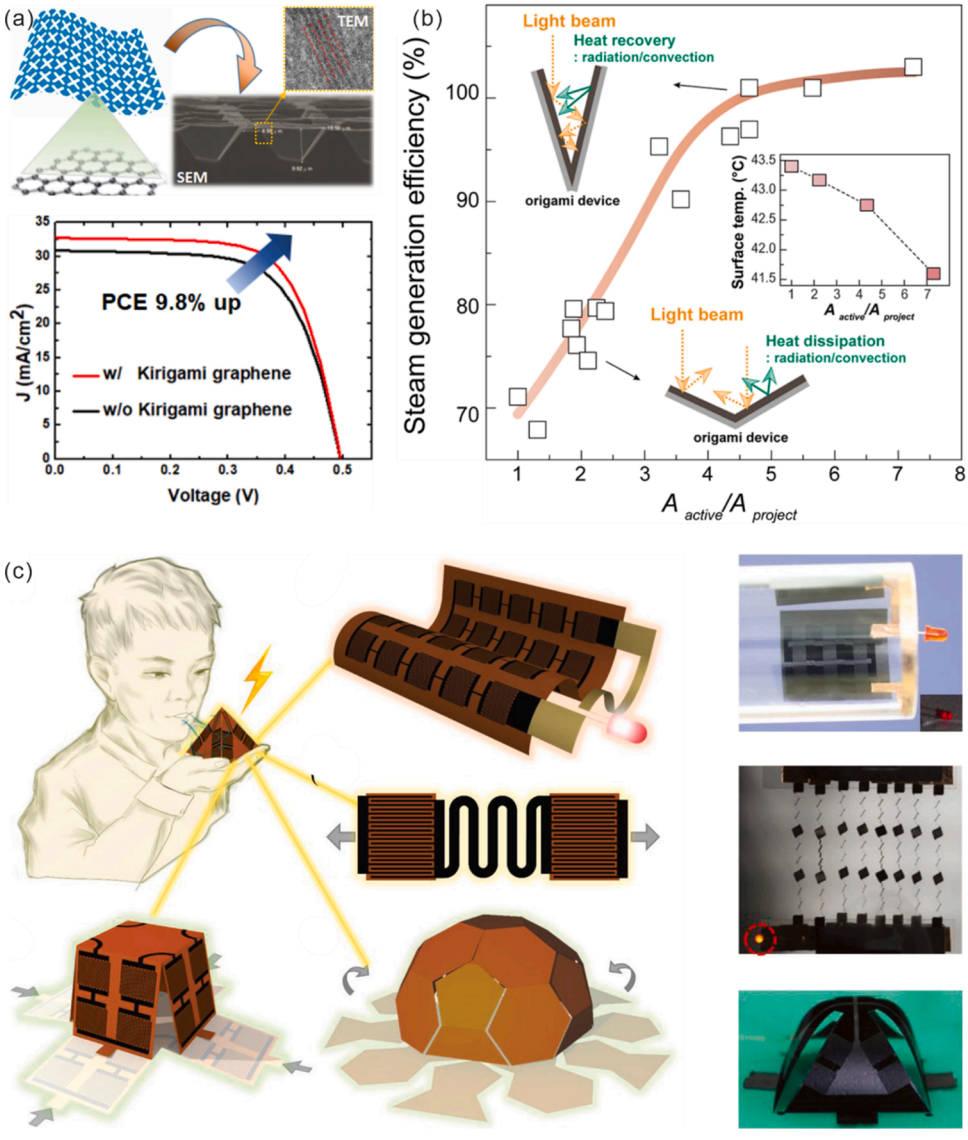

Fig. 19. Energy harvesters. (a) Photovoltaic (PV) cells with textured surface employing the kirigami graphene as the effective transparent electrode for improved conductivity and power conversion efficiency [184]. (b) Graphene oxide composites with origami surface configuration for solar steam generator toward near-full utilization of solar energy [186]. (c) Graphene hydroelectric generators with excellent performance in diverse geometries like rollable, stretchable, and reconfigurable structures [25].

conversion of solar energy [185]. The general idea is to generate solar cells that 'track' the location of the sun without the use of mechanical devices to orient the solar panel. The idea was implemented by cleverly designing a kirigami system of out-of-plane structures that were inherently capable of solar tracking and thus improving the solar harvesting efficiency.

Another approach for light harvesting is to use the light to generate steam. On this basis, a CNT-embedded GO nanocomposite was fabricated with a Miura-ori design to create a deployable 3D origami solar steam generator capable of fully utilizing solar energy [186]. The Miura-ori tessellation structure consists of rigid faces (parallelogram--shaped) formed through a series of folds, producing mountain- and valley-like features. This structure, with its periodic concavity, has an auxetic effect on the reabsorption of heat and thus reduceing energy losses due to radiation and convection. In order to quantify the effect of the origami structure, the efficiency of the steam generator was assessed in relation to a series of structural parameters: area interacting with the light (A_{active}), projected area ($A_{project}$), projection angle (ϕ), and surface areal density ($A_{active}/A_{project}$). Fig. 19b shows the steam generation efficiency and surface temperature (inset) as a function of $A_{active}/A_{project}$. It was observed that the steam generation efficiency increased with the surface areal density, and reached the saturation value at 4.65, which was attributed to the reduction in heat dissipation that occurred due to the enhanced recovery achieved using larger folds. Similar origami designs have also been applied to photothermal materials, which allows more efficient solar energy utilization to be achieved for the distillation of water [187].

The diverse geometries arising from the reshaping of 2D materials can pave the way for more versatile energy harvesters on demand, for instance, in portable or wearable devices [188]. Polypyrrole/graphene-based micro-supercapacitor arrays have been imprinted on paper with interconnects between the origami-folded parts and used for harvesting wind energy [189]. Yang et al. [25] reported a kind of graphene-based hydroelectric generator (GHEG) with excellent performance in a diverse range of geometries that are rollable, stretchable, and reconfigurable, as illustrated schematically in Fig. 19c. In that work, laser processing was used to produce rGO circuits on GO *in situ*. Then, the GO sheets were electrically polarized to produce a gradient of oxygen-containing groups, which led to the formation of an ion concentration gradient in humid conditions, and hence electricity generation [190–192]. Moreover, the GHEGs are mechanically malleable and pliable and can be used for the construction of various structures, thus breaking the inherent limitations existing in conventional rigid structures. The optical images in Fig. 19c show a rolled GHEG, stretchable serpentine bridge-island GHEG, and origami-based GHEG (e.g. pyramid) integrated with LEDs, all of which can operate regularly when triggered by moisture.

6.3. Sensors

To keep up with the rapid rise of interest in smart devices and 'Internet of Things', the mutual interaction between smart devices and the environment, which demands high-performance sensors and even sensor arrays integrated into the system, has been studied intensively. Due to the outstanding sensing capacity of 2D materials (with respect to optoelectrical detection in particular), the rational design of reshaped 2D materials can create surprising sensors that can be utilized in many important fields.

It is well known that nanomembrane microcavities can have a remarkable effect on detection accuracy if advantage is taken of 'whispering-gallery modes' [193,194]. Unfortunately, the fabrication of high-quality rolled-up 2D materials for the construction of ultrasensitive sensors remains challenging. Recently, alternative transfer methods based on conventional nanomembrane microcavities have exhibited

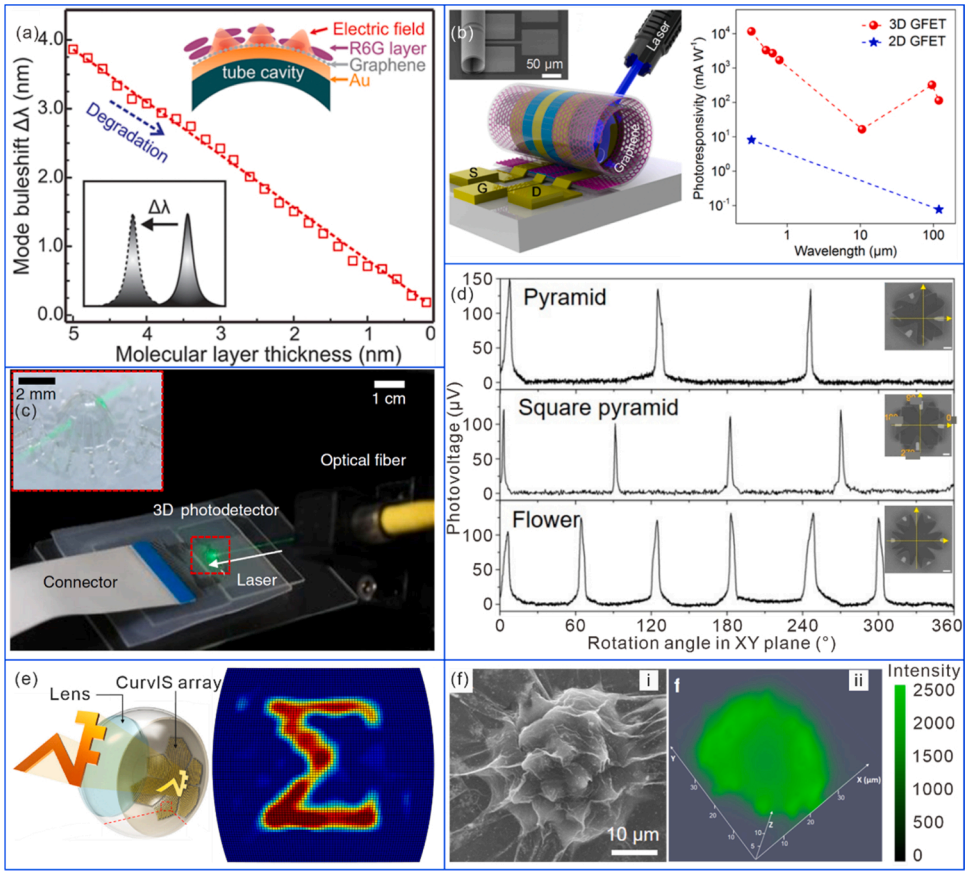

Fig. 20. Sensors. (a) Rolled-up plasmonic nanomembrane cavities with graphene-induced field enhancement effect for photodegradation detection [195]. (b) 3D graphene field-effect transistors with enhanced photoresponsivity and a broad spectral range [196]. (c) Optical images of the 3D photodetection system with 2D materials on the hemispherical surface [21]. (d) SEM images and angular-dependent photovoltage response of the self-folded pyramid, square pyramid, and flower-shaped 3D MoS_2-SU8 photodetectors [14]. (e) Curved image sensor (CurvIS) array based on the MoS_2-graphene heterostructure and the captured image of '∑' [22]. (f) (i) SEM image of hybrid graphene skin wrapping the pollen for 3D biosensing and (ii) 3D surface Raman spectroscopic spatial map for the characterization of spiky features belong to the pollen [197].

preliminary hopes. For example, Fig. 20a shows a rolled-up, gold--coated, nanomembrane cavity covered by the transferred graphene [195]. This sensor was successfully employed to monitor the photodegradation of rhodamine 6 G molecules at a molecular level in real-time. The sensor takes advantage of the coupling between optoplasmonic and graphene-induced field enhancement effects. In addition to promoting the induction of whispering-gallery modes in the metal-coated nanomembrane microcavities, the graphene on the surface is able to effectively enhance the electrical fields involved. Hence, by measuring the resonance shift produced, the photodegradation of the rhodamine 6 G molecules could be accurately monitored in real-time.

Fig. 20b shows a 3D graphene field-effect transistor (GFET) that features enhanced photoresponsivity and broad spectral range [196]. Actually, graphene-based photodetectors generally exhibit broad operation spectra but tend to suffer from poor photosensitivity because of their weak optical absorptivities. However, the tubular nature of the 3D GFET shown facilitates a large increase in the light–matter interaction area. It also promotes the intensity of the optical field via microcavity resonances. Overall, the photosensitivity is remarkably enhanced compared to planar 2D GFETs. Meanwhile, the 3D GFET can operate at high frequencies which can be further elevated using the optimized procedures and may even reach the anticipated terahertz region.

3D architecture can open up access to the enhanced levels of spatial sensing, so that the photodetection or imaging process can yield more information about the orientation of the light detected. Rogers et al. [21] proposed a 3D photodetection/imaging system with the guidance of compressive buckling based on MoS_2, as shown in Fig. 20c. The transparent hemispherical surface of the 3D photodetection system allows that both the intensity and direction of the incident light can be detected by the simultaneous measurement of the entry/exit points of the light. In detail, based on the photoresponse recorded by the photodetectors near the laser, the photocurrent together with the azimuthal and polar angles can be used to interpolate the position of the laser beam.

Fig. 20d shows SEM images and angular-dependent photoresponses from pyramidal, square pyramidal, and flower-shaped 3D MoS_2–SU8 photodetectors which can be used to elucidate the spatial photosensitivity of the origami structures [14]. Through the setting of multiple electrodes according to the structural symmetry, the successive measurement of the photoresponses from structures of different shapes exhibits their own spatially-resolved photovoltaic signals. In addition, the photoresponse detected using a Miura shape was found to be reconfigurable and could be reversibly tuned during folding and unfolding cycles.

The flexible nature of 3D architectures integrating photosensors based on 2D materials means they may play an important role in the development of soft bioelectronic devices (e.g. artificial electronic eyes) which is currently a research hotspot. Fig. 20e illustrates a curved image sensor (CurvIS) array composed of MoS_2–graphene heterostructures with high-density and therefore suitable for use in artificial eye construction [22]. A sigma-shaped image captured by the human-eye inspired soft optoelectronic device is also shown. The device integrates a single lens (like the eye) with the strain-release design of the MoS_2–graphene heterostructures, thus avoiding mechanical failure of the CurvIS array on the concave hemisphere. Furthermore, the imaging process is insensitive to infrared irradiation because of the absorption spectrum of MoS_2. It is also possible that the CurvIS array itself could find application as an implantable retina which would electrically stimulate the optical nerve in response to an optical signal without causing any mechanical damage to the existing retina.

Graphene is considered as an ideal substrate for biosensing applications because of its biocompatibility and Raman-enhanced effect. Furthermore, as graphene can be reshaped, it is very promising for use in 3D biosensing as it can be molded over irregularly-shaped surfaces and provide more information about samples with excellent spatial resolution. For example, a kind of hybrid graphene ‘skin’ was proposed for application in 3D biosensing which exploited the self-folding and encapsulation behavior of the ‘skin’ [197]. Fig. 20f(i) shows SEM image of a pollen grain that was conformally coated with the graphene skin including the spikes (without fracturing the film). The image shown in Fig. 20f(ii) is a spatially-resolved map of the spiky pollen grain obtained using surface-enhanced Raman spectroscopy thanks to the hybrid graphene ‘skin’ which can surround the entire pollen grain.

6.4. Actuators

In the current context, an actuator is a device that generates mechanical locomotion in response to a stimulus from the external environment (rather than transforming the signal for sensing/detection purposes). Combining 2D materials with conventional shape-changing materials (e.g. hydrogels, polymers, etc.), 2D materials can be self-assembled to form 3D architectures, which allows a versatile range of hybrid actuators to be developed to accomplish specific deformations in a reversible manner. This is highly advantageous for the creation of automatic control systems and further applications in advanced robots (discussed in the next subsection).

As already stated, it is the inclusion of the active materials that assists the shaping and structuring of 2D materials used. 2D materials themselves form the material bodies of such actuators and improve their performance.

Light-driven actuators form one of the main groups of actuators conceived so far. Light is an attractive form of stimulus because it can be conveniently applied from afar thus allowing remote control to be realized. The driving force induced by light is generally produced by photothermal effects. For example, the rGO sheets interfaced with elastin-like polypeptides were proposed by Wang et al. [16] to produce nanocomposites with reversible thermal-responsive behavior. These were used to manufacture actuators that could be precisely controlled by the application of near-infrared (NIR) radiation. Based on this actuator, ‘fingers’ of a hydrogel ‘hand’ could be bent by selectively exposing them to NIR light. Besides, a flexible anisotropic actuator was fabricated by combining MoS_2 sheets with a hydrogel [198]. A two-step polymerization method was firstly used to create a thermal-responsive layer (containing MoS_2 as a photothermal transduction agent) and a second temperature-insensitive layer. The mismatch in swelling properties thus produced induced bending when the temperature increased. The anisotropic response of the actuator caused it to bend reversibly under the action of light and even caused the self-wrapping.

As mentioned in Subsection 4.3, graphene-based polymer bilayers can also exhibit photothermal deflection behavior. This has inspired the creation of hinge actuators that can be remotely folded using light, as shown in Fig. 21a [15]. The figure shows a series of hinge actuators fabricated to investigate the relationship between the (controllable) folding angle and (tunable) hinge length. It is shown that the two factors are approximately linearly related. Similar graphene nanocomposite bilayers have been used for actuators in optical switching applications [199].

Bilayers made of GO–polydopamine (PDA) nanocomposite and rGO can also be used to construct photoactuators, driven by the shrinking of the GO upon exposure to NIR light irradiation [18]. In the top panel of Fig. 21b, the bending and unbending of the actuator can be clearly seen as the light is turned on and off sequentially. The bottom panel shows that the folding angle can be programmed by varying the light intensity.

Apart from photothermal actuation, there are many other environmental factors that can effectively stimulate actuators, e.g. pH, humidity, and external fields. Miskin et al. [200] prepared graphene-based bimorphs that could be actuated to induce self-folding. Such an approach can be expected to be a wonderful platform for autonomous origami machines. In addition to their temperature-dependence, the bimorph actuators can produce a sensitive response to the pH of their environment. The top panel in Fig. 21c shows the rapid unfolding of a folded tetrahedron in response to an increase in pH; the lower panel shows the slower sequential folding response to a subsequent lowering

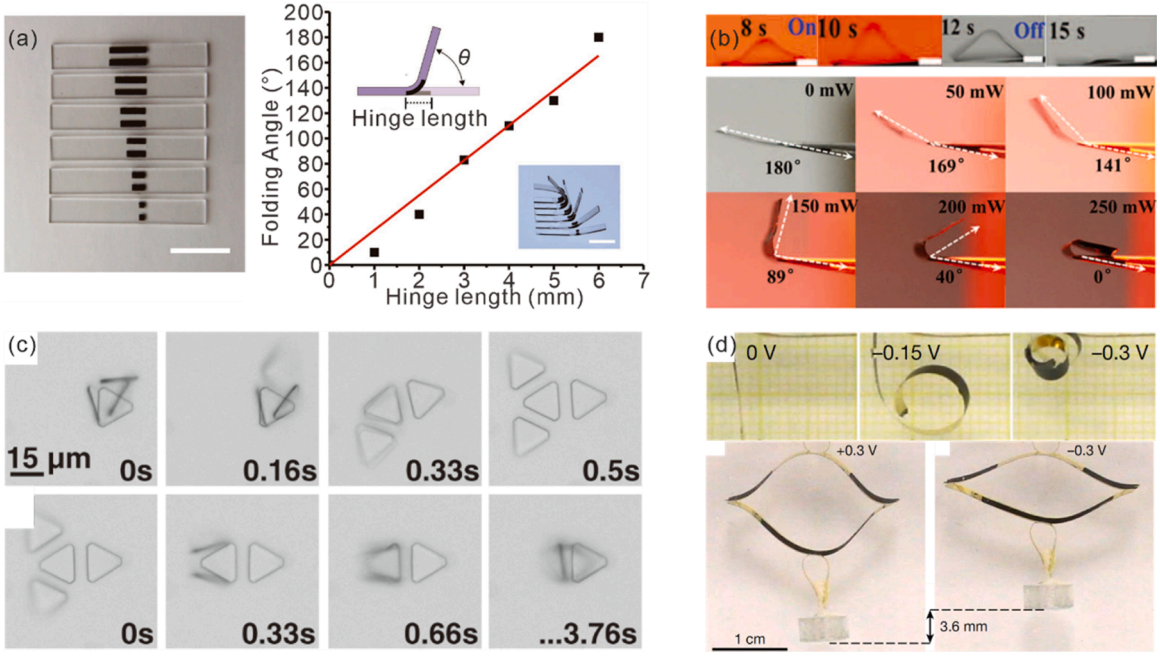

Fig. 21. Actuators. (a) Graphene-based polymer bilayers actuators with remote light controlled folding [15]. All scale bars are 10 mm. (b) GO–PDA/rGO photo-actuators and controlled photothermal actuation upon exposure to NIR light irradiation [18]. All scale bars are 3 mm. (c) Graphene-based bimorphs for the actuator with reversible folding and unfolding responsive to the environmental pH change [200]. (d) MoS_2-based electrochemical actuators with charging triggered rolling and lifting [201].

of pH.

As another example, Fig. 21d shows metallic 1T-MoS_2/Au bimorph actuators that can be triggered by immersing them in electrolyte (or other method of charging) which triggers a response by the intercalation of charged species into the MoS_2 film [201]. The actuators can be used to perform controllable rolling and lifting, and even easily outperform mammalian muscle tissue.

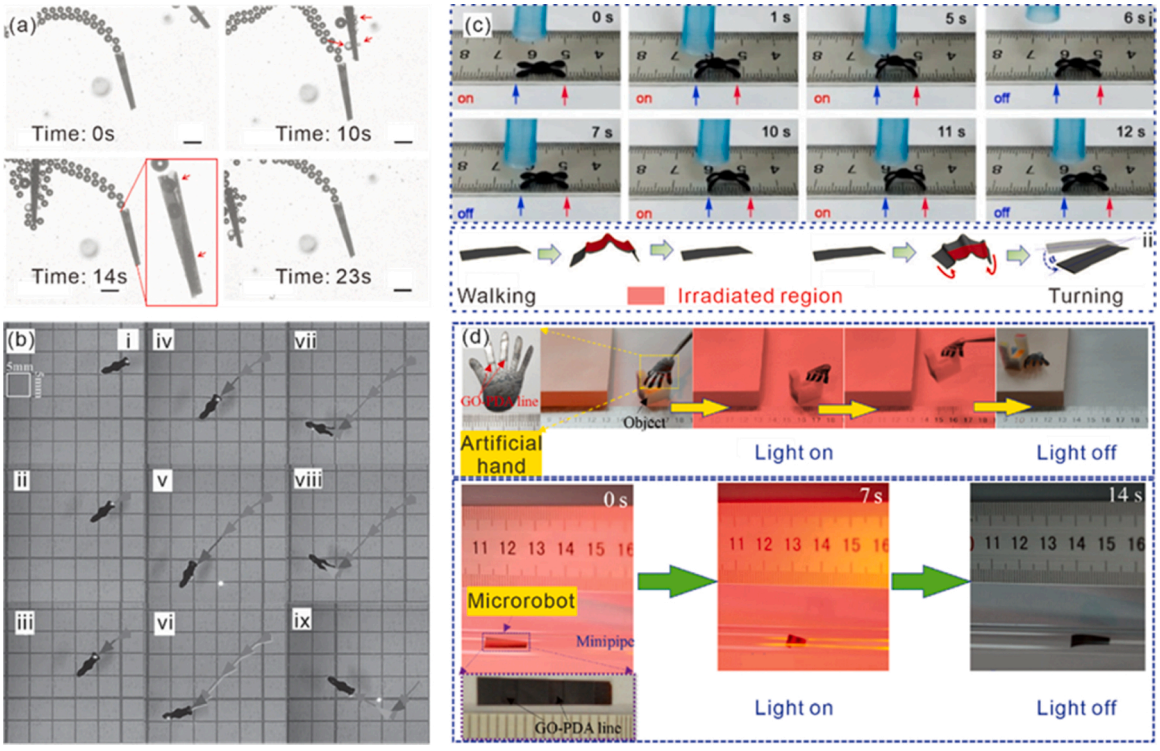

Fig. 22. Micromotors and soft robots. (a) Navigation and oil droplet transport by graphene oxide rolled-up micromotors [17]. Scale bar, 200 μm. (b) Photoresponsive PDMS/graphene nanoplatelets composited layer for soft-robotic design, like microfish with various motions including forward, backward, and turning around [205]. (c) (i) Moving process of moisture-responsive crawler robots actuated by rGO/GO film [207]. (ii) Origami-inspired self-walking robot with crawling and turning mode driven by selectively light irradiation [18]. (d) Artificial robotic hand and moving microrobot under NIR/laser control [18].

6.5. Micromotors and soft robots

The actuation performance of reshaped 2D materials suggests these new materials can be used to drive smart and autonomous modes of manipulation in robotic systems. As such, they may well play a useful role in the manufacturing of multifunctional robots. It is noteworthy that a myriad of robot-like morphologies can be assembled from 2D materials using origami. Thus, it is possible to take advantage of such fabrication methods to ensure that the biomimetic structures produced have sufficient structural flexibility and rigidity, which is particularly important in the emergent field of 'soft robots' [31,202].

On the other hand, the reshaped 3D geometries exhibit the unique advantages for the robotic applications. For instance, one of the most significant applications for rolled-up nanomembranes is the creation of tubular micromotors. These motors are devised as tubular cavities that can undergo catalytic self-propulsion. They can thus serve as motors to propel microrobots in many different fascinating applications in environmental science, biomedicine, and biosensors [203].

A facile method of fabricating micromotors from rolled-up GO sheets, in which wax-printed paper was utilized to allow the shape and size of the motors to be tuned depending on the scrolling path and oxidation extent, was presented by Baptista-Pires et al. [17]. A catalytic coating of platinum was successfully used to propel the rolled-up GO micromotors in H_2O_2 solution (the catalyst facilitates the release of oxygen bubbles from the inner cavity). As a proof of concept, oil droplets in water were collected and transported using the rolled-up GO micromotors (Fig. 22a), which experienced the navigation process driven by the hydrophobicity of the GO. Besides, the similar micromotors made from monolayer graphene were also found to have fast moving speed and interesting antibacterial properties [204].

Fig. 22b shows a biomimetic soft-robotic 'microfish' that can be photothermally deflected using NIR light irradiation, producing a variety of different motions: forwards (i–iii), backwards (iv–vi), and turning (vii–ix) [205]. In this case, a bilayer platform consisting of a composited layer of PDMS/graphene nanoplatelets and a pristine PDMS layer was used. Primarily driven by different coefficients of thermal expansion (CTE) and Young's modulus mismatch in the bilayer, the response of the microfish to NIR light irradiation was very fast (e.g. the platform could be deflected about 1500 μm within 3.4 s). The fact that the remote-controlled microfish swimmer could be moved with some agility suggests that this approach has great potential for drug delivery and creation of biomedical robots.

Artificial muscle is particularly challenging in the design of biomimetic robots. However, it is an essential component, which plays a critical role in facilitating complex maneuvers. Unfortunately, conventional motorized systems consist of many actuators with judicious division of function and appropriate conjunction. This naturally multiplies the complexity and difficulty of the problem. To surmount this barrier, Han et al. [206] proposed an integrated artificial muscle for biomedical robots that uses gold nanorods embedded in GO (AuNRs@GO) and PMMA. The artificial muscle is driven by light without the required joints. A robotic spider and artificial hand were fabricated to demonstrate the manipulation capabilities of the muscle. The response of the muscle could also be selected according to the wavelength of the light used (due to the plasmonic responses of AuNRs of different sizes), thus allowing the complexity of the response to be further increased.

As mentioned above, rGO/GO bilayers provide an excellent platform for fabricating actuators and have therefore been the inspiration behind many stimulus-sensitive robots. Fig. 22c(i) shows a moisture-sensitive rGO/GO crawler robot resembling a four-legged insect that moves forward or stops in response to the switching on/off of the humidity [207]. Similar crawler robots can be fabricated using rGO-based hydrogel and execute the four-stage motion as follows: (1) apply the laser to the back end of the crawler to initiate folding; (2) in response, the gel curls under the crawler at that specific site; (3) as the gel uncurls, the force from the back end drives the front end forwards; (4) the gel returns to its original state and the crawler has moved forwards a short distance [16]. Fig. 22c (ii) shows an origami-inspired self-walking robot that features more programmable locomotion modes including crawling and turning [18]. In this case, rGO sheets were utilized as substrates and lines of GO–PDA created thereon to induce localized bending when irradiated by NIR light. The creative use of GO–PDA lines allows more versatile robotic applications to be devised, such as the artificial robotic hand and a worm-like microrobot shown in Fig. 22d. The hand was able to have a large carry load compared to itself and the motion of the microrobot inside a minipipe could be controlled remotely using NIR/laser light irradiation.

6.6. Mechanical/optical metamaterials

With artificial properties that are hardly ever found in naturally existing materials, metamaterials have emerged as one of the most popular categories of materials designed and conceptualized in various interdisciplinary fields of study. The intrinsic mechanical superiority of 2D materials can be engineered using exotic kirigami/origami reshaping techniques to create various mechanical metamaterials with unusual and desirable mechanical, and even shape-morphing, properties [208–210]. In addition, the sophisticated 3D configurations created may permit electromagnetic waves to be manipulated in special ways and thus enabling novel photonic functionality to be achieved.

Ever since its first conception, graphene kirigami has been suggested to be a promising approach to building mechanical metamaterials, Fig. 23a shows a typical example: a stretchable graphene kirigami spring made by 3D reconstruction [13]. By varying the design of the pattern of cuts, graphene kirigami can be used to develop more interesting structures for the creation of mechanical metamaterials. For instance, it has been shown that graphene kirigami can be used to create auxetic structures consisting of periodic reentrant honeycombs that possess negative Poisson's ratios [211,212]. Fig. 23b shows a practical realization of this kind of behavior based on photothermal actuators made from wavy strips of GO–cellulose bilayers [20]. The two designs shown correspond to mechanical metamaterials possessing an ultra-positive Poisson's ratio (Fig. 23b(i), (ii)) and negative Poisson's ratio (Fig. 23b (iii), (iv)), respectively. In both cases, four of the wavy strips were bonded together at periodic contact points. When the design shown in Fig. 23b(i) was exposed to NIR light irradiation, the structure experienced a slight lateral expansion and large transverse contraction corresponding to a very large and positive Poisson's ratio (Fig. 23b(ii)). In contrast, the structure with additional solid paper formed a reentrant honeycomb lattice, as shown in Fig. 23b(iii). When this structure was irradiated, it expanded in the transverse direction and so the corresponding Poisson's ratio was negative (Fig. 23b(iv)).

Although the strain engineering of 2D materials has experienced rapid advances, the corresponding progress in fabricating functionalized metamaterials in a true sense is still relatively slow, since it is very difficult to devise and fabricate the artificial designs required. Nevertheless, some intriguing proofs of concept have sprung up over recent years which show that functionalized metamaterials can indeed be produced by assembling shaped and structured 2D materials. For example, simulations of graphene origami structures assembled using surface functionalization recently demonstrated that they exhibit coefficients of thermal expansion that can be tuned across a very broad range (from negative to positive) [213,214].

Fig. 23c(i) shows SEM image of an exceptional optical metamaterial based on a sheet of MoS_2 which was strain-textured using a SiO_2 nanocone array, thus essentially forming an optoelectronic crystal of artificial atoms [19]. The other images shown are scanning photoluminescence maps plotting: (ii) the wavelength, and (iii) the peak intensity of the photoluminescence, which reveal the strained nature of the MoS_2 film. The strain induced by the underlying nanopattern can produce a remarkable modulation in the electronic structure of the MoS_2 superlattice. As a result, the adsorption bandwidth increases from 677

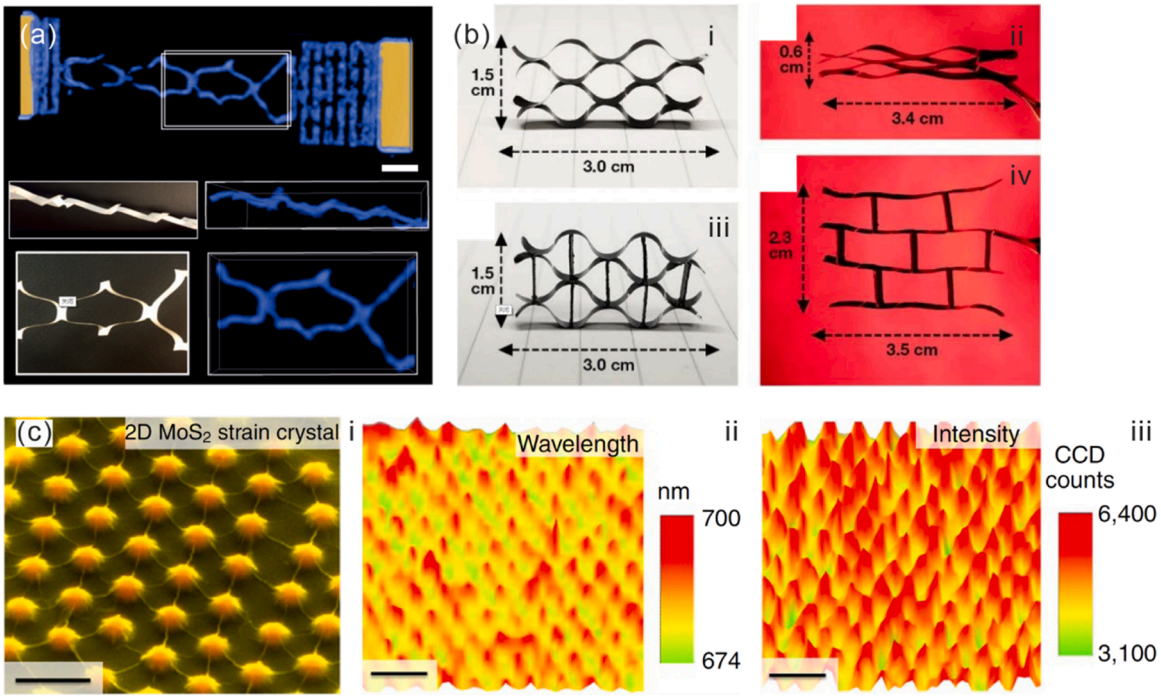

Fig. 23. Mechanical/optical metamaterials. (a) Graphene kirigami inspired stretchable springs [13]. Scale bar, 10 μm. (b) GO-based kirigami structures enabling mechanical metamaterials with ultra-positive (i, original structure; ii, after NIR light irradiation) and negative Poisson's ratio (iii, original structure; iv, NIR light irradiation) [20]. (c) Optoelectronic crystal of artificial atoms in (i) strain-textured MoS_2 (scale bar, 500 nm) and scanning PL maps with (ii) wavelength and (iii) peak intensity (scale bar, 1 μm) [19].

nm (unstrained MoS_2) to 905 nm (most-strained MoS_2) and the metamaterial is endowed with unprecedented strain-textured artificial optical properties.

7. Summary and outlook

In this review, we have summarized the recent progress in the shaping and structuring of 2D materials via kirigami and origami. Some emphasis has been placed on how the desired 3D architectures can be assembled from 2D materials using various strategies, as well as their engineered properties and promising applications. While kirigami/origami assembly strategy has been maturely applied to conventional functional materials, the new regime of 2D materials kirigami/origami still demands more efforts on the detailed investigation at nanoscale. Nevertheless, this nascent field have shown vigorous vitality and creativity, thus exerting a profound effect on the development of cutting-edge researches, e.g. quantum physic, shapeable microelectronics, smart nanorobots, etc.

From the perspective of mechanical properties, the feasibility of shaping and structuring 2D materials has been discussed in terms of their unique mechanical behavior and deformation modes. However, atomically thin 2D materials are easily susceptible to the mechanical stress and chemical environment, which may bring the concern about the stability of both 2D materials themselves and the desired kirigami/origami structures. Although reshaping such materials introduces new degrees of freedom that can be exploited, the fabrication processes are often very challenging. The kirigami/origami approaches, for example, have inspired many assembly/structuring techniques to be devised to achieve the rolling, folding, wrinkling, and buckling of 2D materials in response to internal stresses and external stimuli. The combination of structural construction and lattice deformation has opened up enormous opportunities for the macroscopic integration and strain engineering of 2D materials. It has also allowed a deeper insight to be gained in several areas of frontier science through the leveraging of customized nanostructures.

Many novel 3D functional structures have been designed using 2D materials by following simple geometric and mechanical principles. As the designs have become miniaturized down to nanoscale dimensions, a refreshing new understanding of atomic mechanisms has started to see the dawn. A wide range of compelling applications has subsequently been proposed that covers various fields of study (flexible electronics, energy harvesters, sensors, actuators, robotics, and metamaterials). This progress is paving the way for the next generation of high-performance microelectronic devices and highly-integrated multifunction smart systems.

The ancient papercraft techniques of kirigami and origami have inspired various ways of engineering materials and achieving deterministic assembly in recent years, thus facilitating the construction of various complex 3D structures from 2D materials during the present developmental stages. Although an elementary framework for shaping and structuring 2D materials using kirigami and origami has gradually been established, the researches involved are still at their early stages and there are numerous challenges and limitations that still need to be overcome.

Firstly, graphene and its related derivatives are the main materials used to assemble objects – only rarely are 3D structures fabricated using other 2D materials. More general assembly schemes are needed that offer the option to choose 2D materials used so that the properties of the 3D structures created can be endowed with superior mechanical properties and specialized functionality. Currently, the fabrication methods available differ according to the material platform and assembly strategy used. They thus exhibit their own inherent limitations and drawbacks. On the other hand, universal assembly methods will be rather difficult to exploit under the complex range of circumstances possible. Therefore, more attention should be paid to explore proper methods aimed at key applications, especially with respect to making them more efficient and convenient to use.

Secondly, the scalability and controllability of the fabrication methods are of critical importance when reshaping 2D materials. Up to now, nano-origami using 2D materials remains challenging and is not

conducive for massive fabrication. It is necessary to gain a more thorough knowledge of the atomic mechanisms involved and better (more precise) methods of manipulation. Meanwhile, more complex 3D mesostructures or hybrid systems of as-assembled 2D materials should be developed for a wide range of innovative applications. In this case, the focus should be on inverse design and mechanical principles.

Thirdly, the stability of 2D materials kirigami/origami schemes remains poorly explored. For the pursuit of improved yield and reproducibility, more efforts need to exert on the physical mechanisms of material damage and structure failure associated with multi-step fabrication process since 2D materials are always atomically thin and very vulnerable. Due to the large specific surface areas and high chemical reactivity of 2D materials, the chemicals introduced during the fabrication (e.g. chemical etchant, photoresist) may cause the contamination or damage to the materials used. Furthermore, some intrinsically instable 2D materials like black phosphorus will readily degrade even in ambient atmosphere, which further restricts the enrichment of the candidate materials. Therefore, it is still challenging to optimize the compatible 2D materials and chemical environment involved to avoid the harsh damage. Beyond the chemical failure, the potential fracture or distortion induced by mechanical stress are common in the delicate assembly process. The rational design of both 2D patterns and strain distribution is significant to the availability and stability of target 3D structures, while the inappropriate strain will lead to the deviation of deformation path or even fracture. Therefore, the threshold strain of 2D materials or hybrid system used is critical to the structural stability. The poor performance of the free-standing nature also easily induces the collapse of 3D structures, thus requiring the specific treatment, e.g. supercritical drying after the wet release.

In summary, the challenges that currently exist in the research area of shaping and structuring 2D materials are also stimulating precious opportunities. Likely future research directions include the followings:

(i) Generation of massive, scalable, and versatile fabrication methods for shaping and structuring 2D materials with diverse 2D starting materials beyond graphene. Attempts should also be made to extend the driving methods utilizing more common and effective sources such as electric or magnetic fields.
(ii) Creation of novel nanoscale/atomically-precise methods to architect novel nanostructures based on 2D materials. This should provide new pathways to build suitable platforms for frontier physics investigations and envision proof-of-concept prototype quantum devices, and even machines.
(iii) Using advanced analytical models and computer-aided design (CAD) methodologies to derive new rigorous design schemes, including both the inverse design and validation.
(iv) Constructing complex 3D hierarchical structures of 2D materials with excellent mechanical stability and novel functionality. The structures should be optimized and strain engineering needs to be designed to improve their performance in order to create next-generation multifunctional micro/nanodevices. This can also be conducted in combination with the use of vdW heterostructures and heterogeneous integration.
(v) Converting prototype 3D functional structures made from 2D materials into the critical components needed to create the desired nanoelectromechanical systems (NEMs), as well as developing on-chip and system-level integration strategies.

Declaration of Competing Interest

The authors declare that they have no known competing financial interests or personal relationships that could have appeared to influence the work reported in this paper.

Acknowledgements

The authors thank Key Research Project of Frontier Science, Chinese Academy of Sciences (QYZDB-SSW-JSC021), Science and Technology Innovation Action Plan of Shanghai Science and Technology Committee (20501130700), National Science and Technology Major Project (2016ZX02301003), National Natural Science Foundation of China (Grant No. 51925208, 61974157, 61851401), Strategic Priority Research Program (B) of the Chinese Academy of Sciences (XDB30030000), Science and Technology Commission of Shanghai Municipality (19JC1415500).

Appendix A. Supplementary data

Supplementary material related to this article can be found, in the online version, at doi:https://doi.org/10.1016/j.mser.2021.100621.

References

[1] K.S. Novoselov, D. Jiang, F. Schedin, T.J. Booth, V.V. Khotkevich, S.V. Morozov, A.K. Geim, Proc. Natl. Acad. Sci. U.S.A. 102 (2005) 10451–10453, https://doi.org/10.1073/pnas.0502848102.
[2] S.Z. Butler, S.M. Hollen, L. Cao, Y. Cui, J.A. Gupta, H.R. Gutiérrez, T.F. Heinz, S. S. Hong, J. Huang, A.F. Ismach, E. Johnston-Halperin, M. Kuno, V.V. Plashnitsa, R.D. Robinson, R.S. Ruoff, S. Salahuddin, J. Shan, L. Shi, M.G. Spencer, M. Terrones, W. Windl, J.E. Goldberge, ACS Nano 7 (2013) 2898–2926, https://doi.org/10.1021/nn400280c.
[3] G.R. Bhimanapati, Z. Lin, V. Meunier, Y. Jung, J. Cha, S. Das, D. Xiao, Y. Son, M. S. Strano, V.R. Cooper, L. Liang, S.G. Louie, E. Ringe, W. Zhou, S.S. Kim, R. R. Naik, B.G. Sumpter, H. Terrones, F. Xia, Y. Wang, J. Zhu, D. Akinwande, N. Alem, J.A. Schuller, R.E. Schaak, M. Terrones, J.A. Robinson, ACS Nano 9 (2015) 11509–11539, https://doi.org/10.1021/acsnano.5b05556.
[4] C. Tan, X. Cao, X.-Jun Wu, Q. He, J. Yang, X. Zhang, J. Chen, W. Zhao, S. Han, G.-H. Nam, M. Sindoro, H. Zhang, Chem. Rev. 117 (2017) 6225–6331, https://doi.org/10.1021/acs.chemrev.6b00558.
[5] M.A. Bissett, M. Tsuji, H. Ago, Phys. Chem. Chem. Phys. 16 (2014) 11124–11138, https://doi.org/10.1039/C3CP55443K.
[6] R. Roldán, A. Castellanos-Gomez, E. Cappelluti, Francisco Guinea, J. Phys. Condens. Matter 27 (2015), 313201, https://doi.org/10.1088/0953-8984/27/31/313201.
[7] S. Deng, A.V. Sumant, V. Berry, Nano Today 22 (2018) 14–35, https://doi.org/10.1016/j.nantod.2018.07.001.
[8] D. Karnaushenko, T. Kang, V.K. Bandari, F. Zhu, O.G. Schmidt, Adv. Mater. 32 (2019), 1902994, https://doi.org/10.1002/adma.201902994.
[9] J. Annett, G.L.W. Cross, Nature 535 (2016) 271–275, https://doi.org/10.1038/nature18304.
[10] X. Zhou, Z. Tian, H.J. Kim, Y. Wang, B. Xu, R. Pan, Y.J. Chang, Z. Di, P. Zhou, Y. Mei, Small 15 (2019), 1902528, https://doi.org/10.1002/smll.201902528.
[11] K.-M. Hu, Y.-Q. Liu, L.-W. Zhou, Z.-Y. Xue, B. Peng, H. Yan, Z.-F. Di, X.-S. Jiang, G. Meng, W.-M. Zhang, Adv. Funct. Mater. (2020), 2003273, https://doi.org/10.1002/adfm.202003273.
[12] S. Lim, H. Luan, S. Zhao, Y. Lee, Y. Zhang, Y. Huang, J.A. Rogers, J.-H. Ahn, Adv. Mater. (2020), 2001303, https://doi.org/10.1002/adma.202001303.
[13] M.K. Blees, A.W. Barnard, P.A. Rose, S.P. Roberts, K.L. McGill, P.Y. Huang, A. R. Ruyack, J.W. Kevek, B. Kobrin, D.A. Muller, P.L. McEuen, Nature 524 (2015) 204–207, https://doi.org/10.1038/nature14588.
[14] W. Xu, T. Li, Z. Qin, Q. Huang, H. Gao, K. Kang, J. Park, M.J. Buehler, J. B. Khurgin, D.H. Gracias, Nano Lett. 19 (2019) 7941–7949, https://doi.org/10.1021/acs.nanolett.9b03107.
[15] Z. Tang, Z. Gao, S. Jia, F. Wang, Y. Wang, Adv. Sci. 4 (2017), 1600437, https://doi.org/10.1002/advs.201600437.
[16] E. Wang, M.S. Desai, S.-W. Lee, Nano Lett. 13 (2013) 2826–2830, https://doi.org/10.1021/nl401088b.
[17] L. Baptista-Pires, J. Orozco, P. Guardia, A. Merkoçi, Small 14 (2018), 1702746, https://doi.org/10.1002/smll.201702746.
[18] J. Mu, C. Hou, H. Wang, Y. Li, Q. Zhang, M. Zhu, Sci. Adv. 1 (2015), e1500533, https://doi.org/10.1126/sciadv.1500533.
[19] H. Li, A.W. Contryman, X. Qian, S.M. Ardakani, Y. Gong, X. Wang, J.M. Weisse, C. H. Lee, J. Zhao, P.M. Ajayan, J. Li, H.C. Manoharan, X. Zheng, Nat. Commun. 6 (2015) 7381, https://doi.org/10.1038/ncomms8381.
[20] D. Gao, M.-F. Lin, J. Xiong, S. Li, S.N. Lou, Y. Liu, J.-H. Ciou, X. Zhou, P.S. Lee, Nanoscale Horiz. 5 (2020) 730–738, https://doi.org/10.1039/c9nh00719a.
[21] W. Lee, Y. Liu, Y. Lee, B.K. Sharma, S.M. Shinde, S.D. Kim, K. Nan, Z. Yan, M. Han, Y. Huang, Y. Zhang, J.-H. Ahn, J.A. Rogers, Nat. Commun. 9 (2018) 1417, https://doi.org/10.1038/s41467-018-03870-0.
[22] C. Choi, M.K. Choi, S. Liu, M.S. Kim, O.K. Park, C. Im, J. Kim, X. Qin, G.J. Lee, K. W. Cho, M. Kim, E. Joh, J. Lee, D. Son, S.-H. Kwon, N.L. Jeon, Y.M. Song, N. Lu, D.-H. Kim, Nat. Commun. 8 (2017) 1664, https://doi.org/10.1038/s41467-017-01824-6.

[23] E. Okogbue, S.S. Han, T.-J. Ko, H.-S. Chung, J. Ma, M.S. Shawkat, J.H. Kim, J. H. Kim, E. Ji, K.H. Oh, L. Zhai, G.-H. Lee, Y. Jung, Nano Lett. 19 (2019) 7598–7607, https://doi.org/10.1021/acs.nanolett.9b01726.

[24] W. Zheng, W. Huang, F. Gao, H. Yang, M. Dai, G. Liu, B. Yang, J. Zhang, Y.Q. R. Fu, X. Chen, Y. Qiu, D. Jia, Y. Zhou, P. Hu, Chem. Mater. 30 (2018) 6063–6070, https://doi.org/10.1021/acs.chemmater.8b02464.

[25] C. Yang, Y. Huang, H. Cheng, L. Jiang, L. Qu, Adv. Mater. 31 (2019), 1805705, https://doi.org/10.1002/adma.201805705.

[26] T. Xu, D. Yang, Z. Fan, X. Li, Y. Liu, C. Guo, M. Zhang, Z.-Z. Yu, Carbon 152 (2019) 134–143, https://doi.org/10.1016/j.carbon.2019.06.005.

[27] L. Xu, T.C. Shyu, N.A. Kotov, ACS Nano 11 (2017) 7587–7599, https://doi.org/10.1021/acsnano.7b03287.

[28] J.J. Park, P. Won, S.H. Ko, Int. J. Precis. Eng. Manuf.-Green Tech. 6 (2019) 147–161, https://doi.org/10.1007/s40684-019-00027-2.

[29] S. Chen, J. Chen, X. Zhang, Z.-Y. Li, J. Li, Light Sci. Appl. 9 (2020) 75, https://doi.org/10.1038/s41377-020-0309-9.

[30] X. Ning, X. Wang, Y. Zhang, X. Yu, D. Choi, N. Zheng, D.S. Kim, Y. Huang, Y. Zhang, J.A. Rogers, Adv. Mater. Interfaces 5 (2018), 1800284, https://doi.org/10.1002/admi.201800284.

[31] D. Rus, M.T. Tolley, Nat. Rev. Mater. 3 (2018) 101–112, https://doi.org/10.1038/s41578-018-0009-8.

[32] H. Chen, X.L. Zhang, Y.-Y. Zhang, D. Wang, D.-L. Bao, Y. Que, W. Xiao, S. Du, M. Ouyang, S.T. Pantelides, H.-J. Gao, Science 365 (2019) 1036–1040, https://doi.org/10.1126/science.aax7864.

[33] B. Zhao, Z. Wan, Y. Liu, J. Xu, X. Yang, D. Shen, Z. Zhang, C. Guo, Q. Qian, J. Li, R. Wu, Z. Lin, X. Yan, B. Li, Z. Zhang, H. Ma, B. Li, X. Chen, Y. Qiao, I. Shakir, Z. Almutairi, F. Wei, Y. Zhang, X. Pan, Y. Huang, Y. Ping, X. Duan, X. Duan, Nature 591 (2021) 385–390, https://doi.org/10.1038/s41586-021-03338-0.

[34] D. Akinwande, C.J. Brennan, J.S. Bunch, P. Egberts, J.R. Felts, H. Gao, R. Huang, J.-S. Kim, T. Li, Y. Li, K.M. Liechti, N. Lu, H.S. Park, E.J. Reed, P. Wang, B. I. Yakobson, T. Zhang, Y.-W. Zhang, Y. Zhou, Y. Zhu, Extreme Mech. Lett. 13 (2017) 42–77, https://doi.org/10.1016/j.eml.2017.01.008.

[35] X. Li, M. Sun, C. Shan, Q. Chen, X. Wei, Adv. Mater. Interfaces 5 (2018), 1701246, https://doi.org/10.1002/admi.201701246.

[36] J.H. Kim, J.H. Jeong, N. Kim, R. Joshi, G.-H. Lee, J. Phys. D Appl. Phys. 52 (2019), 083001, https://doi.org/10.1088/1361-6463/aaf465.

[37] C. Lee, X. Wei, J.W. Kysar, J. Hone, Science 321 (2008) 385–388, https://doi.org/10.1126/science.1157996.

[38] G.-H. Lee, R.C. Cooper, S.J. An, S. Lee, Avd. Zande, N. Petrone, A.G. Hammerberg, C. Lee, B. Crawford, W. Oliver, J.W. Kysar, J. Hone, Science 340 (2013) 1073–1076, https://doi.org/10.1126/science.1235126.

[39] C.S. Ruiz-Vargas, H.L. Zhuang, P.Y. Huang, A.M. van der Zande, S. Garg, P. L. McEuen, D.A. Muller, R.G. Hennig, J. Park, Nano Lett. 11 (2011) 2259–2263, https://doi.org/10.1021/nl200429f.

[40] S.P. Koenig, N.G. Boddeti, M.L. Dunn, J.S. Bunch, Nat. Nanotechnol. 6 (2011) 543–546, https://doi.org/10.1038/nnano.2011.123.

[41] S. Bertolazzi, J. Brivio, A. Kis, ACS Nano 5 (2011) 9703–9709, https://doi.org/10.1021/nn203879f.

[42] L. Song, L. Ci, H. Lu, P.B. Sorokin, C. Jin, J. Ni, A.G. Kvashnin, D.G. Kvashnin, J. Lou, B.I. Yakobson, P.M. Ajayan, Nano Lett. 10 (2010) 3209–3215, https://doi.org/10.1021/nl1022139.

[43] N. Jing, Q. Xue, C. Ling, M. Shan, T. Zhang, X. Zhou, Z. Jiao, RSC Adv. 2 (2012) 9124–9129, https://doi.org/10.1039/c2ra21228e.

[44] S.K. Georgantzinos, D.E. Katsareas, N.K. Anifantis, Int. J. Mech. Sci. 55 (2012) 85–94, https://doi.org/10.1016/j.ijmecsci.2011.12.006.

[45] G. López-Polín, C. Gómez-Navarro, V. Parente, F. Guinea, M.I. Katsnelson, F. Pérez-Murano, J. Gómez-Herrero, Nat. Phys. 11 (2015) 26–31, https://doi.org/10.1038/NPHYS3183.

[46] W. Zhou, X. Zou, S. Najmaei, Z. Liu, Y. Shi, J. Kong, J. Lou, P.M. Ajayan, B. I. Yakobson, J.-C. Idrobo, Nano Lett. 13 (2013) 2615–2622, https://doi.org/10.1021/nl4007479.

[47] Z.G. Yu, Y.-W. Zhang, B.I. Yakobson, Nano Lett. 15 (2015) 6855–6861, https://doi.org/10.1021/acs.nanolett.5b02769.

[48] J. Wu, P. Cao, Z. Zhang, F. Ning, S. Zheng, J. He, Z. Zhang, Nano Lett. 18 (2018) 1543–1552, https://doi.org/10.1021/acs.nanolett.7b05433.

[49] N. Ding, C.-M.L. Wu, H. Li, Phys. Chem. Chem. Phys. 16 (2014) 23716–23722, https://doi.org/10.1039/c4cp02521k.

[50] Y. Guo, S. Zhou, J. Zhang, Y. Bai, J. Zhao, 2D Mater. 3 (2016), 025008, https://doi.org/10.1088/2053-1583/3/2/025008.

[51] L. Tapasztó, T. Dumitrică, S.J. Kim, P. Nemes-Incze, C. Hwang, L.P. Biró, Nat. Phys. 8 (2012) 739–742, https://doi.org/10.1038/NPHYS2389.

[52] D.B. Zhang, E. Akatyeva, T. Dumitrică, Phys. Rev. Lett. 106 (2011), 255503, https://doi.org/10.1103/PhysRevLett.106.255503.

[53] M. Zelisko, F. Ahmadpoor, H. Gao, P. Sharma, Phys. Rev. Lett. 119 (2017), 068002, https://doi.org/10.1103/PhysRevLett.119.068002.

[54] R. Nicklow, N. Wakabayashi, H.G. Smith, Phys. Rev. B 5 (1972) 4951–4962, https://doi.org/10.1103/PhysRevB.5.4951.

[55] N. Lindahl, D. Midtvedt, J. Svensson, O.A. Nerushev, N. Lindvall, A. Isacsson, E.E. B. Campbell, Nano Lett. 12 (2012) 3526–3531, https://doi.org/10.1021/nl301080v.

[56] P. Koskinen, O.O. Kit, Phys. Rev. B 82 (2010), 235420, https://doi.org/10.1103/PhysRevB.82.235420.

[57] P. Wang, W. Gao, Z. Cao, K.M. Liechti, R. Huang, J. Appl. Mech. 80 (2013), 040905, https://doi.org/10.1115/1.4024169.

[58] C. Li, Y. Bando, C. Zhi, Y. Huang, D. Golberg, Nanotechnology 20 (2009), 385707, https://doi.org/10.1088/0957-4484/20/38/385707.

[59] A. Castellanos-Gomez, M. Poot, G.A. Steele, H.S.J. van der Zant, N. Agraït, G. Rubio-Bollinger, Adv. Mater. 24 (2012) 772–775, https://doi.org/10.1002/adma.201103965.

[60] X. Chen, C. Yi, C. Ke, Appl. Phys. Lett. 106 (2015), 101907, https://doi.org/10.1063/1.4915075.

[61] G. Wang, Z. Dai, J. Xiao, S. Feng, C. Weng, L. Liu, Z. Xu, R. Huang, Z. Zhang, Phys. Rev. Lett. 123 (2019), 116101, https://doi.org/10.1103/PhysRevLett.123.116101.

[62] P. Jia, W. Chen, J. Qiao, M. Zhang, X. Zheng, Z. Xue, R. Liang, C. Tian, L. He, Z. Di, X. Wang, Nat. Commun. 10 (2019) 3127, https://doi.org/10.1038/s41467-019-11038-7.

[63] P. Zhang, L. Ma, F. Fan, Z. Zeng, C. Peng, P.E. Loya, Z. Liu, Y. Gong, J. Zhang, X. Zhang, P.M. Ajayan, T. Zhu, J. Lou, Nat. Commun. 5 (2014) 3782, https://doi.org/10.1038/ncomms4782.

[64] J. Zhang, J. Zhao, J. Lu, ACS Nano 6 (2012) 2704–2711, https://doi.org/10.1021/nn3001356.

[65] T. Zhang, X. Li, H. Gao, Int J Fract 196 (2015) 1–31, https://doi.org/10.1007/s10704-015-0039-9.

[66] R. Grantab, V.B. Shenoy, R.S. Ruoff, Science 330 (2010) 946–948, https://doi.org/10.1126/science.1196893.

[67] Y. Wei, J. Wu, H. Yin, X. Shi, R. Yang, M. Dresselhaus, Nat. Mater. 11 (2012) 759–763, https://doi.org/10.1038/NMAT3370.

[68] O.V. Yazyev, Y.P. Chen, Nat. Nanotechnol. 9 (2014) 755–767, https://doi.org/10.1038/NNANO.2014.166.

[69] Z. Song, V.I. Artyukhov, B.I. Yakobson, Z. Xu, Nano Lett. 13 (2013) 1829–1833, https://doi.org/10.1021/nl400542n.

[70] Z.D. Sha, S.S. Quek, Q.X. Pei, Z.S. Liu, T.J. Wang, V.B. Shenoy, Y.W. Zhang, Sci. Rep. 4 (2014) 5991, https://doi.org/10.1038/srep05991.

[71] A.W. Robertson, C.S. Allen, Y.A. Wu, K. He, J. Olivier, J. Neethling, A.I. Kirkland, J.H. Warner, Nat. Commun. 3 (2012) 1144, https://doi.org/10.1038/ncomms2141.

[72] T. Zhao, C. Xu, W. Ma, Z. Liu, T. Zhou, Z. Liu, S. Feng, M. Zhu, N. Kang, D.-M. Sun, H.-M. Cheng, W. Ren, Nat. Commun. 10 (2019) 4854, https://doi.org/10.1038/s41467-019-12662-z.

[73] S. Deng, E. Gao, Z. Xu, V. Berry, ACS Appl. Mater. Interfaces 9 (2017) 7812–7818, https://doi.org/10.1021/acsami.6b16175.

[74] C.J. Brennan, J. Nguyen, E.T. Yu, N. Lu, Adv. Mater. Interfaces 2 (2015), 1500176, https://doi.org/10.1002/admi.201500176.

[75] D.A. Sanchez, Z. Dai, P. Wang, A. Cantu-Chavez, C.J. Brennan, R. Huang, N. Lu, Proc. Natl. Acad. Sci. U.S.A. 115 (2018) 7884–7889, https://doi.org/10.1073/pnas.1801551115.

[76] L. Liu, M. Zhou, L. Jin, L. Li, Y. Mo, G. Su, X. Li, H. Zhu, Y. Tian, Friction 7 (2019) 199–216, https://doi.org/10.1007/s40544-019-0268-4.

[77] S. Zhang, T. Ma, A. Erdemir, Q. Li, Mater. Today 26 (2019) 67–86, https://doi.org/10.1016/j.mattod.2018.12.002.

[78] C. Lee, Q. Li, W. Kalb, X.-Z. Liu, H. Berger, R.W. Carpick, J. Hone, Science 328 (2010) 76–80, https://doi.org/10.1126/science.1184167.

[79] X. Wei, Z. Meng, L. Ruiz, W. Xia, C. Lee, J.W. Kysar, J.C. Hone, S. Keten, H. D. Espinosa, ACS Nano 10 (2016) 1820–1828, https://doi.org/10.1021/acsnano.5b04939.

[80] X. Feng, S. Kwon, J.Y. Park, M. Salmeron, ACS Nano 7 (2013) 1718–1724, https://doi.org/10.1021/nn305722d.

[81] X. Cheng, Y. Zhang, Adv. Mater. 31 (2019), 1901895, https://doi.org/10.1002/adma.201901895.

[82] Y. Zhang, F. Zhang, Z. Yan, Q. Ma, X. Li, Y. Huang, J.A. Rogers, Nat. Rev. Mater. 2 (2017) 17019, https://doi.org/10.1038/natrevmats.2017.19.

[83] G. Mao, Q. Wang, Z. Chai, H. Liu, K. Liu, X. Ren, RSC Adv. 7 (2017) 14481–14486, https://doi.org/10.1039/c6ra28482e.

[84] I.D. Barcelos, L.G. Moura, R.G. Lacerda, A. Malachias, Nano Lett. 14 (2014) 3919–3924, https://doi.org/10.1021/nl5012068.

[85] T. Deng, C. Yoon, Q. Jin, M. Li, Z. Liu, D.H. Gracias, Appl. Phys. Lett. 106 (2015), 203108, https://doi.org/10.1063/1.4921530.

[86] W. Xu, Z. Qin, C.-T. Chen, H.R. Kwag, Q. Ma, A. Sarkar, M.J. Buehler, D. H. Gracias, Sci. Adv. 3 (2017), e1701084, https://doi.org/10.1126/sciadv.1701084.

[87] C. Py, P. Reverdy, L. Doppler, J. Bico, B. Roman, C.N. Baroud, Phys. Rev. Lett. 98 (2007), 156103, https://doi.org/10.1103/PhysRevLett.98.156103.

[88] N. Patra, B. Wang, P. Král, Nano Lett. 9 (2009) 3766–3771, https://doi.org/10.1021/nl9019616.

[89] X. Xie, L. Ju, X. Feng, Y. Sun, R. Zhou, K. Liu, S. Fan, Q. Li, K. Jiang, Nano Lett. 9 (2009) 2565–2570, https://doi.org/10.1021/nl900677y.

[90] X. Cui, Z. Kong, E. Gao, D. Huang, Y. Hao, H. Shen, C.-an Di, Z. Xu, J. Zheng, D. Zhu, Nat. Commun. 9 (2018) 1301, https://doi.org/10.1038/s41467-018-03752-5.

[91] U. Mirsaidov, V.R.S.S. Mokkapati, D. Bhattacharya, H. Andersen, M. Bosman, B. Özyilmaz, P. Matsudaira, Lab Chip 13 (2013) 2874–2878, https://doi.org/10.1039/c3lc50304f.

[92] M.F. Reynolds, K.L. McGill, M.A. Wang, H. Gao, F. Mujid, K. Kang, J. Park, M. Z. Miskin, I. Cohen, P.L. McEuen, Nano Lett. 19 (2019) 6221–6226, https://doi.org/10.1021/acs.nanolett.9b02281.

[93] D. Joung, A. Nemilentsau, K. Agarwal, C. Dai, C. Liu, Q. Su, J. Li, T. Low, S. J. Koester, J.-H. Cho, Nano Lett. 17 (2017) 1987–1994, https://doi.org/10.1021/acs.nanolett.6b05412.

[94] D. Xia, Q. Xue, J. Xie, H. Chen, C. Lv, F. Besenbacher, M. Dong, Small 6 (2010) 2010–2019, https://doi.org/10.1002/smll.201000646.

[95] D. Xia, Q. Xue, J. Xie, H. Chen, C. Lv, Comput. Mater. Sci. 49 (2010) 588–592, https://doi.org/10.1016/j.commatsci.2010.05.053.
[96] J. Song, X. Xia, J. Chen, D. Xia, Q. Xue, Q. Li, M. Dong, J. Phys. Chem. C 124 (2020) 10495–10501, https://doi.org/10.1021/acs.jpcc.0c00463.
[97] X. Wang, D.-P. Yang, G. Huang, P. Huang, G. Shen, S. Guo, Y. Mei, D. Cui, J. Mater. Chem. 22 (2012) 17441–17444, https://doi.org/10.1039/c2jm32810k.
[98] S. Kang, J.-B. Pyo, T.-S. Kim, Langmuir 34 (2018) 5831–5836, https://doi.org/10.1021/acs.langmuir.8b01063.
[99] L.X. Li, R.P. Liu, Z.W. Chen, Q. Wang, M.Z. Ma, Q. Jing, G. Li, Y. Tian, Carbon 44 (2006) 1544–1547, https://doi.org/10.1016/j.carbon.2005.12.031.
[100] H.C. Schniepp, K.N. Kudin, J.-L. Li, R.K. Prud´homme, R. Car, D.A. Saville, I. A. Aksay, ACS Nano 2 (2008) 2577–2584, https://doi.org/10.1021/nn800457s.
[101] J.S. Chang, S. Kim, H.-J. Sung, J. Yeon, K.J. Chang, X. Li, S. Kim, Small 14 (2018), 1803386, https://doi.org/10.1002/smll.201803386.
[102] K. Akius, J.V. Ruitenbeek, arXiv:1812.09501 [cond-mat. mes-hall] (2018), 22 December.
[103] C.L. Yi, L.Y. Zhang, X.M. Chen, X.Q. Wang, C.H. Ke, Exp. Mech. 59 (2019) 381–386, https://doi.org/10.1007/s11340-018-00466-z.
[104] Y. Wakafuji, R. Moriya, S. Masubuchi, K. Watanabe, T. Taniguchi, T. Machida, Nano Lett. 20 (2020) 2486–2492, https://doi.org/10.1021/acs.nanolett.9b05228.
[105] S. Xu, Z. Yan, K.-I. Jang, W. Huang, H. Fu, J. Kim, Z. Wei, M. Flavin, J. McCracken, R. Wang, A. Badea, Y. Liu, D. Xiao, G. Zhou, J. Lee, H.U. Chung, H. Cheng, W. Ren, A. Banks, X. Li, U. Paik, R.G. Nuzzo, Y. Huang, Y. Zhang, J. A. Rogers, Science 347 (2015) 154–159, https://doi.org/10.1126/science.1260960.
[106] Y. Zhang, Z. Yan, K. Nan, D. Xiao, Y. Liu, H. Luan, H. Fu, X. Wang, Q. Yang, J. Wang, W. Ren, H. Si, F. Liu, L. Yang, H. Li, J. Wang, X. Guo, H. Luo, L. Wang, Y. Huang, J.A. Rogers, Proc. Natl. Acad. Sci. U. S. A. 112 (2015) 11757–11764, https://doi.org/10.1073/pnas.1515602112.
[107] Z. Yan, F. Zhang, J. Wang, F. Liu, X. Guo, K. Nan, Q. Lin, M. Gao, D. Xiao, Y. Shi, Y. Qiu, H. Luan, J.H. Kim, Y. Wang, H. Luo, M. Han, Y. Huang, Y. Zhang, J. A. Rogers, Adv. Funct. Mater. 26 (2016) 2629–2639, https://doi.org/10.1002/adfm.201504901.
[108] Z. Yan, M. Han, Y. Yang, K. Nan, H. Luan, Y. Luo, Y. Zhang, Y. Huang, J.A. Rogers, Extreme Mech. Lett. 11 (2017) 96–104, https://doi.org/10.1016/j.eml.2016.12.006.
[109] Y. Ling, X. Zhuang, Z. Xu, Y. Xie, X. Zhu, Y. Xu, B. Sun, J. Lin, Y. Zhang, Z. Yan, ACS Nano 12 (2018) 12456–12463, https://doi.org/10.1021/acsnano.8b06675.
[110] T. Sharifi, E. Graci, H.R. Barzegar, X. Jia, F. Nitze, G. Hu, P. Nordblad, C.-W. Tai, T. Wågberg, Nat. Commun. 4 (2013) 2319, https://doi.org/10.1038/ncomms3319.
[111] D. Yu, F. Liu, Nano Lett. 7 (2007) 3046–3050, https://doi.org/10.1021/nl071511n.
[112] S. Zhu, T. Li, ACS Nano 8 (2014) 2864–2872, https://doi.org/10.1021/nn500025t.
[113] A. Sidorov, D. Mudd, G. Sumanasekera, P.J. Ouseph, C.S. Jayanthi, S.-Y. Wu, Nanotechnology 20 (2009), 055611, https://doi.org/10.1088/0957-4484/20/5/055611.
[114] D. Berman, S.A. Deshmukh, S.K.R.S. Sankaranarayanan, A. Erdemir, A.V. Sumant, Science 348 (2015) 1118–1122, https://doi.org/10.1126/science.1262024.
[115] X. Chen, R.A. Boulos, J.F. Dobsonb, C.L. Raston, Nanoscale 5 (2013) 498–502, https://doi.org/10.1039/c2nr33071g.
[116] L.M. Viculis, J.J. Mack, R.B. Kaner, Science 299 (2003) 1361, https://doi.org/10.1126/science.1078842.
[117] F. Zeng, Y. Kuang, Y. Wang, Z. Huang, C. Fu, H. Zhou, Adv. Mater. 23 (2011) 4929–4932, https://doi.org/10.1002/adma.201102798.
[118] C.A. Amadei, I.Y. Stein, G.J. Silverberg, B.L. Wardle, C.D. Vecitis, Nanoscale 8 (2016) 6783–6791, https://doi.org/10.1039/c5nr07983g.
[119] M.M. Fogler, A.H.C. Neto, F. Guinea, Phys. Rev. B 81 (2010), 161408, https://doi.org/10.1103/PhysRevB.81.161408.
[120] O.-K. Park, C.S. Tiwary, Y. Yang, S. Bhowmick, S. Vinod, Q. Zhang, V.L. Colvin, S. A.S. Asif, R. Vajtai, E.S. Penev, B.I. Yakobson, P.M. Ajayan, Nanoscale 9 (2017) 6991–6997, https://doi.org/10.1039/c7nr01054k.
[121] A.P. Rooney, Z. Li, W. Zhao, A. Gholinia, A. Kozikov, G. Auton, F. Ding, R. V. Gorbachev, R.J. Young, S.J. Haigh, Nat. Commun. 9 (2018) 3597, https://doi.org/10.1038/s41467-018-06074-8.
[122] E. Prada, P. San-Jose, L. Brey, Phys. Rev. Lett. 105 (2010), 106802, https://doi.org/10.1103/PhysRevLett.105.106802.
[123] D. Rainis, F. Taddei, M. Polini, G. Léon, F. Guinea, V.I. Fal'ko, Phys. Rev. B 83 (2011), 165403, https://doi.org/10.1103/PhysRevB.83.165403.
[124] F. Queisser, R. Schützhold, Phys. Rev. Lett. 111 (2013), 046601, https://doi.org/10.1103/PhysRevLett.111.046601.
[125] R. Bistritzer, A.H. MacDonald, Proc. Natl. Acad. Sci. U. S. A. 108 (2011) 12233–12237, https://doi.org/10.1073/pnas.1108174108.
[126] E. Koren, E. Lörtscher, C. Rawlings, A.W. Knoll, U. Duerig, Science 348 (2015) 679–683, https://doi.org/10.1126/science.aaa4157.
[127] E. Koren, I. Leven, E. Lörtscher1, A. Knoll, O. Hod, U. Duerig, Nat. Nanotechnol. 11 (2016) 752–757, https://doi.org/10.1038/NNANO.2016.85.
[128] R. Ribeiro-Palau, C. Zhang, K. Watanabe, T. Taniguchi, J. Hone, C.R. Dean, Science 361 (2018) 690–693, https://doi.org/10.1126/science.aat6981.
[129] Y. Cao, V. Fatemi, A. Demir, S. Fang, S.L. Tomarken, J.Y. Luo, J.D. Sanchez-Yamagishi, K. Watanabe, T. Taniguchi, E. Kaxiras, R.C. Ashoori, P. Jarillo-Herrero, Nature 556 (2018) 80–84, https://doi.org/10.1038/nature26154.
[130] Y. Cao, V. Fatemi, S. Fang, K. Watanabe, T. Taniguchi, E. Kaxiras, P. Jarillo-Herrero, Nature 556 (2018) 43–50, https://doi.org/10.1038/nature26160.
[131] M. Yankowitz, S. Chen, H. Polshyn, Y. Zhang, K. Watanabe, T. Taniguchi, D. Graf, A.F. Young, C.R. Dean, Science 363 (2019) 1059–1064, https://doi.org/10.1126/science.aav1910.
[132] X. Lu, P. Stepanov, W. Yang, M. Xie, M.A. Aamir, I. Das, C. Urgell, K. Watanabe, T. Taniguchi, G. Zhang, A. Bachtold, A.H. MacDonald, D.K. Efetov, Nature 574 (2019) 653–657, https://doi.org/10.1038/s41586-019-1695-0.
[133] A.L. Sharpe, E.J. Fox, A.W. Barnard, J. Finney, K. Watanabe, T. Taniguchi, M. A. Kastner, D. Goldhaber-Gordon, Science 365 (2019) 605–608, https://doi.org/10.1126/science.aaw3780.
[134] Y. Jiang, X. Lai, K. Watanabe, T. Taniguchi, K. Haule, J. Mao, E.Y. Andrei, Nature 573 (2019) 91–95, https://doi.org/10.1038/s41586-019-1460-4.
[135] M. Serlin, C.L. Tschirhart, H. Polshyn, Y. Zhang, J. Zhu, K. Watanabe, T. Taniguchi, L. Balents, A.F. Young, Science 367 (2020) 900–903, https://doi.org/10.1126/science.aay5533.
[136] G. Chen, A.L. Sharpe, E.J. Fox, Y.-H. Zhang, S. Wang, L. Jiang, B. Lyu, H. Li, K. Watanabe, T. Taniguchi, Z. Shi, T. Senthil, D. Goldhaber-Gordon, Y. Zhang, F. Wang, Nature 579 (2020) 56–61, https://doi.org/10.1038/s41586-020-2049-7.
[137] D. Wong, K.P. Nuckolls, M. Oh, B. Lian, Y. Xie, S. Jeon, K. Watanabe, T. Taniguchi, B.A. Bernevig, A. Yazdani, Nature 582 (2020) 198–202, https://doi.org/10.1038/s41586-020-2339-0.
[138] U. Zondiner, A. Rozen, D. Rodan-Legrain, Y. Cao, R. Queiroz, T. Taniguchi, K. Watanabe, Y. Oreg, F. von Oppen, A. Stern, E. Berg, P. Jarillo-Herrero, S. Ilani, Nature 582 (2020) 203–208, https://doi.org/10.1038/s41586-020-2373-y.
[139] K.L. Seyler, P. Rivera, H. Yu, N.P. Wilson, E.L. Ray, D.G. Mandrus, J. Yan, W. Yao, X. Xu, Nature 567 (2019) 66–70, https://doi.org/10.1038/s41586-019-0957-1.
[140] K. Tran, G. Moody, F. Wu, X. Lu, J. Choi, K. Kim, A. Rai, D.A. Sanchez, J. Quan, A. Singh, J. Embley, A. Zepeda, M. Campbell, T. Autry, T. Taniguchi, K. Watanabe, N. Lu, S.K. Banerjee, K.L. Silverman, S. Kim, E. Tutuc, L. Yang, A. H. MacDonald, X. Li, Nature 567 (2019) 71–75, https://doi.org/10.1038/s41586-019-0975-z.
[141] C. Jin, E.C. Regan1, A. Yan, M.I.B. Utama, D. Wang, S. Zhao, Y. Qin, S. Yang, Z. Zheng, S. Shi, K. Watanabe, T. Taniguchi, S. Tongay, A. Zettl, F. Wang, Nature 567 (2019) 76–80, https://doi.org/10.1038/s41586-019-0976-y.
[142] E.M. Alexeev, D.A. Ruiz-Tijerina, M. Danovich, M.J. Hamer, D.J. Terry, P. K. Nayak, S. Ahn, S. Pak, J. Lee, J.I. Sohn, M.R. Molas, M. Koperski, K. Watanabe, T. Taniguchi, K.S. Novoselov, R.V. Gorbachev, H.S. Shin, V.I. Fal'ko, A. I. Tartakovskii, Nature 567 (2019) 81–86, https://doi.org/10.1038/s41586-019-0986-9.
[143] W. Chen, Z. Sun, Z. Wang, L. Gu, X. Xu, S. Wu, C. Gao, Science 366 (2019) 983–987, https://doi.org/10.1126/science.aav1937.
[144] G. Hu, Q. Ou, G. Si, Y. Wu, J. Wu, Z. Dai, A. Krasnok, Y. Mazor, Q. Zhang, Q. Bao, C.-W. Qiu, A. Alù, Nature 582 (2020) 209–213, https://doi.org/10.1038/s41586-020-2359-9.
[145] B. Wang, M. Huang, N.Y. Kim, B.V. Cunning, Y. Huang, D. Qu, X. Chen, S. Jin, M. Biswal, X. Zhang, S.H. Lee, H. Lim, W.J. Yoo, Z. Lee, R.S. Ruoff, Nano Lett. 17 (2017) 1467–1473, https://doi.org/10.1021/acs.nanolett.6b04459.
[146] H. Zhao, B. Wang, F. Liu, X. Yan, H. Wang, W.S. Leong, M.J. Stevens, P. Vashishta, A. Nakano, J. Kong, R. Kalia, H. Wang, Adv. Funct. Mater. 30 (2020), 1908691, https://doi.org/10.1002/adfm.201908691.
[147] C. Xu, X. Wu, G. Huang, Y. Mei, Adv. Mater. Technol. 4 (2019), 1800486, https://doi.org/10.1002/admt.201800486.
[148] S. Iijima, Nature 354 (1991) 56–58, https://doi.org/10.1038/354056a0.
[149] S. Iljima, T. Ichihashi, Nature 363 (1993) 603–605, https://doi.org/10.1038/363603a0.
[150] L. Wang, Z. Tian, B. Zhang, B. Xu, T. Wang, Y. Wang, S. Li, Z. Di, Y. Mei, Small 15 (2019), 1805477, https://doi.org/10.1002/smll.201805477.
[151] T.F. Teshima, C.S. Henderson, M. Takamura, Y. Ogawa, S. Wang, Y. Kashimura, S. Sasaki, T. Goto, H. Nakashima, Y. Ueno, Nano Lett. 19 (2019) 461–470, https://doi.org/10.1021/acs.nanolett.8b04279.
[152] S. Deng, V. Berry, Mater. Today 19 (2016) 197–212, https://doi.org/10.1016/j.mattod.2015.10.002.
[153] W. Chen, X. Gui, L. Yang, H. Zhu, Z. Tang, Nanoscale Horiz. 4 (2019) 291–320, https://doi.org/10.1039/c8nh00112j.
[154] W. Bao, F. Miao, Z. Chen, H. Zhang, W. Jang, C. Dames, C.N. Lau, Nat. Nanotechnol. 4 (2009) 562–566, https://doi.org/10.1038/NNANO.2009.191.
[155] W.-K. Lee, J. Kang, K.-S. Chen, C.J. Engel, W.-B. Jung, D. Rhee, M.C. Hersam, T. W. Odom, Nano Lett. 16 (2016) 7121–7127, https://doi.org/10.1021/acs.nanolett.6b03415.
[156] S. Lou, Y. Liu, F. Yang, S. Lin, R. Zhang, Y. Deng, M. Wang, K.B. Tom, F. Zhou, H. Ding, K.C. Bustillo, X. Wang, S. Yan, M. Scott, A. Minor, J. Yao, Nano Lett. 18 (2018) 1819–1825, https://doi.org/10.1021/acs.nanolett.7b05074.
[157] S. Yang, C. Wang, H. Sahin, H. Chen, Y. Li, S.-S. Li, A. Suslu, F.M. Peeters, Q. Liu, J. Li, S. Tongay, Nano Lett. 15 (2015) 1660–1666, https://doi.org/10.1021/nl504276u.
[158] L. Cai, M.J. Shearer, Y. Zhao, Z. Hu, F. Wang, Y. Zhang, K.W. Eliceiri, R.J. Hamers, W. Yan, S. Wei, M. Tang, S. Jin, J. Am. Chem. Soc. 140 (2018) 10980–10987, https://doi.org/10.1021/jacs.8b03399.
[159] C. Zhang, O. Dyck, D.A. Garfinkel, M.G. Stanford, A.A. Belianinov, J.D. Fowlkes, S. Jesse, P.D. Rack, Nanomaterials 9 (2019) 1394, https://doi.org/10.3390/nano9101394.
[160] T.W. Ebbesen, H. Hiura, Adv. Mater. 7 (1995) 582–586, https://doi.org/10.1002/adma.19950070618.
[161] D. Joung, T. Gu, J.-H. Cho, ACS Nano 10 (2016) 9586–9594, https://doi.org/10.1021/acsnano.6b04971.

[162] W. Xu, K.S. Kwok, D.H. Gracias, Acc. Chem. Res. 51 (2018) 436–444, https://doi.org/10.1021/acs.accounts.7b00468.
[163] Z. Dai, L. Liu, Z. Zhang, Adv. Mater. 31 (2019), 1805417, https://doi.org/10.1002/adma.201805417.
[164] Y. Wang, C. Jiang, Q. Chen, Q. Zhou, H. Wang, J. Wan, L. Ma, J. Wang, J. Phys. Chem. Lett. 9 (2018) 6847–6852, https://doi.org/10.1021/acs.jpclett.8b02913.
[165] A.T. Costa, M.S. Ferreira, T. Hallam, G.S. Duesberg, A.H.C. Neto, EPL 104 (2013) 47001, https://doi.org/10.1209/0295-5075/104/47001.
[166] T.C. Shyu, P.F. Damasceno, P.M. Dodd, A. Lamoureux, L. Xu, M. Shlian, M. Shtein, S.C. Glotzer, N.A. Kotov, Nat. Mater. 14 (2015) 785–789, https://doi.org/10.1038/NMAT4327.
[167] B. Wang, Z. Li, C. Wang, S. Signetti, B.V. Cunning, X. Wu, Y. Huang, Y. Jiang, H. Shi, S. Ryu, N.M. Pugno, R.S. Ruoff, Adv. Mater. 30 (2018), 1707449, https://doi.org/10.1002/adma.201707449.
[168] W.J. Yu, S.H. Chae, D. Perello, S.Y. Lee, G.H. Han, M. Yun, Y.H. Lee, ACS Nano 4 (2010) 5480–5486, https://doi.org/10.1021/nn101581k.
[169] R. Xiang, T. Inoue, Y. Zheng, A. Kumamoto, Y. Qian, Y. Sato, M. Liu, D. Tang, D. Gokhale, J. Guo, K. Hisama, S. Yotsumoto, T. Ogamoto, H. Arai, Y. Kobayashi, H. Zhang, B. Hou, A. Anisimov, M. Maruyama, Y. Miyata, S. Okada, S. Chiashi, Y. Li, J. Kong, E.I. Kauppinen, Y. Ikuhara, K. Suenaga, S. Maruyama, Science 367 (2020) 537–542, https://doi.org/10.1126/science.aaz2570.
[170] S.J.P. Callens, A.A. Zadpoor, Mater. Today 21 (2018) 241–264, https://doi.org/10.1016/j.mattod.2017.10.004.
[171] W. Zhao, X. Ren, B. Wang, C. Jin, W. Duan, F. Ding, Phys. Rev. Mater. 3 (2019), 056001, https://doi.org/10.1103/PhysRevMaterials.3.056001.
[172] P.Z. Hanakata, E.D. Cubuk, D.K. Campbell, H.S. Park, Phys. Rev. Lett. 121 (2018), 255304, https://doi.org/10.1103/PhysRevLett.121.255304.
[173] E. Han, J. Yu, E. Annevelink, J. Son, D.A. Kang, K. Watanabe, T. Taniguchi, E. Ertekin, P.Y. Huang, A.M. van der Zande, Nat. Mater. 19 (2020) 305–309, https://doi.org/10.1038/s41563-019-0529-7.
[174] J.A. Rogers, T. Someya, Y. Huang, Science 327 (2010) 1603–1607, https://doi.org/10.1126/science.1182383.
[175] Q. Guo, Z. Di, M.G. Lagally, Y. Mei, Mater. Sci. Eng. R Rep. 128 (2018) 1–31, https://doi.org/10.1016/j.mser.2018.02.002.
[176] S. Huang, Y. Liu, Y. Zhao, Z. Ren, C.F. Guo, Adv. Funct. Mater. 29 (2019), 1805924, https://doi.org/10.1002/adfm.201805924.
[177] D. Qi, Z. Liu, Y. Liu, W.R. Leow, B. Zhu, H. Yang, J. Yu, W. Wang, H. Wang, S. Yin, X. Chen, Adv. Mater. 27 (2015) 5559–5566, https://doi.org/10.1002/adma.201502549.
[178] W.J. Hyun, O.O. Park, B.D. Chin, Adv. Mater. 25 (2013) 4729–4734, https://doi.org/10.1002/adma.201302063.
[179] H.C. Lee, E.Y. Hsieh, K. Yong, S. Nam, Nano Res. 13 (2020) 1406–1412, https://doi.org/10.1007/s12274-020-2662-7.
[180] K. Xu, Y. Lu, S. Honda, T. Arie, S. Akitaa, K. Takei, J. Mater. Chem. C 7 (2019) 9609–9617, https://doi.org/10.1039/C9TC01874C.
[181] D. Yang, H. Wan, S. Luo, C. Wang, S. Zhang, S. Guo, Nanomaterials 9 (2019) 922, https://doi.org/10.3390/nano9070922.
[182] F. Yi, H. Ren, J. Shan, X. Sun, D. Wei, Z. Liu, Chem. Soc. Rev. 47 (2018) 3152–3188, https://doi.org/10.1039/c7cs00849j.
[183] Z. Song, T. Ma, R. Tang, Q. Cheng, X. Wang, D. Krishnaraju, R. Panat, C.K. Chan, H. Yu, H. Jiang, Nat. Commun. 5 (2014) 3140, https://doi.org/10.1038/ncomms4140.
[184] C.-H. Huang, Z.-Y. Chen, C.-L. Chiu, T.-T. Huang, H.-F. Meng, P. Yu, ACS Appl. Mater. Interfaces 11 (2019) 29901–29909, https://doi.org/10.1021/acsami.9b08366.
[185] A. Lamoureux, K. Lee, M. Shlian, S.R. Forrest, M. Shtein, Nat. Commun. 6 (2015) 8092, https://doi.org/10.1038/ncomms9092.
[186] S. Hong, Y. Shi, R. Li, C. Zhang, Y. Jin, P. Wang, ACS Appl. Mater. Interfaces 10 (2018) 28517–28524, https://doi.org/10.1021/acsami.8b07150.
[187] Y. Xu, J. Ma, D. Liu, H. Xu, F. Cui, W. Wang, Chem. Eng. J. 356 (2019) 869–876, https://doi.org/10.1016/j.cej.2018.09.070.
[188] W. Li, Z. Li, K. Bertelsmann, D.E. Fan, Adv. Mater. 31 (2019), 1900720, https://doi.org/10.1002/adma.201900720.
[189] C. Gao, J. Gao, C. Shao, Y. Xiao, Y. Zhao, L. Qu, J. Mater. Chem. A 6 (2018) 19750–19756, https://doi.org/10.1039/C8TA05148H.
[190] Y.X. Huang, H.H. Cheng, G.Q. Shi, L.T. Qu, ACS Appl. Mater. Interfaces 9 (2017) 38170–38175, https://doi.org/10.1021/acsami.7b12542.
[191] Y. Liang, F. Zhao, Z.H. Cheng, Q.H. Zhou, H.B. Shao, L. Jiang, L.T. Qu, Nano Energy 32 (2017) 329–335, https://doi.org/10.1016/j.nanoen.2016.12.062.
[192] F. Zhao, L.X. Wang, Y. Zhao, L.T. Qu, L.M. Dai, Adv. Mater. 29 (2017), 1604972, https://doi.org/10.1002/adma.201604972.
[193] A.M. Armani, R.P. Kulkarni, S.E. Fraser, R.C. Flagan, K.J. Vahala, Science 317 (2007) 783–787, https://doi.org/10.1126/science.1145002.
[194] L. He, Ş.K. Özdemir, J. Zhu, W. Kim, L. Yang, Nat. Nanotechnol. 6 (2011) 428–432, https://doi.org/10.1038/NNANO.2011.99.
[195] Y. Yin, J. Pang, J. Wang, X. Lu, Q. Hao, E.S.G. Naz, X. Zhou, L. Ma, O.G. Schmidt, ACS Appl. Mater. Interfaces 11 (2019) 15891–15897, https://doi.org/10.1021/acsami.9b00733.
[196] T. Deng, Z. Zhang, Y. Liu, Y. Wang, F. Su, S. Li, Y. Zhang, H. Li, H. Chen, Z. Zhao, Y. Li, Z. Liu, Nano Lett. 19 (2019) 1494–1503, https://doi.org/10.1021/acs.nanolett.8b04099.
[197] W. Xu, S.K. Paidi, Z. Qin, Q. Huang, C.-H. Yu, J.V. Pagaduan, M.J. Buehler, I. Barman, D.H. Gracias, Nano Lett. 19 (2019) 1409–1417, https://doi.org/10.1021/acs.nanolett.8b03461.
[198] Z. Lei, W. Zhu, S. Sun, P. Wu, Nanoscale 8 (2016) 18800–18807, https://doi.org/10.1039/c6nr07265h.
[199] D. Niu, W. Jiang, H. Liu, T. Zhao, B. Lei, Y. Li, L. Yin, Y. Shi, B. Chen, B. Lu, Sci. Rep. 6 (2016) 27366, https://doi.org/10.1038/srep27366.
[200] M.Z. Miskin, K.J. Dorsey, B. Bircan, Y. Han, D.A. Muller, P.L. McEuen, I. Cohen, Proc. Natl. Acad. Sci. U. S. A. 115 (2018) 466–470, https://doi.org/10.1073/pnas.1712889115.
[201] M. Acerce, E.K. Akdoğan, M. Chhowalla, Nature 549 (2017) 370–373, https://doi.org/10.1038/nature23668.
[202] W. Xu, D.H. Gracias, ACS Nano 13 (2019) 4883–4892, https://doi.org/10.1021/acsnano.9b03051.
[203] Y. Mei, A.A. Solovev, S. Sanchez, O.G. Schmidt, Chem. Soc. Rev. 40 (2011) 2109–2119, https://doi.org/10.1039/c0cs00078g.
[204] B. Zhang, G. Huang, L. Wang, T. Wang, L. Liu, Z. Di, X. Liu, Y. Mei, Chem. Asian J. 14 (2019) 2479–2484, https://doi.org/10.1002/asia.201900301.
[205] W. Jiang, D. Niu, H. Liu, C. Wang, T. Zhao, L. Yin, Y. Shi, B. Chen, Y. Ding, B. Lu, Adv. Funct. Mater. 24 (2014) 7598–7604, https://doi.org/10.1002/adfm.201402070.
[206] B. Han, Y.-L. Zhang, L. Zhu, Y. Li, Z.-C. Ma, Y.-Q. Liu, X.-L. Zhang, X.-W. Cao, Q.-D. Chen, C.-W. Qiu, H.-B. Sun, Adv. Mater. 31 (2019), 1806386, https://doi.org/10.1002/adma.201806386.
[207] Y.-Q. Liu, J.-N. Ma, Y. Liu, D.-D. Han, H.-B. J, J.-W. Mao, C.-H. Han, Z.-Z. Jiao, Y.-L. Zhang, Opt. Mater. Express 7 (2017) 2617–2625, https://doi.org/10.1364/OME.7.002617.
[208] A.A. Zadpoor, Mater. Horiz. 3 (2016) 371–381, https://doi.org/10.1039/c6mh00065g.
[209] K. Bertoldi, V. Vitelli, J. Christensen, M. van Hecke, Nat. Rev. Mater. 2 (2017) 17066, https://doi.org/10.1038/natrevmats.2017.66.
[210] J.U. Surjadi, L. Gao, H. Du, X. Li, X. Xiong, N.X. Fang, Y. Lu, Adv. Eng. Mater. 21 (2019), 1800864, https://doi.org/10.1002/adem.201800864.
[211] G. Qin, Z. Qin, NPJ Comput. Mater. 6 (2020) 51, https://doi.org/10.1038/s41524-020-0313-x.
[212] K. Cai, J. Luo, Y. Ling, J. Wan, Q.-h. Qin, Sci. Rep. 6 (2016) 35157, https://doi.org/10.1038/srep35157.
[213] D.T. Ho, V.H. Ho, V. Babar, S.Y. Kim, U. Schwingenschlögl, Nanoscale 12 (2020) 10172–10179, https://doi.org/10.1039/d0nr01733g.
[214] D.T. Ho, H.S. Park, S.Y. Kim, U. Schwingenschlögl, ACS Nano 14 (2020) 8969–8974, https://doi.org/10.1021/acsnano.0c03791.

Ziyang Zhang received his B.S. degree in Nano Materials and Technology from Nanjing University of Science and Technology. He is persuing his Ph.D. degree in Microelectronics and Solid-State Electronics at Shanghai Institute of Microsystem and Information Technology. His current research interests focus on the strain engineering and origami-based assembly of two-dimensional materials.

Ziao Tian received his B.S. and M.S. degrees from University of Shanghai for Science and Technology and Ph.D. degree in physics from Fudan University. He is an associate professor at Shanghai Institute of Microsystem and Information Technology. Before that, he worked as a postdoctoral researcher in the Department of Material Science at Fudan University. His research is focused on the development of micro/nanotubes fabricated by rolled-up nanotechnology and their functionalization with smart materials.

Yongfeng Mei received his BS and MS in physics from Nanjing University and PhD in materials physics from City University of Hong Kong. He is a professor in materials physics and chemistry and associated department head in the Department of Materials Science at Fudan University (China). Before that, he worked as a post-doctoral researcher in the Max Planck Institute for Solid State Research (Germany) and then led a research group in the Leibniz Institute for Solid State and Materials Research Dresden (Germany) as a staff scientist. His research interest focuses on the nanomembrane materials development in micro/nanorobotics, flexible electronics/optoelectronics and nanophotonics.

Zengfeng Di received his B.S. degree in biochemistry from Nanjing University and PhD in microelectronics and solid state electronics from Shanghai Institute of Microsystem and Information Technology (SIMIT), Chinese Academy of Sciences (CAS). He is a professor in microelectronics and solid state electronics and a deputy director of SIMIT CAS. Prior to join SIMIT, CAS as a professor, he worked as a Director's Postdoctoral Fellow in Los Alamos National Laboratory (LANL) in US. His research interest covers advanced silicon-on-insulator (SOI) materials, two dimensional materials, microelectronic and optoelectronic devices